

Immune and Stromal Cell Characterization of Abdominal Adipose Deposits

By

Beth McKendrick

A thesis submitted to the University of Birmingham

For the Degree of MASTER OF SCIENCE BY RESEARCH

Institute of Immunology and Immunotherapy

College of Medical and Dental Sciences

University of Birmingham

March 2017

UNIVERSITY OF
BIRMINGHAM

University of Birmingham Research Archive

e-theses repository

This unpublished thesis/dissertation is copyright of the author and/or third parties. The intellectual property rights of the author or third parties in respect of this work are as defined by The Copyright Designs and Patents Act 1988 or as modified by any successor legislation.

Any use made of information contained in this thesis/dissertation must be in accordance with that legislation and must be properly acknowledged. Further distribution or reproduction in any format is prohibited without the permission of the copyright holder.

Abstract

Type 2 immunity has been recently shown to play a key role in adipocyte homeostasis, and a relatively novel cell type, group 2 innate lymphoid cells (ILC2s), are instrumental in many homeostatic pathways in adipose tissue. A novel lymphoid structure, fat-associated lymphoid clusters (FALCs), have been recently identified in adipose deposits but their broader function(s) in adipocyte homeostasis are unknown, and it is unclear what the most appropriate adipose deposit might be for further study. The aim of this investigation was to characterize the FALCs, ILC populations, and IL-33-producing stromal populations in three types of adipose tissue, to understand which might be the most appropriate for further study into adipocyte homeostasis.

The results reveal that the most commonly studied adipose deposit (gonadal fat) has similar characteristics to the deposit that was hypothesized to be more physiologically appropriate (mesenteric fat). Subtle differences are apparent, including differing ILC2 populations, but the body of evidence is not sufficient to confidently suggest that mesenteric fat should replace gonadal as the *in vivo* model tissue of choice for obesity studies. However, omental fat does fulfill the criteria as an appropriate candidate tissue to explore questions around the role(s) of FALC in metabolic homeostasis, because of relatively high number of FALCs, ILC2s, and IL-33⁺ stromal cells. In addition, an improved imaging technique has been developed to allow the exploration of immune cell localization within the FALCs – critical for any future studies into FALC function in metabolic homeostasis.

Contents

1. Introduction	1
1.1. Adipose tissue and obesity-associated inflammation.....	5
1.2. Innate Lymphoid Cells	7
1.2.1. Group 1 ILCs	11
1.2.2. Group 2 ILCs	12
1.2.3. Group 3 ILCs	13
1.3. Stromal cells of the mLN and adipose tissues	14
1.3.1. Production of IL-33 by stromal cells.....	15
1.4. Metabolic homeostasis and obesity (i): Brown, white, and beige.....	16
1.5. Metabolic homeostasis and obesity (ii): a role for ILC2s.....	17
1.6. Atypical secondary lymphoid structures: FALCs.....	22
1.7. Project Aims.....	24
2. Materials and Methods	26
2.1. Mice	26
2.2. Isolation of cells from the mesenteric lymph node	27
2.3. Isolation of cells from adipose deposits	27
2.4. Flow Cytometry.....	28
2.5. Whole-Mount Immunofluorescence	31
2.6. FALC counts	33
2.7. FALC removal experiments	33
2.8. Zymosan Immunization.....	33
2.9. Statistical analysis	33
3. Results	35
3.1. FALCs can be identified and enumerated in abdominal adipose deposits.....	35
3.2. Identification of ILC1s, ILC2s and ILC3s in mLN and abdominal adipose deposits	40
3.3. Isolation of FALC from mesenteric fat deposits	51
3.4. Enumerating FALC in IL-33 ^{cit/+} and IL-33 ^{cit/cit} mice.....	57
3.5. Identification of IL-33 ⁺ cells.....	59
3.6. Further characterization of Gp38 ⁺ citrine ⁺ stromal populations.....	70
3.7. Effects of zymosan-induced peritoneal inflammation on Gp38 ⁺ citrine ⁺ stromal populations	76

3.8. Components of FALCs identified by whole mount immunofluorescence and confocal microscopy	79
4. Discussion.....	85
4.1. The presence of FALCs in adipose tissues.....	86
4.2. Differential ILC profiles of adipose tissues	88
4.3. The location of ILC2s in mesenteric fat.....	91
4.4. IL-33 ^{cit/+} and IL-33 ^{cit/cit} mice as tools to investigate IL-33- producing stromal cells	92
4.5. Further characterization of citrine ⁺ stromal cells	95
4.6. The effect of zymosan on adipose stromal populations	96
4.7. Development of a whole mount immunofluorescence staining method for confocal microscopy	98
5. Concluding Remarks	100
Appendix A: Supplementary Figures	104
Appendix B: List of References	108

List of Figures

Figure 1.1: Locations of abdominal adipose deposits in the mouse peritoneal cavity.....	4
Figure 1.2: Summary schematic of ILC development pathways.	10
Figure 1.3: Summary schematic of the IL-33-ILC2 adipocyte beiging pathways.	2120
Figure 3.1: Visualising and enumerating FALC in abdominal adipose deposits.....	38
Figure 3.2: Identification of ILC1 in the mesenteric lymph node, and abdominal fat depots.....	41
Figure 3.3: Identification of ILC2 and ILC3 populations in mesenteric lymph node, and abdominal fat depots.....	43
Figure 3.4: Quantitation of total ILC populations in the mesenteric lymph node and abdominal adipose depots.....	47
Figure 3.5: Quantitation of ILC populations in the mesenteric lymph node and abdominal adipose depots.....	49
Figure 3.6: Isolation of FALC from mesenteric fat.....	53
Figure 3.7: Removal of FALC from mesenteric fat does not impact ILC2 populations as assessed by flow cytometry.....	55
Figure 3.8: Enumerating FALC in IL-33 ^{cit/+} and IL-33 ^{cit/cit} mice.....	58
Figure 3.9: Identification of IL-33 ⁺ cells in citrine reporter mice.....	62
Figure 3.10: Identification of IL-33 ⁺ cells in citrine reporter mice.....	64
Figure 3.11: IL-33 ⁺ stromal cell composition in mesenteric lymph node and adipose tissues from IL-33 ^{cit/+} (+/-) mice.....	66
Figure 3.12: IL-33 ⁺ stromal cell composition in mesenteric lymph node and adipose tissues from IL-33 ^{cit/cit} (-/-) mice.....	67
Figure 3.13: Comparison of Gp38 ⁺ Citrine ⁺ populations in mLN and adipose deposits in IL-33 ^{cit/+} and IL-33 ^{cit/cit} mice.....	68
Figure 3.14: Comparison of citrine ⁺ cells in IL-33 ^{cit/+} and IL-33 ^{cit/cit} mice.....	69
Figure 3.15: Further characterization of Gp38 ⁺ IL33 ⁺ stromal populations in the mesenteric lymph node and adipose deposits of IL-33 ^{cit/+} and IL-33 ^{cit/cit} mice.....	73
Figure 3.16: Further characterization of Gp38 ⁺ IL33 ⁺ stromal populations in the mesenteric lymph node and adipose deposits of IL-33 ^{cit/+} and IL-33 ^{cit/cit} mice.....	75
Figure 3.17: Effect of Zymosan-induced peritoneal inflammation on Gp38+IL-33+ stromal populations in IL-33 ^{cit/+} mice.....	77
Figure 3.18: Components of FALC identified by whole mount immunofluorescence and confocal microscopy.....	81
Figure 3.19: IL-33 expressing cells in FALC identified by whole mount immunofluorescence and confocal microscopy.....	83
Figure S1: Gating strategy for identifying ILCs in the mesenteric lymph node and gonadal fat.....	104
Figure S2: Gating strategy for identifying ILCs in mesenteric fat and omental fat.....	105
Figure S3: Gating strategy for identifying IL-33 producing stromal cells in the mesenteric lymph node and gonadal fat of IL-33 ^{cit/+} mice.....	106
Figure S4: Gating strategy for identifying IL-33 producing stromal cells in mesenteric fat and omental fat of IL-33 ^{cit/+} mice.....	107

List of Tables

Table 1: Details of mouse strains used in this study	266
Table 2: Fluorescently conjugated cell labelling reagents and antibodies used for flow cytometry	30
Table 3: Fluorescently conjugated cell labelling reagents and antibodies used for whole-mount immunofluorescence	32

List of Abbreviations

AAMs	Alternatively Activated Macrophages
AP	Adipocyte Precursors
BMI	Body Mass Index
CD3i	Internal CD3
CLP	Common Lymphoid Progenitor
CXCL13	Chemokine Ligand 13
DAMPs	Danger-associated Molecular Patterns
Dapi	4',6-diamidino-2-phenylindole
EDTA	Ethylenediaminetetraacetic acid
ELISA	Enzyme-Linked Immunosorbant Asssay
FALC	Fat Associated Lymphoid Cluster
GATA3	GATA-binding protein 3
FCS	Fetal Calf Serum
ID2	Inhibitor of DNA binding 2
IFN γ	Interferon Gamma
IgM	Immunoglobulin M
ILCs	Innate Lymphoid Cell
IL	Interleukin
iNKT	Invariant Natural Killer T cells
K.O	Knock Out
Lin	Lineage
LT β R	Lymphotoxin Beta Receptor
LTi	Lymphoid Tissue Inducer
mLN	Mesenteric Lymph Node
MetEnk	Met-Enkephalin
mRNA	Messenger Ribonucleic Acid
NK	Natural Killer (cell)

NRLP3	NACHT, LRR and PYD domains-containing protein 3
NCR	Natural Cytotoxicity Receptors
PAMPs	Pathogen-Associated Molecular Patterns
<i>Pcsk1</i>	Proprotein Convertase Subtilisin/kexin type 1
PDGFR α	Platelet-derived growth factor alpha
PLZF	Promyelocytic leukaemia zinc finger protein
<i>Ppara</i>	Peroxisome proliferator activated receptor alpha
RAG	Recombination-activating genes
ROR α	Retinoic acid receptor -related orphan receptor alpha
ROR γ t	Retinoic acid receptor -related orphan receptor gamma T
RPMI	Roswell Park Memorial Institute
Sca-1	Stem cell antigen 1
<i>Srebp1c</i>	Sterol regulatory element-binding transcription factor 1
SVF	Stromal Vascular Fraction
T _H 1/2	T-helper 1/2
TLR	Toll-like Receptor
TNF	Tumour Necrosis Factor
UCP1	Uncoupling Protein 1
WT	Wild Type

1. Introduction

In the year 2000, the World Health Organization (WHO) stated that “one of the greatest public health challenges in first half of the 21st century is preventing the epidemic of obesity” (WHO *et al.*, 2000). Almost two decades later, the global obesity crisis has worsened considerably and the headline figure quoted in government literature estimates that obesity-associated costs reached upwards of £25 billion in the UK alone in 2015 (Butland *et al.* 2007). The real figure is unknown but likely to be somewhat higher, as this estimate is the result of a modelled projection from research conducted in 2007. A significant proportion of these costs result from associated co-morbidities such as type 2 diabetes, which drastically reduce quality of life for obese patients.

During the development of obesity, individual adipocytes will undergo hypertrophy and hyperplasia in response to over-nutrition, and hence fat deposits expand (Faust *et al.*, 1978). In many cases sensitivity to insulin and glucose tolerance is decreased. Reduced insulin sensitivity can develop into type 2 diabetes and an excess of visceral fat is considered to be strongly associated with the development of the condition, more so than factors such as high body mass index (BMI) and general adiposity (Neeland *et al.*, 2012). Up until very recently all abdominal visceral fat deposits were simply considered as just “visceral fat” regarded as a homogenous tissue group, with little attention paid to location or functional differences. However, evidence from studies into different deposits which examined parameters such as differential mitochondrial densities (an indicator of metabolic activity) (Deveaud *et al.*, 2004), mRNA levels of peroxisome proliferator activated receptor alpha (*ppara*) (signaling of which is linked to adipogenesis and lipid metabolism) (Vidal-Puig *et al.*, 1997; Yang *et al.*, 2008), and gene expression of

lipogenic transcription factors *Ppar γ* and Sterol regulatory element-binding transcription factor 1 (*Srebp1c*) (Palou *et al.*, 2009), suggest that visceral fat deposits possess distinct characteristics deserving of further study.

The vast majority of rodent studies focusing on obesity, diabetes and metabolic syndrome still refer simply to “visceral fat” with no further detail or, more commonly, investigate only the perigonadal fat pad, also known as epididymal fat in males or periovarian fat in females. For simplicity, this deposit shall be referred to as gonadal fat in this study. This focus on gonadal fat is understandable due to its accessible location in rodents but is also problematic, not least because an analogous deposit does not exist in humans (Chusyd *et al.*, 2016). Therefore, findings from studies of this nature may only have limited application to human biology.

There are two other alternative visceral fat deposits that should be considered alongside gonadal fat (Figure 1.1). The first, mesenteric fat, is widely regarded as the most analogous to the abdominal adipose deposit found in humans (Chusyd *et al.*, 2016), due to its anatomical location and link to the portal vein. Indeed, it has recently been designated an organ (Coffey & O’ Leary, 2016). The mesenteric adipose tissue is connected to the small intestine and surrounds the mesenteric lymph node (mLN). It is however poorly understood in rodents because it is not easy to access or manipulate during live-animal studies. The second, the omentum, is a long and narrow strip of adipose tissue, usually located next to the spleen and stomach. The omentum has several well-established functions during peritoneal inflammation. It is one of only two documented sites that can physically absorb and remove bacteria and foreign particles from the site of inflammation (Shipley & Cunningham, 1916). In addition, previous

studies in healthy humans have documented that the omentum is a vast reservoir of macrophages and also contains significant proportions of B and T cells. (Krist *et al.*, 1995). Finally, the omentum is also able to migrate (not move *per se*, rather, utilize endogenous mechanisms such as intestinal peristalsis) to sites of inflammation or infection, and will rapidly produce fibrin to seal off the contaminated area (Konturek *et al.*, 1994). This phenomenon has even been observed with surgically implanted devices such as catheters (Agrama *et al.*, 1976). The ability of the omentum to seal up sites of inflammation, along with the fact it is heavily vascularized means it has become a critical part of the surgeon's tool kit. Omentoplasty is used by surgeons all over the world to revascularize organs (Vineberg *et al.*, 1966) and ischemic limbs (Agarwal & Bajaj, 1987), as well as to aid wound healing (De Broux *et al.*, 2005). The risk of developing obesity-related diseases is best documented for mesenteric and omental fat, yet the properties of these tissues, especially their immunological characteristics, are incompletely understood. This is concerning as there is known to be a significant immunological component, particularly type 2 immunity, active within adipose tissue during homeostasis and decreased during obesity (Wu *et al.*, 2011; Molofsky *et al.*, 2013). It is obvious that the picture regarding abdominal adipose deposits is far from clear and therefore additional characterization of gonadal, mesenteric and omental fat is required. Improving the understanding of *in vivo* models used and refining them where appropriate will lead to more biologically relevant data with better application to human disease.

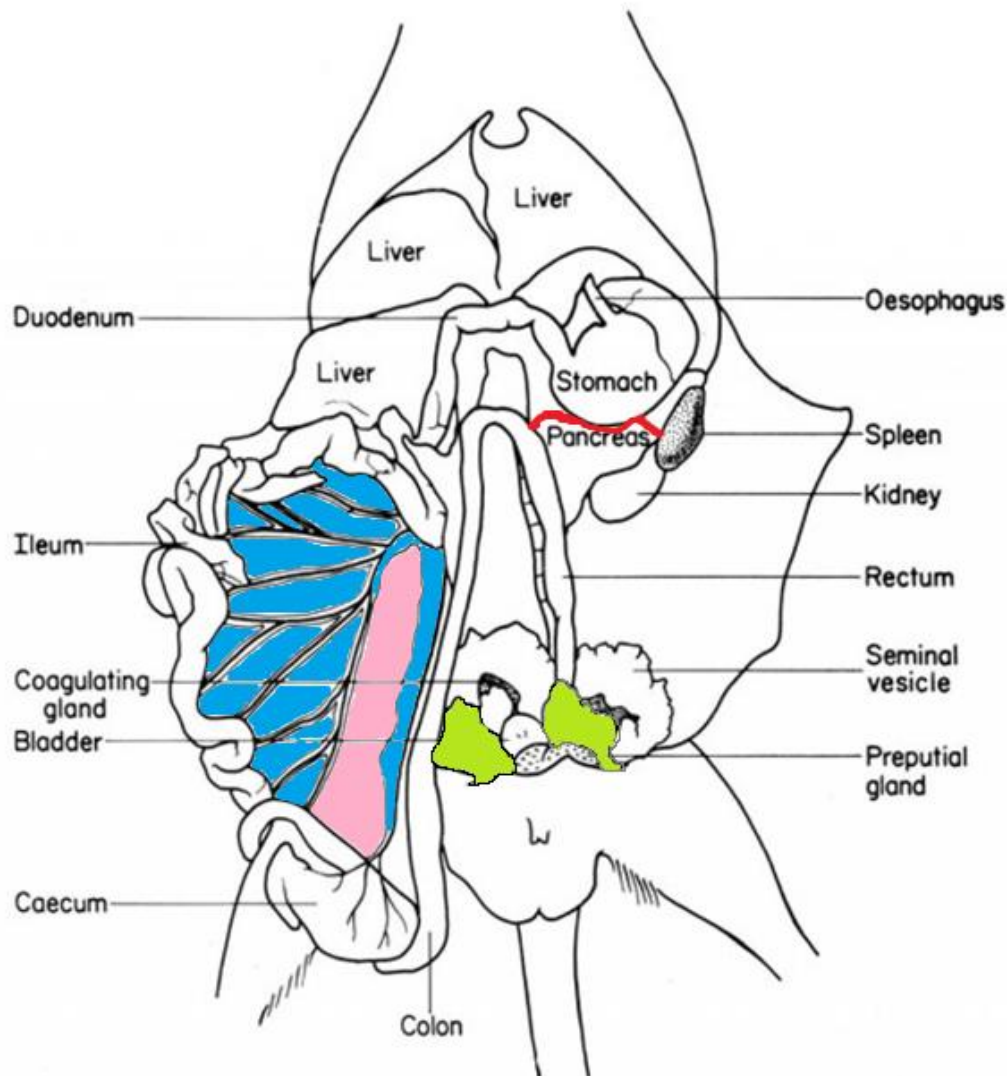


Figure 1.1: Locations of abdominal adipose deposits in the mouse peritoneal cavity (adapted from original image by anatomylibrary.us). Gonadal fat (green) is located next to the bladder and genital region of the mouse. Mesenteric fat (blue) is connected to the small intestine and surrounds the mesenteric lymph node (pink). Omental fat (red) is a thin strip of adipose tissue normally situated next to the stomach and spleen, but can use the inherent movements of the peritoneal cavity, such as peristalsis, to move around the cavity to sites of infection.

1.1. Adipose tissue and obesity-associated inflammation

A growing body of evidence suggests that, contrary to popular thought, adipose tissues are not just inert energy storage sites, but instead comprise a large and immunologically active organ. Adipose tissue has the ability to secrete a cocktail of adipokines, cytokines that can directly influence local insulin sensitivity, as well as a classic array of pro- and anti-inflammatory cytokines (Ouchi *et al.*, 2011). Adipocytes are not the only component of adipose tissue. The stromal-vascular fraction (SVF), which can be isolated by enzymatic digestion of adipose, contains myriad other cell types such as pre-adipocytes, blood endothelium and immune cells. Recent quantification of the SVF in obese animals determined that up to two-thirds of the cells are hematopoietic cells such as T cells, B cells, and macrophages (Grant *et al.*, 2013). The physiological hallmark of obesity is chronic, low-grade inflammation, and several immunological and structural changes have been observed in obese adipose tissues which are linked to this. Crown-like structures, comprised of macrophages and other immune cells, appear in murine adipose tissues upon onset of high fat feeding and peak around four months later, coinciding with a peak in adipocyte death (up to 80%). By month five, adipocyte death and crown-like structure numbers are decreased and insulin sensitivity even improves marginally, although is still markedly worse than WT controls (Strissel *et al.*, 2007). This suggests adipose tissue remodels in an attempt to mitigate the consequences of over-nutrition, but cannot deal with the problem in its entirety. Obesity-associated inflammation is thought to be the result of massive adipocyte cell death such as that seen in the Strissel study (Strissel *et al.*, 2007) via a putative mechanism known as pyroptosis, a NLRP3 inflammasome-dependent Caspase-1 mediated mechanism of cell

death, in which there is a measure of cytosolic leakage from adipocytes into the extracellular environment (Giordano *et al.*, 2013). This leakage triggers the release of danger signals known as DAMPs (danger-associated molecular pattern), such as high-mobility group box 1 (HMGB1) (Yang *et al.*, 2015) and heat shock proteins (Ohashi *et al.*, 2000), from surrounding cells. These signals are mostly detected by Toll-like receptors (TLRs) on innate immune cells in much the same way as PAMPs (pathogen-associated molecular patterns) are; For example the detection of the bacterial endotoxin lipopolysaccharide (LPS) is predominantly mediated by TLR4 (Poltorak *et al.*, 1998; Lu *et al.*, 2008). However other varieties of DAMP receptors exist, such as the P2X7 receptor that signals upon interaction with adenosine triphosphate (ATP) (Cicko *et al.*, 2015). Over time, exposure of macrophages to most types of DAMPs will skew their polarization from the regulatory M2 phenotype to the proinflammatory M1 phenotype. M1 macrophages can drive T cell proliferation in adipose tissues and also induce their differentiation towards the Th1 phenotype, leading to increases in pro-inflammatory type 1 cytokine production in adipose tissues, feeding the cycle of inflammation (Morris *et al.*, 2013). This is the basis of the chronic low-grade inflammation observed in obesity. However, not all DAMPs exclusively promote the M1 macrophage phenotype. IL-33, a DAMP released by a number of stromal cells such as endothelium, epithelium, and adipocytes, has been found to promote the M1 phenotype in naïve human macrophages. However, when added to human macrophages already in the M2 state (*in vitro*) IL-33 contributed to the maintenance of M2 characteristics, which are associated with the prevention of obesity (Joshi *et al.*, 2010).

Recently, a novel set of immune cells, known as innate lymphoid cells, have been implicated in regulation of metabolic homeostasis and the development of obesity. This is a heterogeneous new family of cells and some subsets are more involved in the immunological features of adipose tissues than others.

1.2. Innate Lymphoid Cells

Innate Lymphoid Cells (ILCs) are a relatively new subset of immune cells characterized by their lack of recombination-activating genes (RAG)-dependent antigen receptors such as those found on B and T cells, lack of phenotypic markers used to define specific lineages such as those found on macrophages and dendritic cells (Lin^-), and general lymphoid morphology (Spits *et al.*, 2013). Like all lymphocytes, ILCs are derived from a common lymphoid progenitor (CLP) although there are several downstream progenitors that can give rise to different subsets (Figure 1.2). ID2 (inhibitor of DNA binding 2) is the key transcriptional regulator that is required at some stage for the development of all ILC subsets (Boos *et al.*, 2007). Many other transcription factors including, GATA Binding Protein 3 (GATA3), retinoic acid receptor-related orphan receptor gamma (ROR γ t), and Tbet are involved in the development of individual subsets, which are summarized in Figure 1.2. A degree of plasticity is thought to exist in some ILC populations and this is influenced by transcription factors, for example increased expression of Tbet and a loss of ROR γ t expression gives rise to a population of ILC3s with ILC1-like characteristics. Expression of interleukin receptor subunits, such as interleukin (IL)2–receptor- α (also known as CD25) and IL-7 receptor- α (also known as CD127) are critical for the further development and function of all ILC subsets (Artis & Spits, 2015). International nomenclature guidelines classify ILCs into three subsets,

ILC1s, ILC2s, and ILC3s, based on their secretory cytokine profiles and the presence of specific transcription factors (Spits *et al.*, 2013).

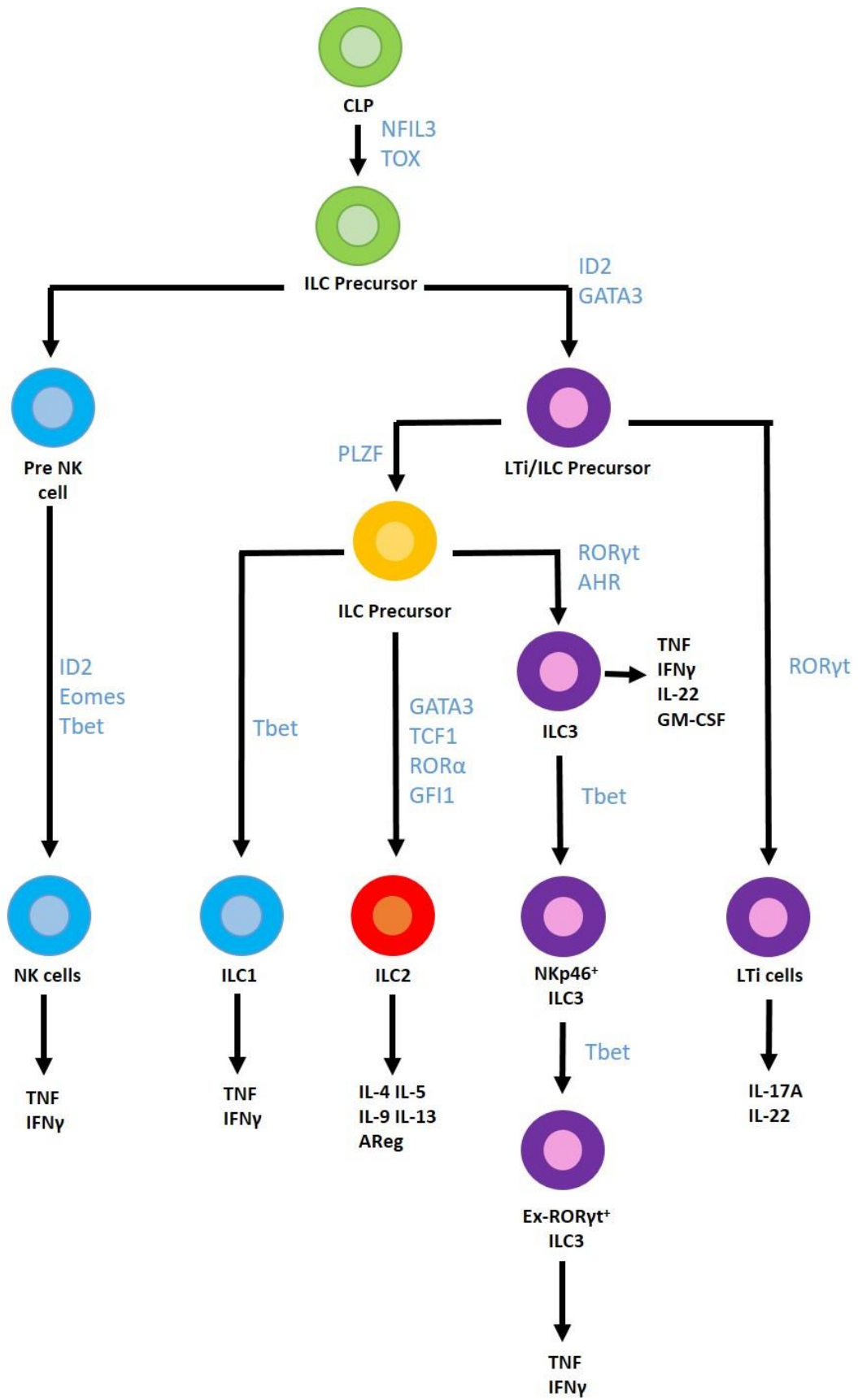


Figure 1.2: Summary schematic of ILC development pathways (image adapted from Artis & Spits, 2015). All ILC subsets arise from a CLP. ILC precursors and pre-NK cells express NFIL3 and TOX transcription factors, and can give rise to subsequent ILC precursors or developed NK cells, depending on the transcription factors expressed. Different populations of ILCs arise from differential expression of specific transcription factors such as GATA3, Tbet, and ROR γ t, and ILC3s can even develop into ILC1-like cells with increased expression of Tbet and loss of ROR γ t expression (inset box). Once fully developed NK cells and ILCs express different cytokine profiles, of which key ones are noted above, which can aid identification by flow cytometry.

CLP - Common Lymphoid Progenitor, ***ILC*** – Innate Lymphoid Cell, ***NK*** – Natural Killer (cell), ***LTi*** – lymphoid tissue inducer (cell), ***NFIL3*** - Nuclear factor, interleukin 3 regulated, ***TOX***- Thymocyte Selection Associated High Mobility Group Box, ***ROR γ t*** - RAR-related orphan receptor gamma, ***AHR***- aryl hydrocarbon receptor, ***ID2***- Inhibitor of DNA binding 2-, ***Eomes***- Eomesodermin, ***GATA3***- GATA-binding protein 3, ***TCF1***- Transcription factor 1, ***GFI1***- Zinc finger protein Gfi-1, ***TNF***- tumour necrosis factor, ***IFN γ*** - interferon gamma, ***GM-CSF***- granular macrophage-colony stimulating factor, ***AReg***- amphiregulin, ***PLZF*** - promyelocytic leukaemia zinc finger protein

1.2.1. Group 1 ILCs

Group 1 ILCs are defined by their ability to produce the classical type 1 cytokines interferon gamma (IFN γ) and tumour necrosis factor (TNF). They are unable to produce cytokines associated with T_H2 and T_H17 cells. Natural killer (NK) cells are considered the prototypical member of this subset and have a number of diverse functions from cytotoxic activity against tumours (Kiessling *et al.*, 1975) to regulation of dendritic cells in early stage inflammation (Moretta *et al.*, 2005). In addition, a second lineage has been described that fits the criteria of group 1 ILCs and these have been designated ILC1s. In humans they have been found to express high levels of the transcription factor Tbet and low levels of Retinoid-orphan receptor (ROR) γ t (Bernink *et al.*, 2013). However, this study provides evidence that under certain conditions expression levels of transcription factors can change, influencing the subtype of the cell. For example, non-NK ILC1 cells could develop from NKp44⁺ROR γ t⁺ cells, a defining feature of human ILC3s, when stimulated with IL-12. This resulted in the loss of ROR γ t upon differentiation. Conversely, in short term culture with IL-2 and IL-23 ILC1s were found to decrease expression of *tbx21* mRNA – the gene that encodes Tbet. These results suggest there is a certain level of plasticity between ILC1s and ILC3 in which Tbet and ROR γ t are implicated. Further work has confirmed the existence of ILC plasticity, in this case between ILC3s and ILC1-like cells (Klose *et al.*, 2013). This study described a population of CCR6⁻ ILC3s that were able to upregulate Tbet and express NKp46 in response to IL-12, and subsequently downregulate ROR γ t. This was accompanied by the population switching from a regulatory phenotype (IL-22 production) to a proinflammatory phenotype (IFN γ production) in response to *Salmonella* infection

(Klose *et al.*, 2013). This population has been described as both “Ex-ROR γ t ILC3s” and “ILC1-like cells” (Figure 1.2). There is still some debate as to whether ILC1s and ILC3s are indeed distinct subsets, or the same subset at different stages of differentiation (Walker *et al.*, 2013). A recent study has implicated ILC1s in promotion of obesity-induced insulin resistance, whereby ILC1-derived IFN γ drove macrophage polarization to the M1 pro-inflammatory phenotype, leading to insulin resistance (O’Sullivan *et al.*, 2016).

1.2.2. Group 2 ILCs

Group 2 ILCs, or ILC2s, produce classical T_H2 cytokines (such as IL-4, IL-5, IL-9, and IL-13) in response to stimulation with the epithelial cytokines IL-25, IL-33, or thymic stromal lymphopoietin (Halim *et al.*, 2012a). They require the transcription factor retinoic acid receptor-related orphan receptor- α (ROR α) and GATA-binding protein 3 (GATA3) for their development and function (Halim *et al.*, 2012b; Hoyler *et al.*, 2012). In 2010, three papers reported a novel innate cell type integral for helminth expulsion, which were designated “natural helper cells”, “nuocytes” and “innate helper 2 cells” respectively (Moro *et al.*, 2010; Neill *et al.*, 2010; Price *et al.*, 2010), and the 2013 nomenclature guidelines classified them as ILC2s (Spits *et al.*, 2013). ILC2 involvement in type 2 immunity is critical for the resolution of intestinal worm infections, and dysregulation of type 2 responses is responsible for atopic asthma (Robinson *et al.*, 1992). More recently, a role has been suggested for ILC2s in metabolic homeostasis and limiting obesity in mice (Brestoff *et al.*, 2015), which is explored in detail in section 1.5.

1.2.3. Group 3 ILCs

Group 3 ILCs produce IL-17A and/or IL-22, and depend on the transcription factor ROR γ t for their development and function, much like T_H17 cells. Lymphoid tissue-inducer (LTi cells), required for secondary lymphoid organ formation, are the classical example of a group 3 ILC. Two other key members of the group 3 ILCs have been designated natural cytotoxicity triggering receptor (NCR)⁺ILC3 and NCR⁻ILC3 (Spits *et al.*, 2013). All three of these ILC3 subsets play major roles in gut homeostasis, in many cases through their production of IL-22. NCR⁺ILC3s secrete IL-22 which helps to protect the gut epithelium during inflammation (Zenewicz *et al.*, 2008). They have also been found critical in the innate immune response mediated by IL-22 that controls infections by the extracellular bacterium *Citrobacter rodentium* (Sato-Takayama *et al.*, 2008) although recent evidence suggests that they may be dispensable in animals that have a competent T cell response (Rankin *et al.*, 2016). LTi cell-derived IL-22 has also been shown to play a critical role in innate defense in response to *C.rodentium*, with host mortality increasing in a murine model where LTI cells were absent (Sonnenberg *et al.*, 2011).NCR⁻ILC3s are also able to produce IL-22 but are not sufficient to protect against *C.rodentium* infection in T cell compromised mice – NCR⁺ILC3s are required too in this instance (Rankin *et al.*, 2016). NCR⁻ILC3s were also found to have a potential pathogenic role in some circumstances, as they mediated a murine model of colitis through dysregulation of IL-17A signaling (Buonocore *et al.*, 2010a). Group 3 ILCs are perhaps the most heterogeneous subset of ILCs and it is not clear if cells categorized as non-LTi ILC3s comprise *bona fide* separate populations or are just phenotypically

plastic (Figure 1.2). Little, if any, evidence exists for ILC3 activity in obesity and development of type 2 diabetes at this time.

1.3. Stromal cells of the mLN and adipose tissues

Stromal cells are traditionally considered to constitute the structural components of an organ, such as the vasculature. In many cases their roles are determined by their location, and the same cell type can have multiple functions dependent on the organ they reside in. Stromal cells are derived from mesenchymal stem cells, which give rise to a number of mesenchymal precursor cells (MPCs). In the context of lymph node development, MPCs give rise to CXCL13⁺ early lymphoid tissue organizer cells (LTos), in response to retinoic acid release from neurons (van de Pavert *et al.*, 2009). Adipose surrounding the developing lymph node can also be a source of stromal precursor cells. LTβR-dependent signaling recruits pre-adipocyte precursors into the developing lymph node, where they develop into CXCL13⁺ early LTos (Bénézech *et al.*, 2012). LTos mature with increased expression of VCAM1 and ICAM1, and also require LTβR signaling (Cupedo *et al.*, 2004). Mature LTos can differentiate into fibroblastic reticular cells (FRCs), residing in the T cell zone of the lymph node, and marginal reticular cells (MRCs), located close to the subcapsular sinus (Fletcher *et al.*, 2015). Specific populations of MRCs can also develop into follicular dendritic cells (FDCs) that are found in the B cell follicles (Jarjour *et al.*, 2014 & Fletcher *et al.*, 2015).

Numerous types of stromal cells are also present in adipose tissues. Analysis of preadipocyte factor 1⁺ (Pref-1⁺) adipocyte progenitor cells for the stromal markers Gp38 (a.k.a podoplanin) and CD31, led to the identification of four stromal populations: i) Gp38⁺CD31⁻ cells, designated as fibroblastic reticular cells that contain adipocyte

precursors. Gp38⁺ stromal cells are known to produce IL-7 (key for ILC development) and CXCL13 (key for FALC and mLN formation) (Barone *et al.*, 2013). ii) Gp38⁺CD31⁺ cells, designated as lymphatic endothelium. Lymphatic stromal cells are known to play roles in immune regulation, such as via expression of decoy chemokine receptor D6, which scavenges proinflammatory chemokines (Nibbs *et al.*, 2001). iii) Gp38⁻CD31⁺ cells, designated as blood endothelium. Blood endothelia are activated during stress and inflammation and are able to recruit and educate T lymphocytes through expression of markers such as ICOS, OX40, and CD2 (Shiao *et al.*, 2005). iv) Gp38⁻CD31⁻ cells, a large double negative stromal population (Bénézech *et al.*, 2012). These populations are investigated in more detail in this study, particularly in their ability to produce IL-33.

1.3.1. IL-33

IL-33 is a member of the IL-1 family of cytokines and is predominantly expressed by stromal cells such as endothelium, epithelium, and adipocytes (Schmitz *et al.*, 2005). IL-33 is stored in the nuclear compartment of the cell where it has a transcriptional regulatory role (Carriere *et al.*, 2007), and is only released in response to cellular insult or injury. It is therefore described as an “alarmin”. IL-33 exerts a number of responses upon its release, through interaction with its cognate receptor, ST2, but is quickly inactivated through cleavage by caspase-3 and caspase-7 to prevent prolonged activity (Lüthi *et al.*, 2009). ST2 receptors are expressed on numerous cell types, but particularly type 2 immune cells such as ILC2s, T_H2s and eosinophils, where receptor signaling induces the production of type-2 cytokines (Schmitz *et al.*, 2005). IL-33 is known to play a role in metabolic homeostasis mechanisms in adipose tissue, by maintaining ILC2 populations in these tissues, leading to the recruitment of “beige”

adipocytes that increase the caloric expenditure of white adipose tissue (detailed in section 1.5 and Figure 1.3) (Brestoff *et al.*, 2015). However, the cellular source(s) of this cytokine in adipose tissues are currently unknown, and this is one of the key areas under investigation in this study.

1.4. Metabolic homeostasis and obesity (i): Brown, white, and beige

Up until recently, adipose tissues were thought to exist in two forms: white adipose and brown adipose. These two colours reflect the differing functions of the tissues, particularly with regard to their metabolic activity. Adipocytes in white fat deposits are used for storage, and an excess of nutrients leads to accumulation of triglycerides in these stores. Brown adipose responds to cold-induced sympathetic nervous system activity, and adipocytes in these stores upregulate UCP1 (mitochondrial uncoupling protein 1) expression to stimulate non-shivering heat production (Kozak & Anunciado-Koza, 2008). The thermogenesis process dramatically increases energy expenditure. Metabolically active brown adipose stores are prevalent in newborns but their activity has been found to decrease significantly with age and accumulation of white adipose stores (Yoneshiro *et al.*, 2011). However, a third type of adipose tissue, which also contributes to thermogenesis, has recently come under the spotlight. These are beige, or brown-like, adipocytes and they have been located in white adipose deposits and were found to become more numerous upon cold-stimulation (Loncar *et al.*, 1986; Loncar *et al.*, 1988). Further evidence suggests that white adipocytes undergo a “beiging” process under certain conditions to become beige adipocytes, increasing energy expenditure through thermogenesis (Qiu *et al.*, 2014). However, during obesity both brown and beige thermogenic activity decreases, correlating with the rise in

chronic, low-grade inflammation that is characteristic of the condition. Evidence suggests that this may be linked with a decrease in type 2 immunity within adipose tissue during the obese state, such as increases in proinflammatory cytokines, and macrophage polarization away from the protective M2 phenotype and towards the proinflammatory M1 phenotype. Components of type 2 immunity have been shown clearly to be protective in obesity. M2 macrophages are one such example. A study showed that deletion of PPAR γ in mice, known to be critical for polarization of macrophages to their M2 phenotype, led to diminished M2 macrophage activity, resulting in increased likelihood to develop diet-induced obesity, as well as insulin resistance and glucose intolerance (Odegaard *et al.*, 2007). In addition, the classical type 2 cytokine IL-4 (produced by ILC2s and T_H2 cells), was found to be important in nutrient metabolism homeostasis and insulin sensitivity. Treatment of high fat diet-fed WT mice with IL-4 reduced weight gain and adiposity, and improved glucose homeostasis and insulin sensitivity in these animals (Ricardo-Gonzalez *et al.*, 2010). Taken together, these studies suggest type 2 immunity plays a key role in limiting obesity and metabolic dysfunction and that decreases in type 2 activity in adipose tissues are clearly problematic and lead to metabolic disease.

1.5. Metabolic homeostasis and obesity (ii): a role for ILC2s

ILC2s are thought to be highly influential in adipose type 2 immunity for several reasons. ILC2s have been detected in adipose tissues (Molofsky *et al.*, 2013), and within atypical secondary lymphoid structures in the mesenteric fat known as fat-associated lymphoid clusters (FALC) (Moro *et al.*, 2010). They have been found to contribute a higher proportion of type 2 cytokines than T helper 2 (T_H2) cells in response

to exogenous IL-25 and IL-33 (Hams *et al.*, 2013; Molofsky *et al.*, 2013). ILC2s are also known to promote eosinophil accumulation through their secretion of IL-5, and polarize macrophages to the regulatory M2 phenotype, also known as alternatively activated macrophages (AAMs), through secretion of IL-13 (Molofsky *et al.*, 2013). AAMs can also be stimulated by eosinophil derived IL-4, inducing noradrenaline production (Qiu *et al.*, 2014), which has been discovered to be influential in the “beiging” of white adipocytes to beige. Given the protective roles of type 2 immunity against obesity, and the clear influence ILC2s exert within adipose tissues it is particularly striking that in obese individuals, both mice and humans, ILC2 numbers are depleted when compared to non-obese controls (Brestoff *et al.*, 2015). This apparent correlation of decreased ILC2 numbers and decreased adipose thermogenic activity with the rise of the obese state suggests the existence of a pathway that could lend itself to pharmacological or physiological manipulation. These ideas have been explored in detail in two key recent papers.

The laboratories of David Artis, Ajay Chawla and Richard Locksley have investigated the role of IL-33 and ILC2s in the beiging of white adipose. Previous work had already identified roles for eosinophils, AAMs, IL4/13 and cold stimulus in the beiging process (Qiu *et al.*, 2014). ILC2s are well known producers of type 2 cytokines that interact directly with eosinophils (via IL-5) and indirectly with AAMs (via eosinophil-derived IL-4), but it was unknown whether ILC2s had any direct effect on the beiging process. IL-33 activates and expands ILC2 populations via engagement of the ST2 receptor, and induces production of type 2 cytokines. Both of the two key papers (Lee *et al.*, 2015 & Brestoff *et al.*, 2015) involved administering recombinant IL-33 and both concluded that

IL-33-activated ILC2s were sufficient to promote functional beige fat, but each study focused on a different mechanism. Lee and colleagues (Lee et al., 2015) discovered that activated ILC2s could promote the proliferation of PDGFR α ⁺ adipocyte precursors through an IL-4 dependent mechanism, and that IL-4 interaction with adipocyte precursors lead to an upregulation of several genes associated with beige adipocytes, included UCP1. A recent study has demonstrated a requirement for IL-33 for appropriate UCP1 splicing, without which thermogenesis in brown and beige adipocytes cannot occur in perinatal mice (Odegaard *et al.*, 2016). This process of IL-33/ILC2 mediated beiging is linked to that of the “IL-4–AAMs–Noradrenaline” beiging mechanism (Figure 1.3). Using a different approach, Brestoff and colleagues (Brestoff *et al.*, 2015) compared obesity-associated genes expressed in ILC2s, to those found in ILC3s and discovered ILC2s were significantly enriched for the proprotein convertase Subtilisin/kexin type 1 (*Pcsk1*) gene. This enzyme converts prohormones into their active forms and its action in ILC2s leads to the production of significant levels of an endogenous opioid-like molecule, methionine-enkephalin (MetEnk). Exogenous recombinant IL-33 delivery lead to increased production of MetEnk by ILC2s, and administration of MetEnk to mice lead to accumulation of UCP1⁺ beige adipocytes in white adipose deposits. In both studies, exogenous IL-33 application lead to increased caloric expenditure, as well as decreased weight gain in the Brestoff high fat diet study. Taken together these studies show that IL-33-activated ILC2s directly affect adipocyte beiging by at least two separate mechanisms, in addition to their indirect effects on the eosinophil-AAM-Noradrenaline beiging axis (summarized in Figure 1.3), and that these mechanisms contribute to metabolic homeostasis.

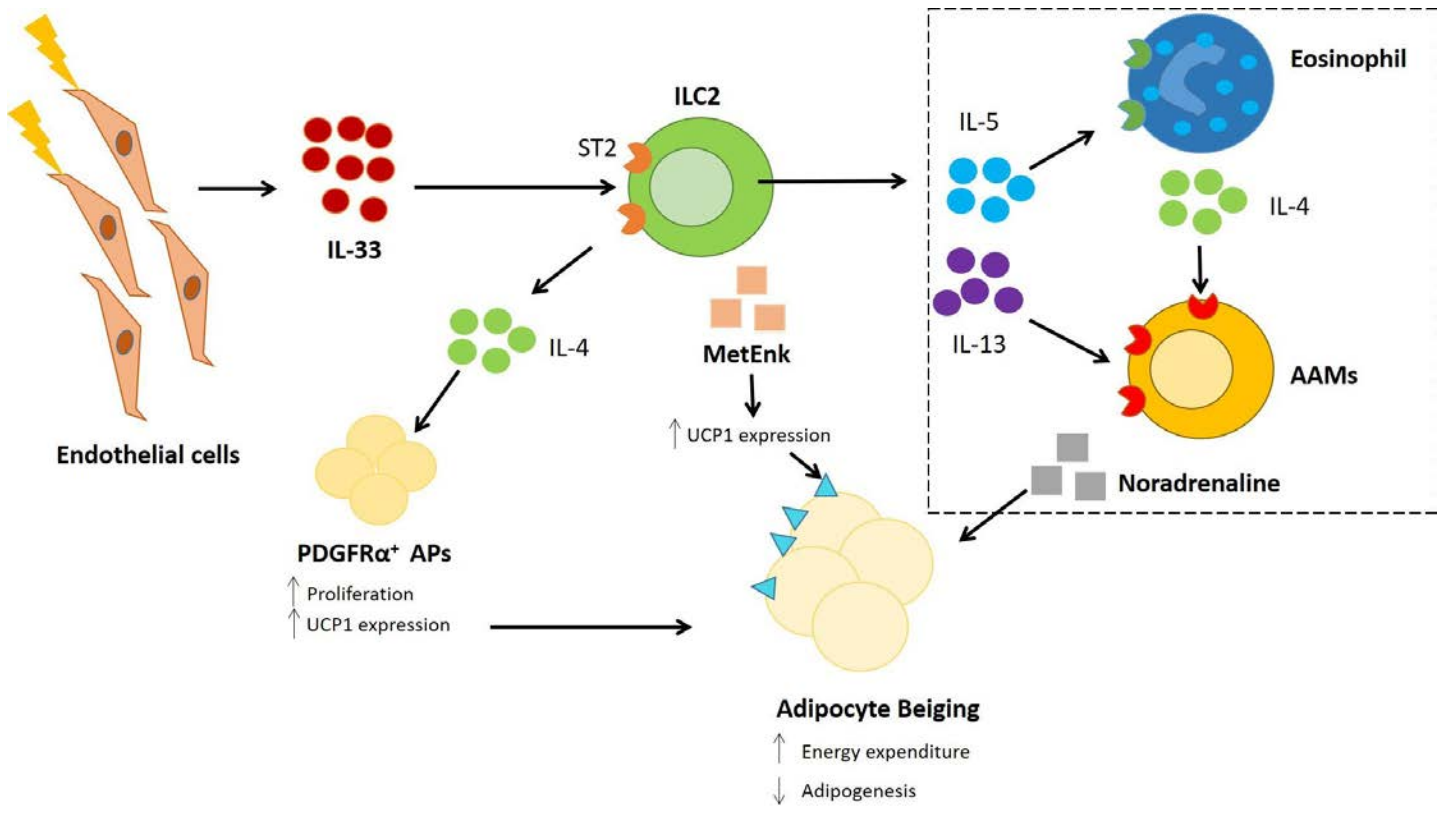


Figure 1.3: Summary schematic of the IL-33-ILC2 adipocyte beiging pathways (adapted from Brestoff et al., 2015 and Uhm et al., 2015). IL-33 is released from stromal cells such as endothelial and epithelial cells in response to insult or injury. IL-33 is the ligand for ST2 (also known as interleukin 1 receptor-like 1) which is highly expressed on immune cells such as ILC2s and T_H2 cells. ILC2s can produce a wide repertoire of type 2 cytokines such as IL-4, IL-5 and IL-13 and these feed into three pathways leading to adipocyte beiging. The first pathway involves indirect action of ILC2s on adipocyte through production of IL-5, acting on eosinophils, and IL-13 acting on macrophages. Eosinophils produce IL-4 that polarizes macrophages to their regulatory M2 phenotype, which are also known as AAMs. AAMs induce production of catecholamines such as noradrenaline which act on adipocytes to increase UCP1 expression, leading to adipocyte beiging. Cold stimulus can also induce catecholamine production through stimulation of the sympathetic nervous system. The second pathway arises from ILC2 production of opioid-like compound MetEnk, which acts on adipocytes to increase the expression of UCP1, leading to adipocyte beiging. The final pathway arises from ILC2 production of IL-4, which acts on populations of PDGFR α ⁺ adipocyte precursors, leading to their expansion. IL-4 also induces upregulation of several genes including UCP1, committing the adipocyte precursors to the beige lineage. All three pathways lead to an increase in beige adipocytes, and hence an increase in energy expenditure and a decrease in adipogenesis.

***ILC2** – Group 2 innate lymphoid cells, **AAMs** – alternatively activated macrophages, **PDGFR α** – platelet derived growth factor alpha, **APs**- adipocyte precursors, **MetEnk** – methionine-enkephalin, **UCP1** – uncoupling protein 1, **ST2** – IL-33 receptor.*

1.6. Atypical secondary lymphoid structures: FALCs

Further investigation of the novel IL-33-ILC2 being axis is of particular interest in the context of FALCs. These small atypical secondary lymphoid structures were only recently identified (Moro *et al.*, 2010) and there is much that is unknown about these structures. The brief description of FALCs contained within the Moro study details FALCs as small clusters of lymphocytes in close proximity to the blood vessels of murine mesenteric fat. Clusters were not surrounded by a fibrous capsule, as is the case with lymph nodes, and lymphocytes were in constant contact with adipocytes. A population of Lin⁻c-Kit⁺Sca-1⁺ cells (c-kit a.k.a Mast/stem cell growth factor receptor) (Sca-1: stem cell antigen 1), which are now known to be ILC2s, were identified within the FALCs, and the focus of the study then moved to further characterization of these cells.

Most subsequent characterization completed so far has been conducted by the Caamano lab, along with this study. In their 2015 paper Bénézech and colleagues presented some basic cellular components of FALCs and elucidated some of their developmental requirements (Bénézech *et al.*, 2015). FALCs were identified in all adipose tissues investigated, which included subcutaneous deposits along with visceral deposits in the peritoneal and pleural cavities. The omentum is well known for having structures known as milky spots, which bear striking resemblance to the FALCs identified in other adipose deposits. There is no consensus yet on whether the milky spots of the omentum should be considered as FALCs in the same way as the clusters identified in other adipose deposits, as there are differences in the number, distribution,

and morphology of clusters in the omentum, compared with other locations (Bénézech *et al.*, 2015). Nevertheless, as the development of both structures is strikingly similar (Rangel-Moreno *et al.*, 2009; Bénézech *et al.*, 2015), all clusters in this study are referred to as FALCs for simplicity of notation. The 2015 Bénézech study demonstrated that IgM⁺ B cells comprised the majority of the cells in FALC, along with small numbers of CD4⁺ T cells and CD11b⁺ myeloid cells. CXCL13⁺ stromal cells were also found within the FALC and CXCL13 is a key chemoattractant for B cells. FALCs develop independently of the usual processes required for secondary lymphoid organs, with no requirement for LTi cells of the group 3 ILCs or lymphotoxin β receptor (LT β R) engagement. Instead postnatal FALC development was found to be partially dependent on macrophage TNF production, TNF signaling in stromal cells, and the commensal flora of the gut. Expansion of FALC numbers were observed in inflammation models, and it was found that invariant natural killer T cells (iNKT) and their production of IL-4 interacting with IL-4R α was required for FALC development in response to inflammation (Bénézech *et al.*, 2015).

The studies reviewed here show there is a clear axis implicated in obesity and metabolic disorder that involves IL-33 and ILC2s. It is unknown whether the FALCs are involved at any point in the beiging axis. To complicate matters, the vast majority of studies cited here focus on one visceral adipose tissue deposit, usually the gonadal deposit but occasionally the mesenteric fat, or refer simply to “white adipose tissue”. There are several elementary questions still to answer, particularly in regards to the ILC profile and cellular source(s) of IL-33 in each abdominal adipose tissue.

1.7. Project Aims

This study was designed with three key aims in mind. The first aim of this study was to characterize the FALCs, immune cells, and stromal cells of gonadal, mesenteric, and omental fat, in order to provide a profile of evidence on which to base tissue selection for *in vivo* and *ex vivo* obesity studies. Mesenteric fat has been postulated to be a more representative model of human visceral fat deposits than gonadal fat and so one objective was to compare characteristics of both deposits to deduce whether they have distinct ILC and stromal cell profiles. The immunological properties of the omentum are also poorly understood in an obesity context, and so this study has also compared the characteristics of the omentum with the current model of choice, gonadal fat, as well as the proposed replacement model tissue, mesenteric fat. In order to achieve this primary aim the following experimental targets were met:

- Investigate FALC numbers in each tissue
- Compile data to draw up an ILC profile for each tissue
- Identify phenotype of the major cellular source(s) of IL-33 in each tissue

The second key aim of the study was to propose a candidate tissue for further studies to interrogate the role of FALC in the beiging process. Based on studies cited above it is hypothesized that the best candidate tissue to address this question should have a high prevalence of FALCs, ILC2s and IL-33-producing cells. The tissue characterization performed in this study should indicate whether any of the examined adipose deposits fit these criteria. In order to facilitate these future studies into FALC and the beiging process, a method of interrogating the localization of immune cells within the FALCs is

required. Therefore, the third key aim of this study was the development of a FALC imaging protocol.

2. Materials and Methods

2.1. Mice

WT C57Bl/6, WT Balb/c, Rosa26-EYFP, and IL-33 reporter mice (Dr Andrew McKenzie, University of Cambridge) were bred and maintained under specific pathogen-free conditions in [REDACTED] (Table 1). All experiments were performed in accordance with Home Office and local ethics committee regulations.

Strain	Host Isotype	Phenotype
C57Bl/6	CD45.2	Wild Type
BALB/C	CD45.2	Wild Type
ROSA26-EYFP (C57Bl/6)	CD45.2	All cells express EYFP (Em:527nm) and appear yellow/green.
IL-33 ^{cit/+} (Balb/c)	CD45.2	IL-33 ⁺ cells produce functional IL-33 and citrine (Em:529nm), appearing green.
IL-33 ^{cit/cit} (Balb/c)	CD45.2	IL-33 ⁺ cells produce citrine only, appearing green. IL-33 is not produced.

Table 2.1: Details of mouse strains used in this study

2.2 Isolation of cells from the mesenteric lymph node

Mice were culled by Schedule 1 cervical dislocation and mesenteric lymph nodes were removed immediately *post mortem*. *Ex vivo* tissues were stored in fresh Roswell Park Memorial Institute (RPMI) medium (Life Technologies) with 2% fetal calf serum (FCS) (Life Technologies) on ice until processing. During lymphocyte extraction excess fat was removed from mLNs, which were then manually chopped and enzymatically digested for 20 minutes in 100mg/ml Collagenase Dispase (Roche), 10mg/ml DNase I (Roche) and 100mg/ml Collagenase P (Roche) in RPMI medium with 2% FCS at 37°C. In the case of stromal cell extraction from mLN, tissues were cleaned of excess fat and the digestion was performed essentially as described (Fletcher *et al.*, 2011). In brief, the capsules of mLN were manually pierced and digested initially for 20 minutes in 2ml of digestion mix comprised of 0.8mg/ml Collagenase Dispase (Roche), 0.2mg/ml DNase I (Roche) and 0.2mg/ml Collagenase P (Roche) in fresh RPMI medium at 37°C with constant shaking (120rpm). The digestion media was siphoned off for centrifugation and replaced with a further 2ml of digestion mix for an additional 10 minutes at 37°C with constant shaking. This cycle was repeated until the tissues had undergone a total of 50 minutes of digestion. The pellet derived from supernatant centrifugation was resuspended in a suitable volume for the number of stains required, and approximately 25% of the cells were plated per well.

2.3 Isolation of cells from adipose deposits

Mice were culled by Schedule 1 cervical dislocation and gonadal fat, mesenteric fat and omental fat were removed immediately *post mortem*. *Ex vivo* tissues were stored in

fresh RPMI medium with 2% FCS on ice until processing. The method of enzymatically digesting adipose remained the same for both lymphocyte and stromal cell extraction. Tissues were checked for contaminating elements (e.g pancreatic fat or remnants of intestine on the mesenteric fat) and manually chopped until a lumpy paste formed. Tissues were digested for a total of 30 minutes in 5ml of digestion mix comprised of 100mg/ml Collagenase Dispase, 10mg/ml DNase I and 100mg/ml Collagenase P in fresh RPMI with 2% FCS at 37°C with constant shaking (120rpm), and inversion of the tubes every 10 minutes.

Digested samples were filtered through 20-75µm nylon mesh (John Stanier and Co.) into 5ml of fresh RPMI with 2% FCS and centrifuged at 1700rpm for 10 minutes. The supernatant was removed and samples were resuspended in fresh RPMI with 2% FCS. Gonadal and mesenteric fat were resuspended in an appropriate volume and 50% of the cells were plated per well required. Omental fat was resuspended in an appropriate volume and 100% of the cells were plated per well, except in experiments where stromal cells were examined for markers Sca-1 and PDGFR-α where 50% of the cells were plated per well.

2.4. Flow Cytometry

Once isolated and plated, cells were incubated with LIVE/DEAD® Fixable Near-IR viability stain (Invitrogen) diluted in PBS (Phosphate buffered saline) for 30 minutes on ice. Cells were washed with staining buffer (PBS with 2mM EDTA (Sigma Aldrich) and 2% FCS) then stained for surface markers with 50µl of antibody master mix, diluted in staining buffer for 30 minutes on ice. All incubations took place in the dark. If intracellular staining was required, cells were first fixed with 100µl/sample of FoxP3

fixation/permeabilization buffer kit (1:4 fixative: diluent) (Ebioscience) for 30 minutes on ice, and permeabilized through subsequent 100µl washes with 1x FoxP3 permeabilization buffer (10x concentrate). A master mix of intracellular antibodies was diluted in permeabilization buffer and samples were stained with 50µl of intracellular staining mix for 30 minutes at room temperature. Samples were washed again with permeabilization buffer and resuspended in an appropriate final volume of staining buffer, filtered, and transferred into flow cytometry tubes. 5ul counting beads (1 million/ml) (Spherotech) were added to the appropriate tubes. Flow cytometry was performed on an LSRFortessa X20 (BD Bioscience) and data were analyzed with FlowJo software (TreeStar). Antibodies used for flow cytometry are listed in table 2.

Antibody Specificity	Conjugate (Dilution)	Clone	Concentration (mg/ml)	Manufacturer
B220	FITC (1:300)	RA3-6B2	0.5	BD Pharmingen
	PE-Cy7 (1:500)	RA3-6B2	0.2	Biolegend
CD3	FITC (1:100)	145-2C11	0.5	BD Pharmingen
	PE-Cy7 (1:200)	145-2C11	0.2	eBioscience
CD3(internal)	AlexaFluor700 (1:100)	500A2	0.2	eBioscience
CD5	FITC (1:100)	53-7.3	0.5	BD Pharmingen
	PE-Cy7 (1:200)	53-7.3	0.2	eBioscience
CD11b	FITC (1:300)	M1/70	0.5	Biolegend
	PE-Cy7 (1:500)	M1/70	0.2	eBioscience
CD11c	FITC (1:300)	N418	0.5	Biolegend
	PE-Cy7 (1:500)	N418	0.2	eBioscience
CD25	BV650 (1:200)	PC61	0.2	Biolegend
CD31	eFluor450 (1:200)	390	0.2	eBioscience
CD45.2	BV510 (1:100)	104	0.1	Biolegend
	BV786 (1:200)	104	0.2	BD Horizon
GATA3	PerCP-eFluor710 (1:50)	TWAJ	0.06µg	eBioscience
Gp38	PE (1:800)	Ebio8.1.1	0.2	eBioscience
IgG2ak isotype	APC (1:200)	eBR2a	0.2	eBioscience
IL-7Rα	BV421 (1:100)	A7R34	0.05	Biolegend
Live/Dead	APC-Cy7 (1:1000)	-	-	Invitrogen
NKp46	PE-Cy7 (1:100)	29A1.4	0.2	eBioscience
PDGFRα	APC (1:200)	APA5	0.2	Biolegend
RORyt	PE (1:50)	Q31-378	0.2	BD Pharmingen
Sca-1	APC (1:200)	D7	0.2	Biolegend
ST2 (IL-33R)	PE (1:50)	DIH9	0.2	Biolegend
Tbet	eFluor660 (1:50)	4B10	0.2	eBioscience
Ter119	PerCP-Cy5.5 (1:1000)	Ter-119	0.2	eBioscience

Table 2.2: Fluorescently conjugated cell labelling reagents and antibodies used for flow cytometry

2.5. Whole-Mount Immunofluorescence

Adipose tissues were fixed in 2% paraformaldehyde (PFA) for 30 minutes on ice whilst on a gyratory rocker (Stuart). After PBS washing for 5 minutes, samples were permeabilized with 1x Triton (Sigma Aldrich) at room temperature. Samples were blocked with 10% horse serum in staining solution for 30 minutes at room temperature. Further blocking was conducted using an Avidin/Biotin blocking kit (Vector Labs) for 15 minutes at room temperature, with a 5 minute PBS wash in between steps. Primary antibodies made up in staining solution (2% BSA in PBS) were applied to the sample and incubated overnight at 4°C. Secondary and tertiary antibody stains, if required, were applied for 1hr each on ice, with 5 minute PBS washes in between. Tissues were incubated with Dapi (4',6-diamidino-2-phenylindole) (1:300) for 20 minutes, washed in PBS and mounted immediately on slides with VectorShield mounting medium (Vector Labs). Antibodies used for immunofluorescence are listed in table 3. Images were collected on a Zeiss 780 Zen confocal microscope.

Primary Antibodies used for Immunofluorescence					
Host	Antibody specificity	Conjugate (dilution)	Clone	Concentration (mg/ml)	Manufacturer
Rat	B220	Biotin (1:200)	RA3-6B2	0.5	eBioscience
Armenian Hamster	CD3ε	FITC (1:50)	145-2C11	0.5	BD Pharmingen
Rat	CD4	AlexaFluor647(1:100)	GK1.5	0.5	Biolegend
Rat	CD31	Biotin (1:100)	390	0.5	eBioscience
Mouse	CD45.2	FITC (1:200)	104	0.5	eBioscience
Goat	IL-33	Unconjugated (1:200)	Poly	0.2	R&D systems
Rat	Lyve-1	eFluor660(1:50)	ALY7	0.2	eBioscience
-	Nuclear	DAPI (1:300)	-	5	Life Technologies
Secondary Antibodies used for Immunofluorescence					
Donkey	Anti-Goat IgM (H+L)	AlexaFluor647(1:200)	-	2	Life Technologies
-	Streptavidin	AlexaFluor555 (1:200)	-	1	Life Technologies

Table 2.3: Fluorescently conjugated cell labelling reagents and antibodies used for whole-mount immunofluorescence

2.6. FALC counts

Adipose tissues were prepared as described for whole-mount immunofluorescence and stained with CD45-FITC antibody for 2hrs on ice. Blocking steps are not strictly necessary for tissues used for FALC counts only but many tissues were counted and subsequently imaged by confocal microscopy, and were therefore blocked and stained for whole-mount immunofluorescence concurrently with CD45-FITC. Samples were counted under a stereo fluorescence microscope (Olympus SZX12) and images were taken with a linked digital camera (Olympus C50-60).

2.7. FALC removal experiments

Mesenteric fat deposits from ROSA26-EYFP mice were examined under a stereo fluorescence microscope and visible lymphoid clusters were removed with forceps. Tissues were then washed in PBS before digestion for flow cytometry.

2.8. Zymosan Immunization

Zymosan A powder from *Saccharomyces cerevisiae* (Sigma Aldrich) was resuspended in sterile PBS at 5mg/ml and 200 μ l was injected i.p into IL-33 het and K.O mice. Control mice were injected i.p with 200 μ l sterile PBS. After 72 hours mice were culled by schedule 1 cervical dislocation and their tissues harvested.

2.9. Statistical analysis

Flow cytometry data was processed using Flow Jo software. Raw flow cytometry data was processed using Microsoft Excel. Graphs were produced using GraphPad Prism 6, and statistical analysis was calculated using this software. Non parametric statistical

analyses such as an unpaired Mann-Whitney or Kruskal-Wallis were conducted in the first instance and the test used is clearly stated in each case. Where appropriate, a Dunn's *post hoc* test was used following a significant finding from a Kruskal-Wallis analysis. * = $p < 0.05$, ** = $p < 0.01$, *** = $p < 0.001$. Where no p value is stated, no statistical significance is observed.

3. Results

3.1. FALCs can be identified and enumerated in abdominal adipose deposits

FALCs are defined as clusters of lymphocytes and other cells within adipose tissues measuring approximately 100-500µm in diameter (Moro *et al.*, 2010). Differences in the number of FALCs across adipose deposits may be indicative of functional differences between those tissues, and numbers have been previously reported to increase during inflammation (Bénézech *et al.*, 2015). Therefore, a baseline number of FALCs in homeostatic conditions was required as a starting point for this study. FALCs are similar in size and morphology across gonadal, mesenteric and omental fat and can be easily identified and counted by immunofluorescence staining with a FITC conjugated anti-CD45 antibody and a stereo-fluorescence dissecting microscope (Figure 3.1A). No scale bar has been included in these images as they were taken with a digital camera attached to the stereo-fluorescence microscope, and are for illustrative purposes. In future work a reference object such as a coin or small ruler should be included where practicable, although this may not always be technically feasible due to the changes of focus used in capturing the images. All well-defined clusters such as those seen in Figure 3.1A were considered to be FALCs and included in the tally. First, the overall number of FALCs per tissue was assessed. Gonadal fat was found to contain a median number of 2 FALCs per tissue, all detected within the thinner surface tissue at the edge of the fat deposit. There was substantial autofluorescence in gonadal fat samples but this was not considered to affect FALC counting as the samples could be manually manipulated under the dissecting microscope to assess presence of FALC deep in the tissues by eye – none were detected. Mesenteric fat was found to contain a

median of 14 FALCs per tissue, and omental fat contained a median of 60 FALC per tissue, significantly more than those seen in gonadal fat despite the much smaller tissue mass of the omentum (Figure 3.1B). Both these tissues are substantially thinner than gonadal fat, and it is easy to distinguish FALCs from small patches of autofluorescence by eye. To control for tissues of different weights, FALC counts were normalized to the weight of the tissue and the number of FALCs per 100mg was calculated for each deposit (Figure 3.1B). Normalized FALC numbers produced similar results to those seen with overall counts. Median normalized counts were as follows: gonadal fat had 0.5 clusters per 100mg, mesenteric fat had 17 clusters per 100mg, and omental fat had 580 clusters per 100mg. Once again omental fat contained significantly more FALCs than gonadal fat, despite the average gonadal fat tissue mass (250mg) vastly outweighing an average omentum (10mg).

Finally, FALC numbers were compared between male and female animals to investigate whether FALC numbers are different between the sexes. Overall FALC counts show that no significant difference exists between male and female animals in gonadal, mesenteric or omental fat (Figure 3.1C). A broader spread of data is observed in omental fat, and while not significant, more animals could be counted to give more confidence to that conclusion. In both the tissue counts and counts normalized to weight there is a trend in the number of FALCs per tissue in the following order: gonadal<mesenteric<omental. This is supported broadly by the observation of significant differences in omental vs gonadal comparisons and mesenteric vs gonadal comparisons when looking at the tissue as a whole, despite differences being more

modest when counts are normalized to weight (significance of omental vs gonadal comparisons only).

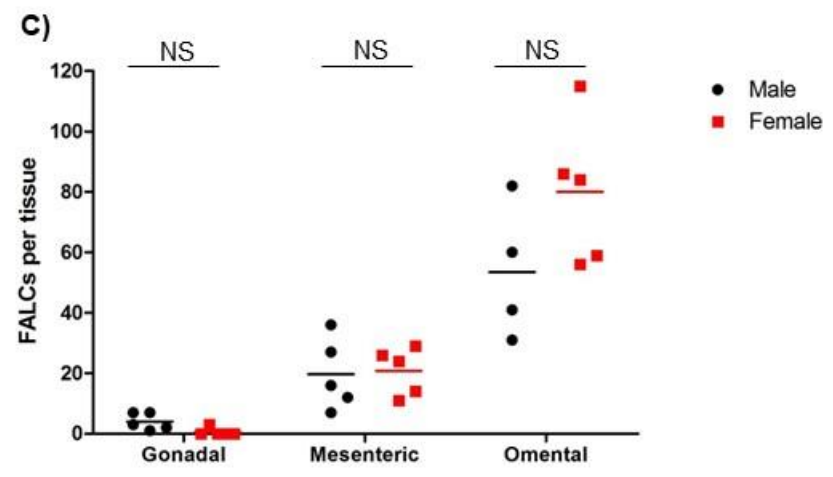
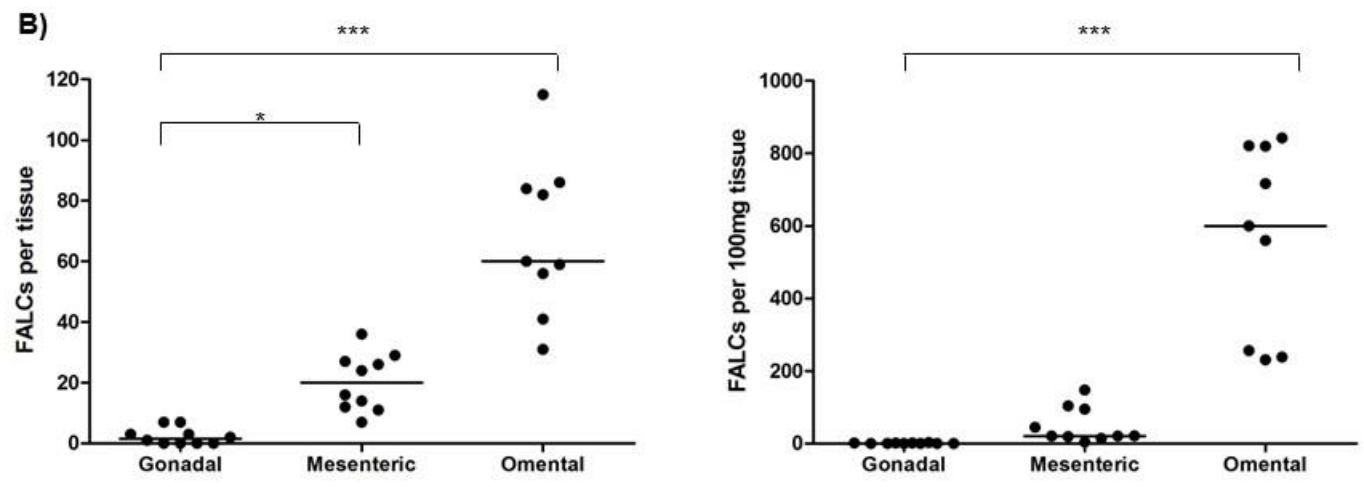
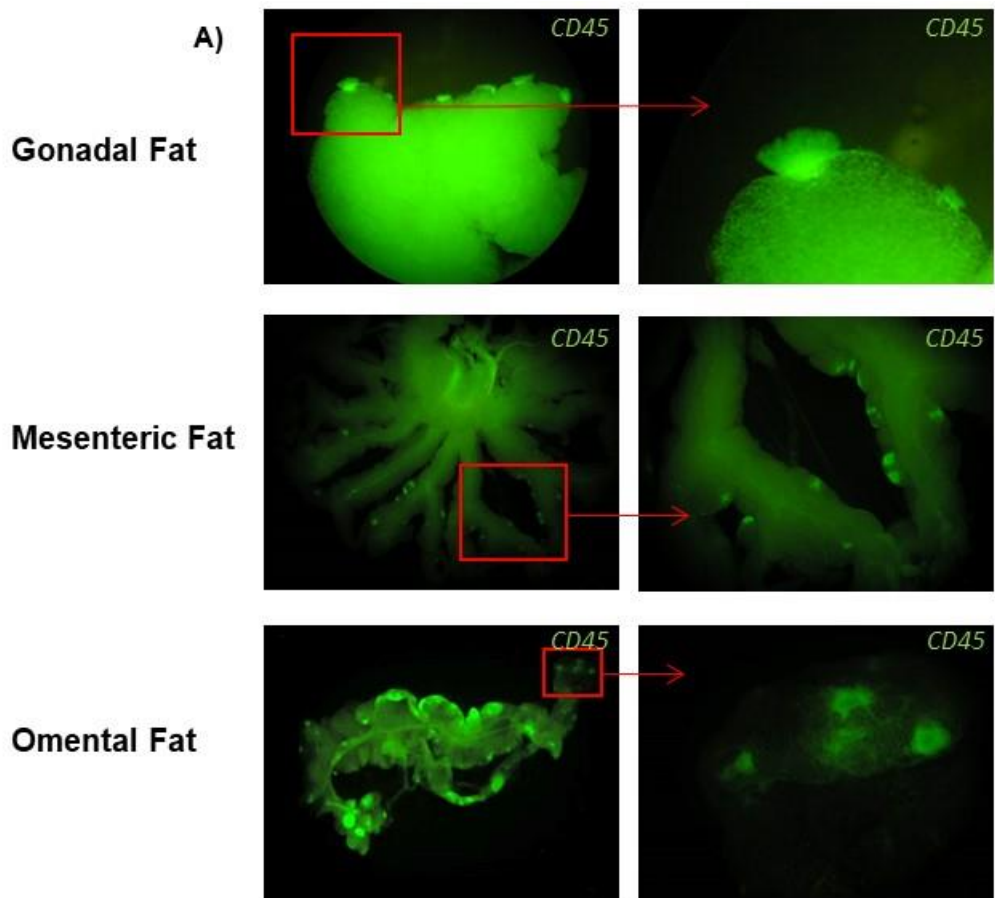


Figure 3. 1: Visualising and enumerating FALC in abdominal adipose deposits

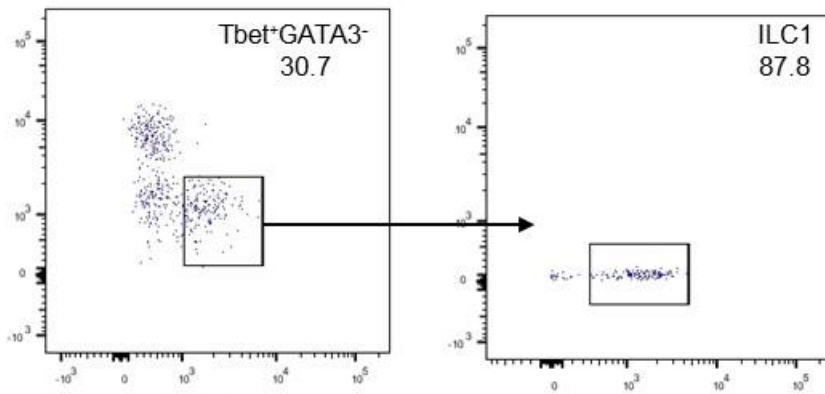
Staining with FITC labelled anti-CD45 in samples of gonadal fat, mesenteric fat, and omental fat (A), with FALC visible as bright spots. Scale bar omitted intentionally. (B) Quantitation of FALC counts displayed as total tissue numbers and normalised to weight. (C) Comparison of total tissue FALC numbers by sex. Statistical significance was assessed by a Kruskal-Wallis test followed by a Dunn's *post hoc* test if appropriate (D) or by unpaired Mann-Whitney test (E). * $p < 0.05$, ** $p < 0.01$, *** $P < 0.001$. Horizontal lines represent the median. Group size $n = 8-9$ C57Bl/6 pooled data from at least three independent experiments. Equal numbers of males and females were used and animals were age-matched (13 weeks).

3.2. Identification of ILC1s, ILC2s and ILC3s in mLN and abdominal adipose deposits

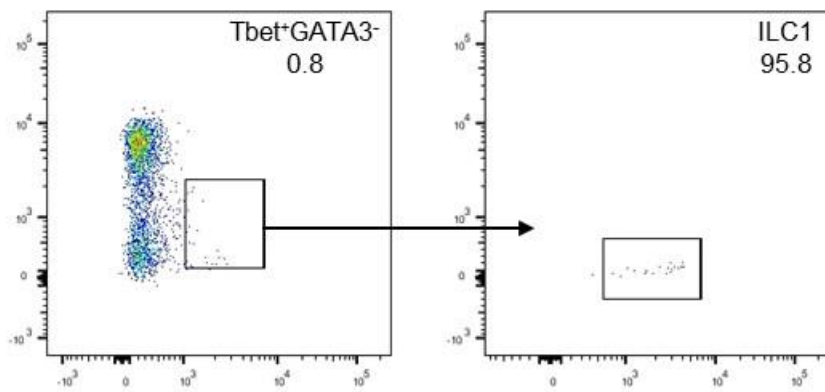
ILCs are lymphocytes of the innate immune system and are defined as being negative for lineage (Lin⁻) markers present on other lymphocytes, such as T or B cells, or myeloid cells, such as macrophages and dendritic cells. They are unable to react in an antigen-specific manner due to their lack of RAG-dependent antigen receptors (Spits *et al.*, 2013). ILCs have also been characterized as CD45⁺ (lymphoid cells) and IL-7R α ⁺ (critical for ILC development) (Artis & Spits, 2015). Staining for intracellular CD3 (CD3i) is also included in the general ILC staining panel as some immature T cells contain CD3i where it is not yet expressed on the cell surface. The full gating strategies for ILC1s, ILC2s, and ILC3s, are provided in the supplementary results (S1-S2). ILC1s can be identified from Live CD45⁺Lin⁻IL-7R α ⁺CD3i⁻ ILCs by staining for the transcription factors GATA-3 and Tbet (Figure 3.2). ILC1s are GATA-3⁻Tbet⁺ and a discrete population fitting this profile is evident in both the mLN and the adipose deposits. Two additional markers are used to give further confidence in the identified ILC1 population: ST2 (IL-33R) and NKp46. ILC1s are ST2⁻NKp46⁺; this step eliminated any stray ILC2s (ST2⁺) that may have been mistakenly included in the original GATA-3⁻Tbet⁺ gate.

ILC2s and ILC3s can also be identified from Live CD45⁺Lin⁻IL-7R α ⁺CD3i⁻ ILCs by transcription factor staining, in this case using GATA-3 and ROR γ t (Figure 3.3). In these plots, there are distinct GATA-3⁺ (ILC2s) and GATA-3⁻ (mostly ILC1s) populations, but the boundary between ROR γ t⁺ and ROR γ t⁻ is less obvious. In this case the ROR γ t⁺ (ILC3) gate was based on the location of the GATA-3⁺ and GATA-3⁻ populations, as both ILC1s and ILC2s are ROR γ t⁻.

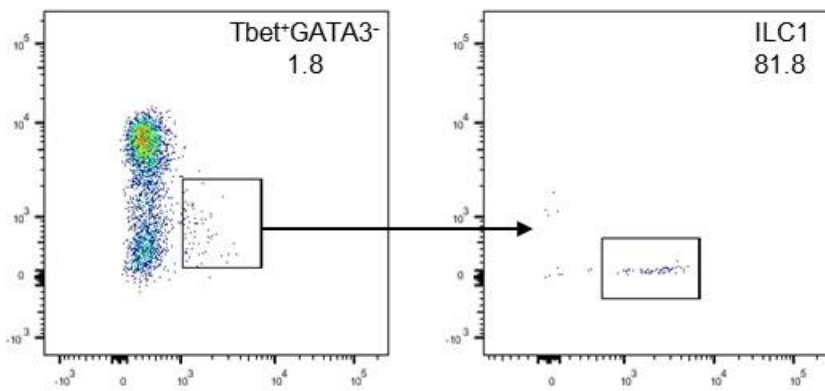
Mesenteric Lymph Node



Gonadal Fat



Mesenteric Fat



Omental Fat

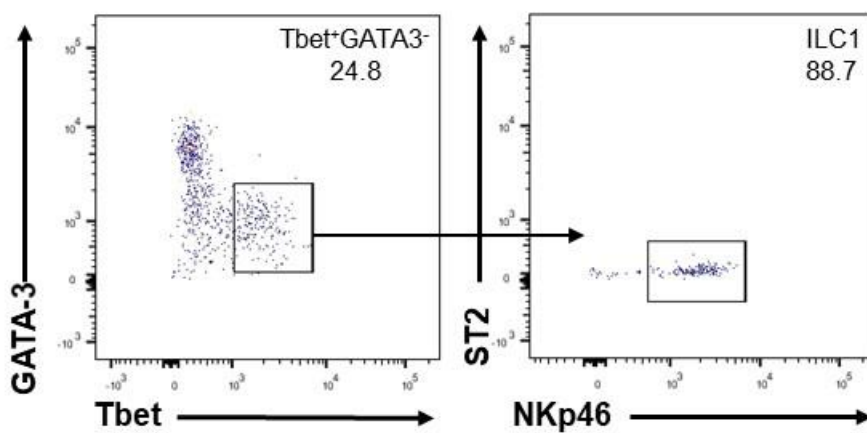
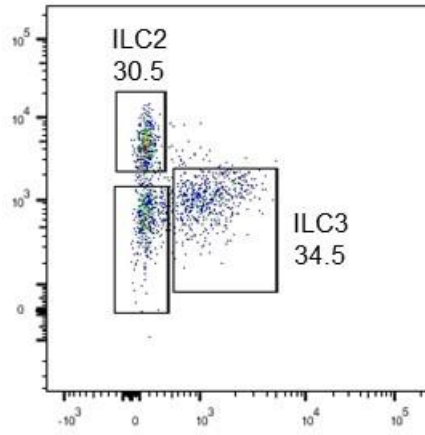


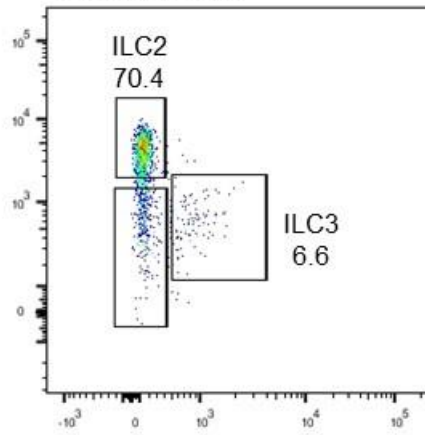
Figure 3.2: Identification of ILC1 in the mesenteric lymph node, and abdominal fat depots.

Representative flow cytometry plots showing the ILC1 population in mesenteric lymph node, gonadal fat, mesenteric fat, and omental fat. Using a combination of cell surface and intracellular markers, a LiveCD45.2⁺ IL-7R α ⁺Lin⁻CD3i⁻ population of ILCs were isolated (*S1-S2: supplementary figures*) and ILC1s were separated based on GATA-3, Tbet, ST2 and NKp46 expression. Indicative data for group size n=4 C57Bl/6 mice pooled from two independent experiments. Equal numbers of males and females were used and were aged between 14-20 weeks.

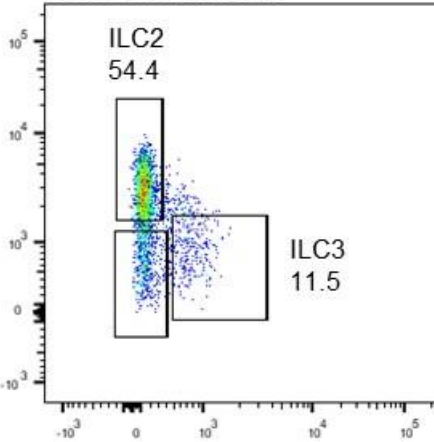
Mesenteric Lymph Node



Gonadal Fat



Mesenteric Fat



Omental Fat

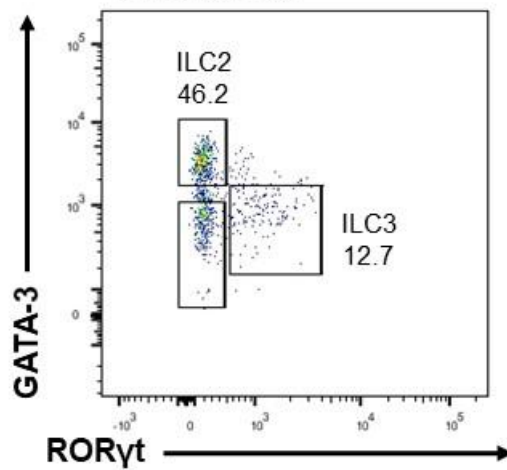


Figure 3.3: Identification of ILC2 and ILC3 populations in mesenteric lymph node, and abdominal fat depots.

Representative flow cytometry plots showing the ILC2 and ILC3 populations in mesenteric lymph node, gonadal fat, mesenteric fat, and omental fat. Using a combination of cell surface and intracellular markers, a LiveCD45.2⁺IL-7R α ⁺Lin⁻CD3i⁻ population of ILCs were isolated (*S1-S2: supplementary information*) and ILC2s and ILC3s were separated based on GATA-3 and ROR γ t expression. Indicative data for group size n=5-9 C57Bl/6 mice pooled from 3 independent experiments. Efforts were made to use equal numbers of males and females, but where the sample number was odd an additional female was used. Animals were aged matched (13 weeks).

Using these gating strategies, quantitation of ILC populations in the mLN and adipose deposits was possible. First, an overview profile of ILC populations was established for each tissue (Figure 3.4). This is useful to examine because there is reportedly plasticity between ILC subsets (Bernink *et al.*, 2013; Klose *et al.*, 2013), which may mean expression levels of markers included in the ILC subset staining panels may be lower on some target cells, leading to their exclusion. An overview of total ILCs uses markers that should detect all subtypes of ILCs, so the data seen in Figure 3.4 will not be affected by phenotypic plasticity. Examining total ILC numbers normalized to weight show that there are significantly more ILCs by tissue weight in the omental fat than the gonadal fat. The mesenteric fat contains the highest numbers of ILCs per tissue, but when the data is normalized to the tissue weights, then numbers are comparable to gonadal fat and omental fat. Subsequently, data on individual ILC populations was examined (Figure 3.5). ILC2s comprise the largest median proportions of ILCs in the gonadal fat (65.7%), mesenteric fat (69.2%), which both have significantly higher proportions compared with omental fat (33%). Data for the mLN is included for reference and in this tissue ILC2s represent a median of 27.1% of total ILCs. However, ILC2 counts normalized to tissue weight show the reverse trend. In this case the omental fat and the mesenteric fat contain significantly more ILC2s per 100mg than gonadal fat (3859 cells and 2537 cells vs 870 cells, respectively). Median values for ILC1s on the other hand do not make up a large proportion of total ILCs in gonadal (1.2%) and mesenteric fat (1.4%). ILC1s comprise just under a fifth of total ILCs in the omentum (17.7%), which although suggests an increased trend of ILC1s in this tissue, is not statistically significant. This is also the case when looking at median ILC1

numbers normalized to weight, where the omental fat (1859 cells) appears to have many more ILC1s than gonadal (16 cells) and mesenteric fat (93 cells). Although the trend appears obvious, it is not significant ($p=0.052$). However, it must be acknowledged that the sample size used for looking at ILC1 populations is very small ($n=4$) and that this is possibly below the number required for appropriate statistical power.

The profile of ILC3s across the different adipose deposits broadly resembles that of ILC1s. Again, ILC3s make up a very small proportion of the total ILCs of gonadal (1.7%) and mesenteric fat (0.8%). Conversely, they comprise just under a fifth of the omental fat ILC profile (17.9%). Differences in proportions of ILC3s across the different tissues were not significant. Median ILC3 numbers normalized to weight for each tissue were as follows: 32 cells in gonadal fat, 26 cells in mesenteric fat, and 1775 cells in omental fat. The omental fat has significantly more ILC3s per weight than both the gonadal fat and mesenteric fat. There are few clear differences in ILCs between gonadal and mesenteric fat, except in total ILC2 numbers where mesenteric fat contains significantly more. There are more points of difference for the ILC profile of omental fat vs gonadal and mesenteric fat, for example higher numbers of ILC3s (both) and higher numbers of ILC2s (gonadal), but the ILC profile of the omentum is not significantly different across the board.

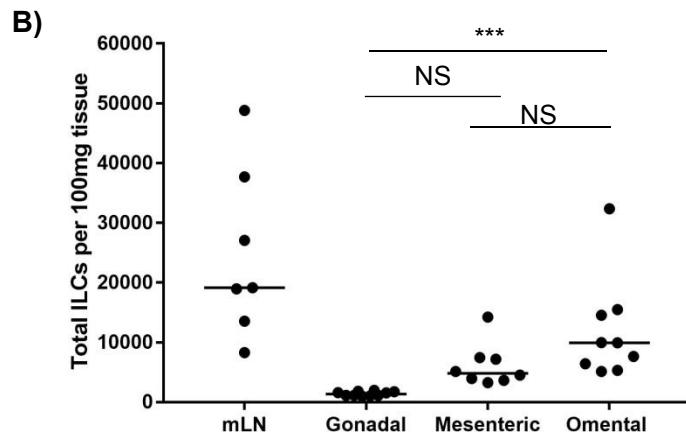
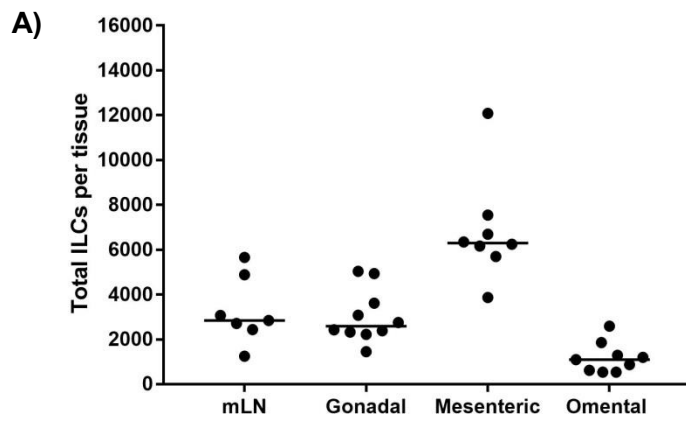


Figure 3.4: Quantitation of total ILC populations in the mesenteric lymph node and abdominal adipose depots.

Total ILC populations shown as the median numbers of total ILCs per tissue (A) and median numbers normalized to tissue weight (B). Statistical significance in B was assessed by a Kruskal-Wallis test, followed by a Dunn's *post hoc* test if appropriate * $p < 0.05$, ** $p < 0.01$, *** $P < 0.001$. Statistical testing was not conducted on data in A. Horizontal lines represent the median. Group size $n = 7-10$ C57Bl/6 pooled from at least three independent experiments. Efforts were made to use equal numbers of males and females, but where the sample number is odd an additional female was used. Animals were between 14-20 weeks of age.

Figure 3.5: Quantitation of ILC populations in the mesenteric lymph node and abdominal adipose depots.

Each ILC population shown as the median proportion of total ILCs and median absolute numbers normalized to tissue weight for (A) ILC1s, (B) ILC2s, and (C) ILC3s. Statistical significance was assessed by a Kruskal-Wallis test, followed by a Dunn's *post hoc* test if appropriate * $p < 0.05$, ** $p < 0.01$, *** $P < 0.001$. Horizontal lines represent the median. Group size $n = 5-9$ C57Bl/6 from at least three independent experiments. Equal numbers of males and females were used in (A), and efforts were made to use equal numbers of males and females in (B) and (C), although in instances where the sample numbers are odd, an additional female was used. Animals were age-matched in (B) and (C) (13 weeks), and were between 14-20 weeks in (A).

3.3. Isolation of FALC from mesenteric fat deposits

Once a profile of ILC populations had been established for the fat deposits as a whole, it was of interest to develop a method to examine the FALCs specifically, by flow cytometry. ILC2s have been previously described in the FALCs (Moro *et al.*, 2010) and it was of interest to investigate whether ILC2s are located predominantly in the FALCs, or whether they are also dispersed in the surrounding tissue. Initially FALCs were to be removed from the tissue and analyzed for ILCs. However, results from a pilot experiment (data not shown) indicated that cell loss from the digestion process was too great to obtain sufficient data for analysis from the flow cytometer with this method. It was then decided that instead a comparison of ILC composition could be made between naïve tissues and tissues where the FALCs had been removed, thus giving an indication of where the majority of ILCs were located.

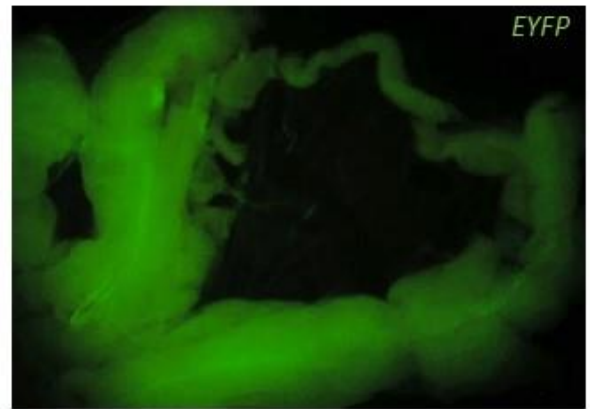
These experiments were conducted only on mesenteric fat for technical reasons. FALC count data suggested that gonadal fat contained a very low number of clusters, while imaging of omental fat suggests that the large number and arrangement of clusters in this tissue would preclude their successful removal and analysis of the remaining tissue. Mesenteric fat on the other hand was found to consistently contain moderate numbers of FALCs and imaging showed that the tissue would likely be robust enough to endure FALC removal without destroying the remaining adipose. It was also decided that the focus of this series of experiments would be the ILC2 population, as this population is the most abundant, both proportionally and numerically, found in mesenteric fat as previously discussed.

All visible FALCs were excised from the mesenteric fat of EYFP⁺ mice by forceps and scalpel (Figure 3.6). These images are displayed without a scale bar for reasons stated in section 3.1. Three populations were examined: Live CD45⁺ cells, total ILCs, and ILC2s. In each case no significant differences in median proportions or numbers normalized to weight were observed between tissues with FALCs or those with FALCs removed (Figure 3.7A-C). This suggested that the majority of Live CD45⁺ cells, total ILCs, and ILC2s are dispersed in the adipose tissue rather than located in the FALCs, although the analysis is based on only the SVF.

A)



Before FALC removal



After FALC removal

B)

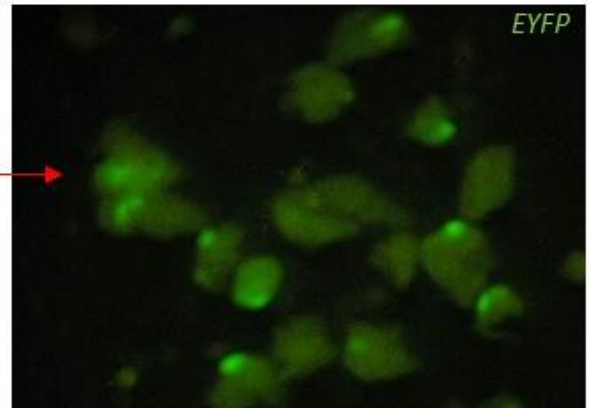
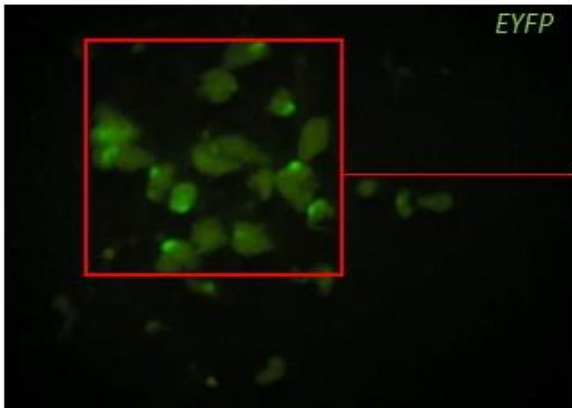


Figure 3.6: Isolation of FALC from mesenteric fat.

Representative images of mesenteric fat from EYFP⁺ mice, taken by a digital camera connected to a stereo fluorescence microscope. (A) Mesenteric FALC are shown as bright green clusters *in situ* and are absent in the subsequent image following removal. (B) Excised FALC are shown as bright green clusters surrounded by small pads of adipose tissue (dull green), enlarged in the subsequent image for clarity. Scale bar omitted intentionally. Indicative data for group size n=6 C57Bl/6 pooled from three independent experiments. Equal numbers of males and females were used and animals were age-matched (13 weeks).

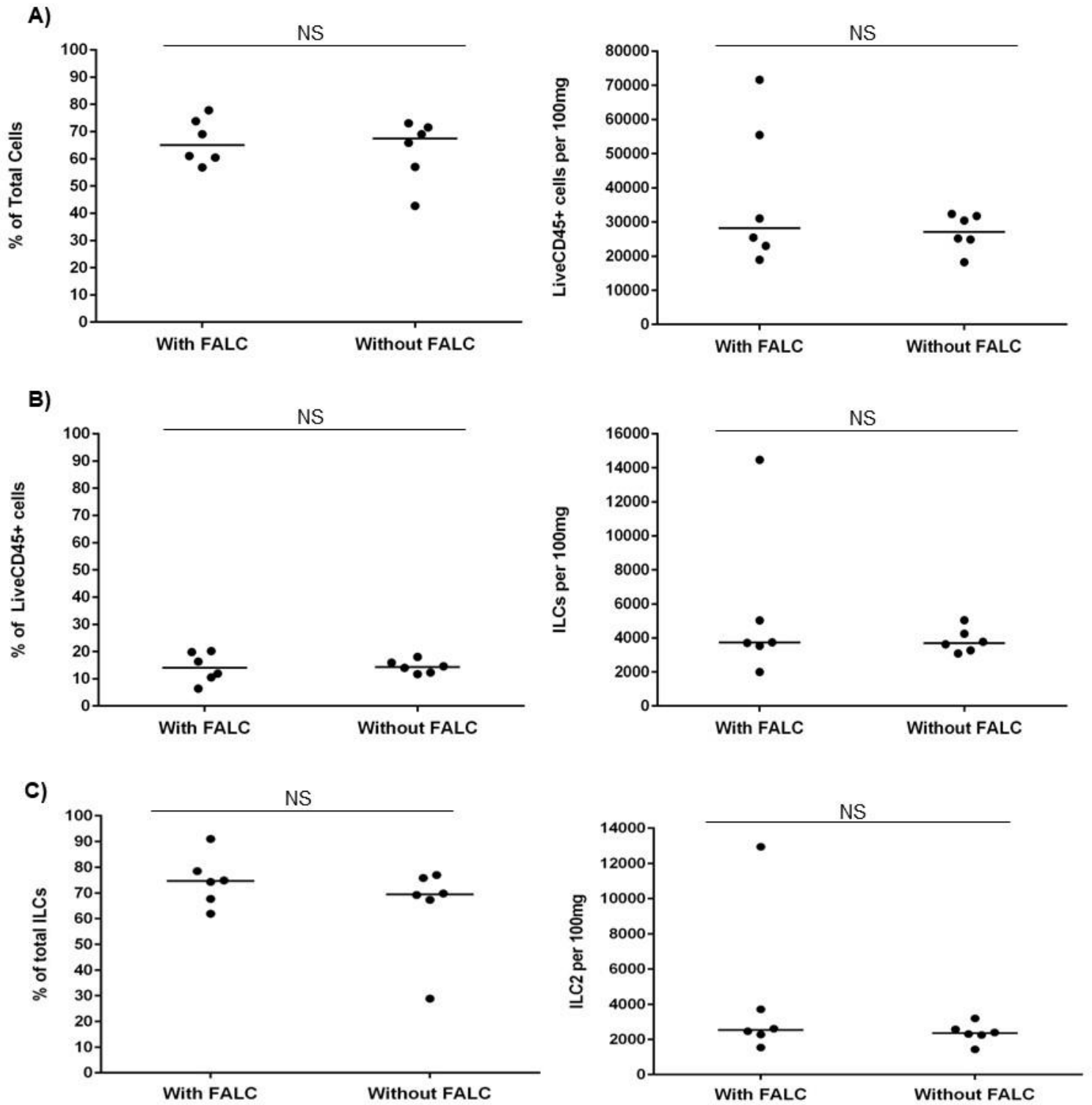


Figure 3.7: Removal of FALC from mesenteric fat does not impact ILC2 populations as assessed by flow cytometry.

(A) Live CD45⁺ cells are shown as a proportion of total cells and as absolute numbers normalized to tissue weight. (B) Total ILCs are shown as a proportion of live lymphocytes and as absolute numbers normalized to tissue weight. (C) ILC2s are shown as a proportion of total ILCs and absolute numbers normalized to tissue weight. Statistical significance was assessed by an unpaired Mann-Whitney test. *p<0.05, **p<0.01, ***P<0.001. Horizontal lines represent the median. Group size n=6 C57Bl/6 pooled from three independent experiments. Equal numbers of males and females were used and animals were age-matched (13 weeks).

3.4. Enumerating FALC in IL-33^{cit/+} and IL-33^{cit/cit} mice

Much of this study so far has focused on FALC counts and ILC populations in WT mice. Another integral player in the adipose tissue microenvironment is IL-33, and the stromal cells that produce it. A novel tool to explore the role of IL-33 has been created recently: the IL-33 reporter mice (Hardman *et al.*, 2013). There are two genotypes of IL-33 reporter mice. The first is IL-33^{cit/+}, a knock-in mouse that produces both functional IL-33 and the citrine reporter protein in cells that produce IL-33. The second is IL-33^{cit/cit}, a mouse that does not produce IL-33, but instead only produces the citrine reporter protein in cells that would normally produce this cytokine. The citrine reporter protein therefore represents a proxy marker for IL-33.

IL-33^{cit/+} and IL-33^{cit/cit} mice are not well characterized in terms of their adipose immunology, therefore homeostatic FALC counts were required as a good foundation for further experiments. There were no significant differences in FALC counts in either gonadal, mesenteric or omental fat (Figure 3.8). However, there is a trend seen in gonadal and omental fat that IL-33^{cit/cit} tissues appear to have fewer FALC than IL-33^{cit/+}, but p numbers are stated for the avoidance of doubt (gonadal, p=0.054, mesenteric, p=0.06). It could very well be the case, as discussed earlier, that the sample size (n=6 per genotype) is too small for sufficient statistical power.

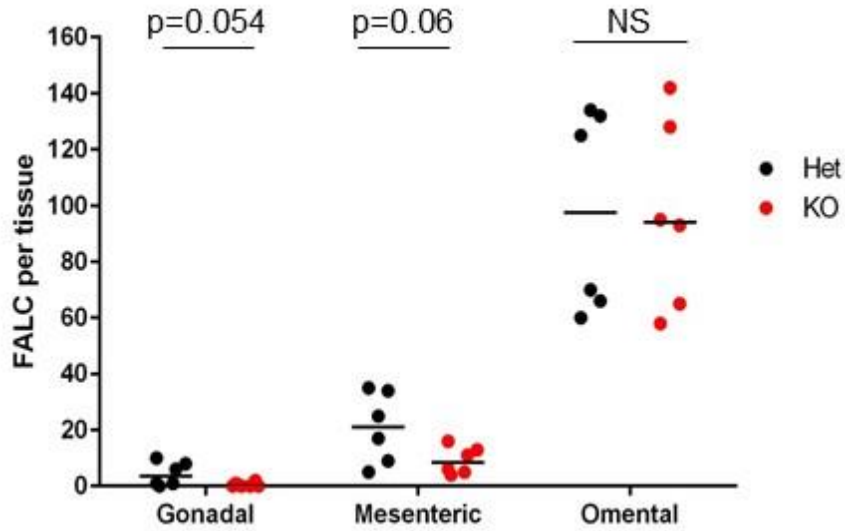


Figure 3.8: Enumerating FALC in IL-33^{cit/+} and IL-33^{cit/cit} mice.

Tissues from IL-33^{cit/+} and IL-33^{cit/cit} were stained with FITC labelled anti-CD45 in order to visualise the FALC and the FALC were counted. Statistical significance was assessed by unpaired Mann-Whitney test. *p<0.05, **p<0.01, ***P<0.001. Horizontal lines represent the median. Group size n=6 pooled from three independent experiments, one independent experiment was conducted by Dr Sara Cruz Migoni. Equal numbers of males and females were used and animals were aged between 12 and 16 weeks.

3.5. Identification of IL-33⁺ cells

IL-33 is released from stromal cells such as endothelial cells, epithelial cells, and adipocytes (Wood *et al.*, 2009; Pichery *et al.*, 2012). However, the precise phenotype of IL-33⁺ cells in adipose deposits has not been elucidated. A 2012 paper by Bénézech and colleagues (Bénézech *et al.*, 2012) identified stromal populations within embryonic fat pads using the markers Gp38 (also known as Podoplanin) and CD31. This previous work was used as the partial basis of the present study and expanded to investigate the cell populations expressing IL-33 in the adipose tissues of adult mice. A population of Live CD45⁻Ter119⁻ stromal cells were identified in the mLN and adipose deposits. The inclusion of Ter119 ensured red blood cells were gated out. Gp38 and CD31 were then used to separate out the stromal cells into four distinct populations (Figure 3.9 and Figure 3.10), as previously described by Bénézech *et al.*: i) Gp38⁺ cells, designated as fibroblastic reticular cells that contain adipocyte precursors, ii) Gp38⁺CD31⁺ cells, designated as lymphatic endothelium, iii) Gp38⁻CD31⁺ cells, designated as blood endothelium, and iv) Gp38⁻CD31⁻ cells, a large double negative population. Each population was then examined for expression of citrine, the reporter marker for IL-33⁺. It is clear from the flow cytometry plots in Figures 3.9-3.10 that there appear to be large differences in the proportion of citrine expressing cells between the different stromal cell populations in the fat deposits.

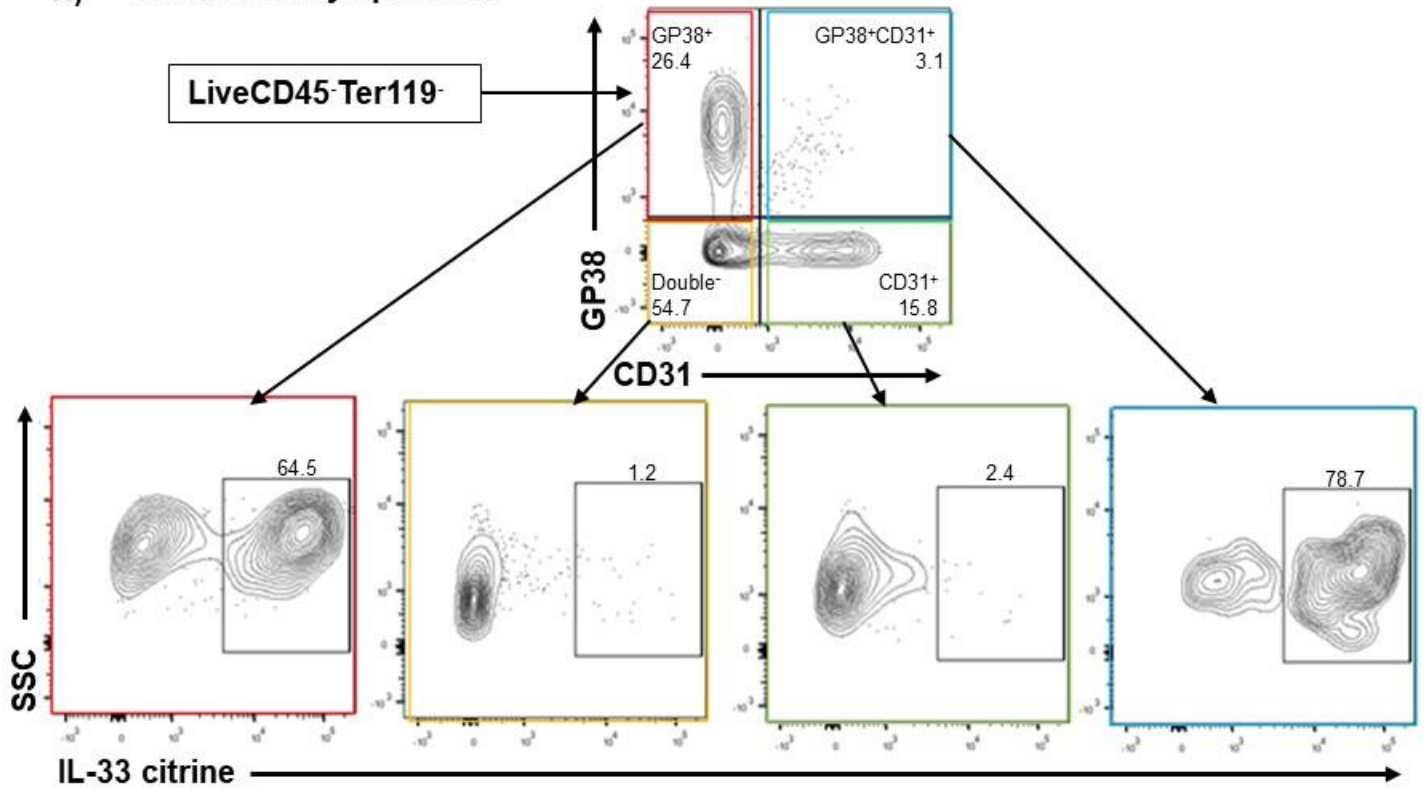
When this data is collated for both IL-33^{cit/+} mice (Figure 3.11) and IL-33^{cit/cit} mice (Figure 3.12), there are some clear differences in the proportions of citrine⁺ cells between each of the stromal populations. For both IL-33^{cit/+} and IL-33^{cit/cit} mice, there is a clear trend suggesting that the highest proportion of citrine⁺ cells in each tissue are of the Gp38⁺

phenotype (median of 10% & 15% in the mLN, 1.9% & 3.8% in gonadal fat, 18.8% & 19.3% in the mesenteric fat and 38.6% & 38.1% in omental fat of IL-33^{cit/+} and IL-33^{cit/cit} mice, respectively). Indeed, the proportions of the citrine⁺Gp38⁺ populations are, on the whole, significantly higher than most of the other stromal populations examined, across all tissue types. Very small proportions of the total stroma are comprised of CD31⁺citrine⁺ and Gp38⁻CD31⁻citrine⁺ populations (median<0.5% in all tissues). Gp38⁺CD31⁺citrine⁺ also comprise a very small proportion of the total stroma (median<0.5% in gonadal and mesenteric fat), although these proportions are slightly increased in the mLN (1.5% and 2.3% of IL-33^{cit/+} and IL-33^{cit/cit} mice, respectively). The Gp38⁺citrine⁺ population data for each deposit was compiled and compared across gonadal, mesenteric and omental fat from both IL-33^{cit/+} (Figure 3.13A) and IL-33^{cit/cit} mice (Figure 3.13B). There is a trend of increased proportions in the order: gonadal<mesenteric<omental fat and the total stroma of the omental fat was found to contain a significantly higher proportion Gp38⁺citrine⁺ cells than gonadal fat for both mouse genotypes.

Finally, to see whether the lack of IL-33 in IL-33^{cit/cit} mice had any bearing on the total numbers of citrine⁺ stromal cells, cell numbers normalized to tissue weight were calculated for each adipose deposit. These data (Figure 3.14A-D) are the result of additional analysis of the proportions data shown in Figure 3.11-3.12. The data on the proportions of citrine⁺ stroma suggested that there is no trend to difference between citrine⁺ cells in both the IL-33^{cit/+} and IL-33^{cit/cit} mice. The normalized cell number comparisons also mirror this finding. There were no significant differences between IL-

33^{cit/+} and IL-33^{cit/cit} mice, regarding any phenotype of stromal cells, in any tissue type (Figure 3.14A-D).

A) Mesenteric Lymph Node



B) Gonadal Fat

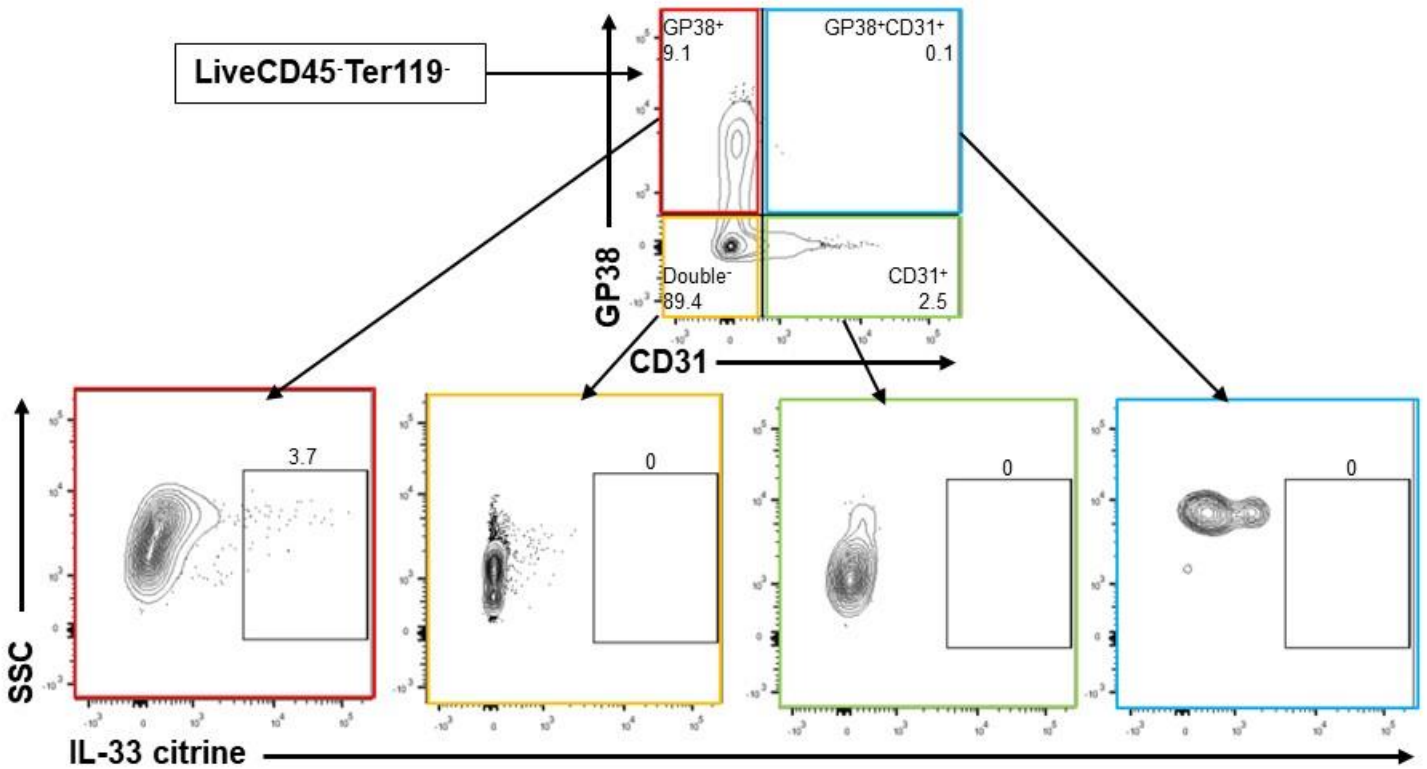
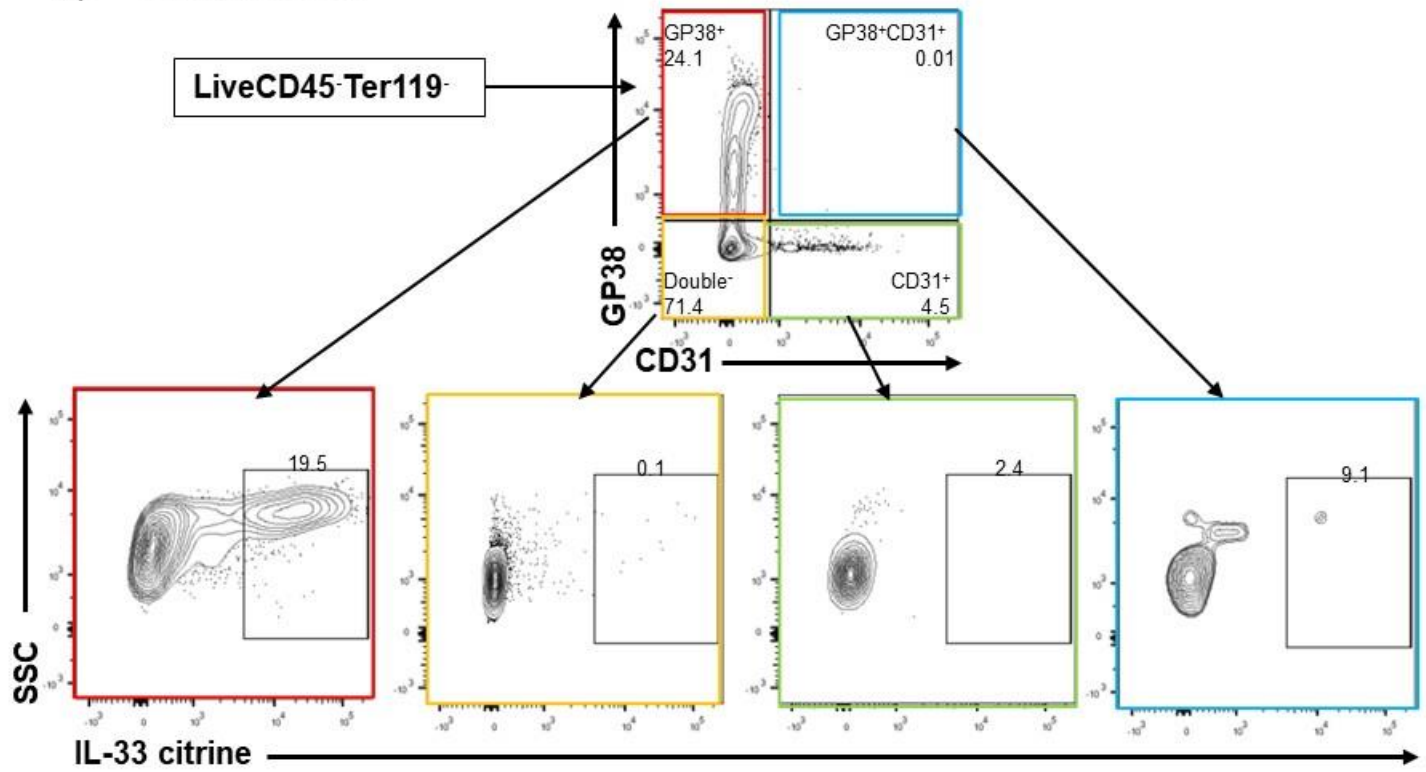


Figure 3.9: Identification of IL-33⁺ cells in citrine reporter mice.

Representative flow cytometry plots from an IL-33^{cit/+} mouse showing citrine⁺ (IL-33⁺) stromal cells in (A) mesenteric lymph node and (B) gonadal fat. Using a combination of cell surface markers, a population of LiveCD45⁻Ter119⁻ cells were isolated (see supplementary figure S3-S4 for full gating). Further identification of the stroma was achieved using Gp38 and CD31, and those cells expressing the fluorescent protein citrine were deemed to be IL-33-expressing cells. Indicative data for group size n=4 IL-33^{cit/+} on a Balb/c background mice pooled from two independent experiments. Equal numbers of males and females were used and animals were between 13-22 weeks old.

A) Mesenteric Fat



B) Omental Fat

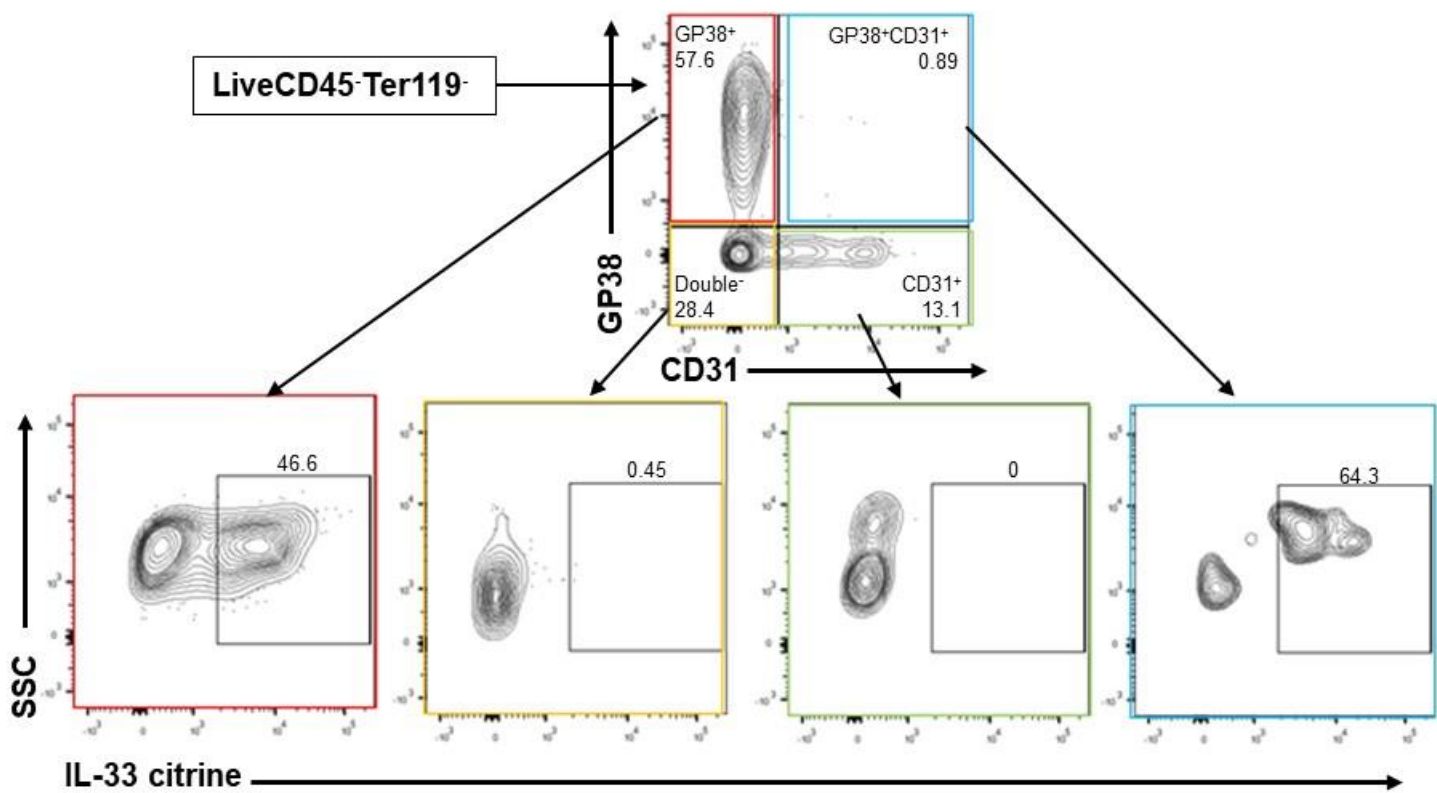


Figure 3.10: Identification of IL-33⁺ cells in citrine reporter mice.

Representative flow cytometry plots from an IL-33^{cit/+} mouse showing citrine⁺ (IL-33⁺) stromal cells in (A) mesenteric fat and (B) omental fat. Using a combination of cell surface markers, a population of LiveCD45⁻Ter119⁻ cells were isolated (see supplementary figure S3-S4 for full gating). Further identification of the stroma was achieved using Gp38 and CD31, and those cells expressing the fluorescent protein citrine were deemed to be IL-33-expressing cells. Indicative data for group size n=4 IL-33^{cit/+} on a Balb/c background mice pooled from two independent experiments. Equal numbers of males and females were used and animals were between 13-22 weeks old.

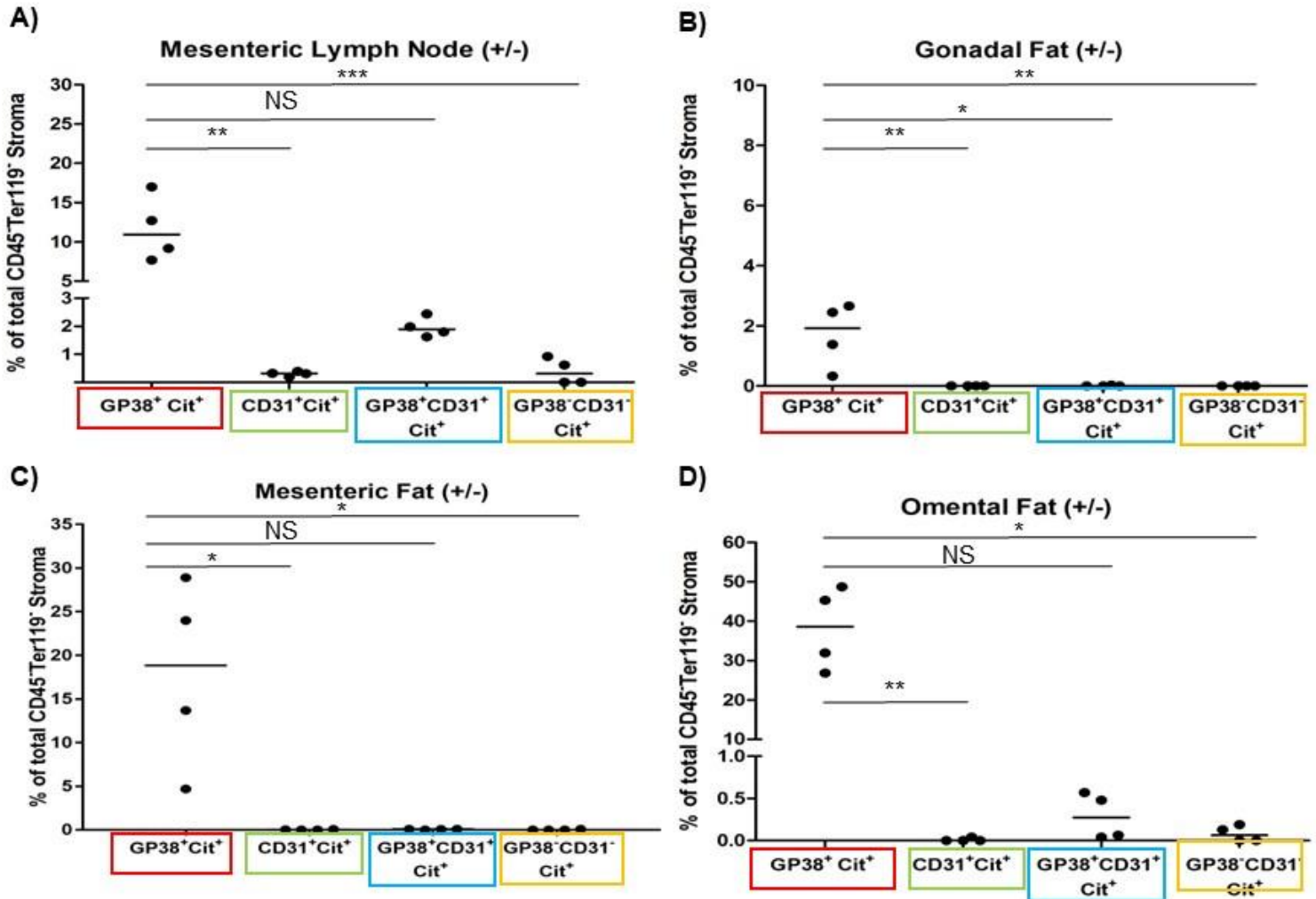


Figure 3.11: IL-33⁺ stromal cell composition in mesenteric lymph node and adipose tissues from IL-33^{cit/+} (+/-) mice.

Citrine⁺ IL33 expressing cells from each stromal phenotype are shown as proportions of the total stroma in (A) mesenteric lymph node, (B) gonadal fat, (C) mesenteric fat and (D) omental fat. Statistical significance was assessed by a Kruskal-Wallis test, followed by a Dunn's *post hoc* test if appropriate **p*<0.05, ***p*<0.01, ****P*<0.001. Horizontal lines represent the median. Group size n=4 IL-33^{cit/+} mice on a Balb/c background pooled from two independent experiments. Equal numbers of males and females were used and animals were between 14-22 weeks old.

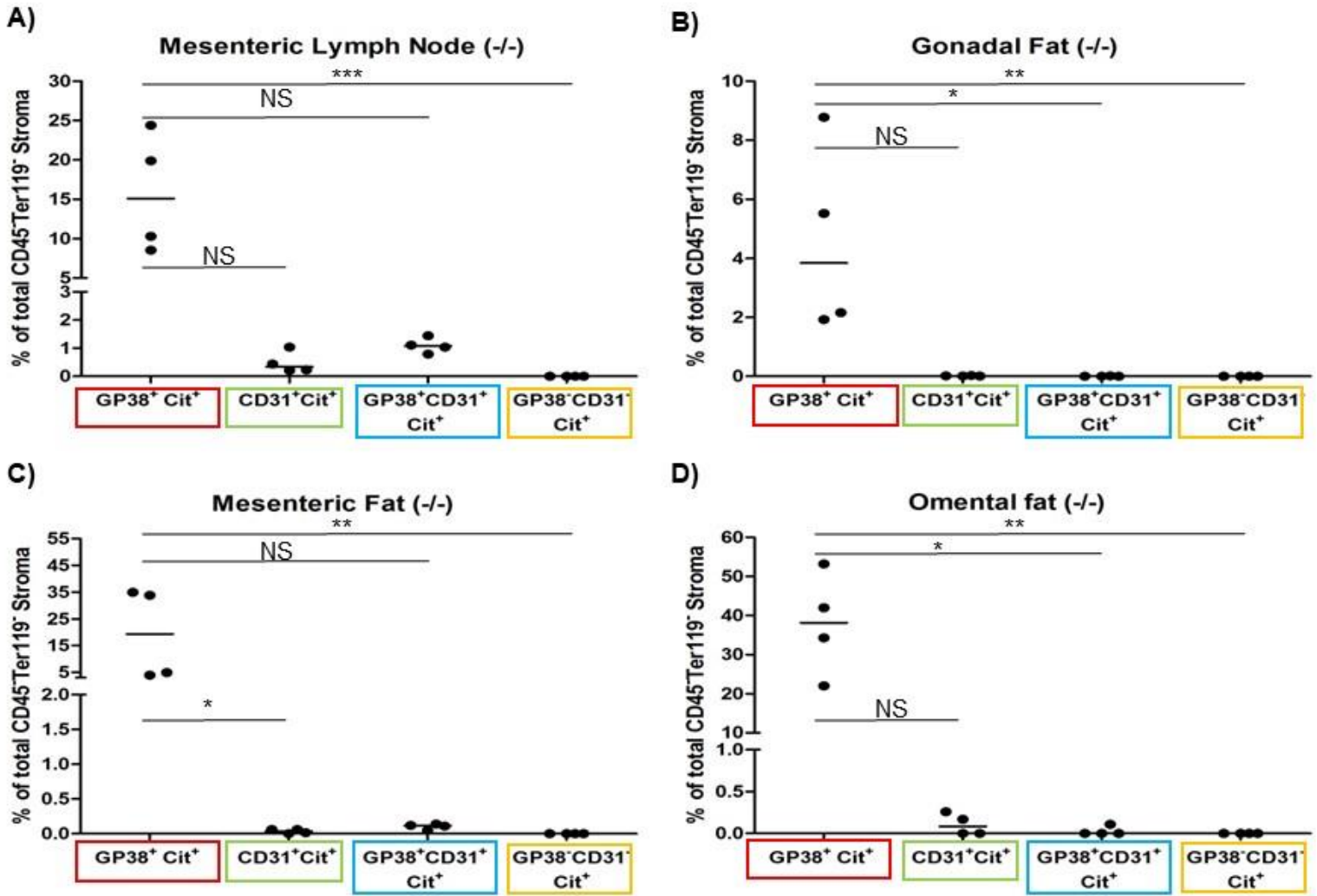


Figure 3.12: IL-33⁺ stromal cell composition in mesenteric lymph node and adipose tissues from IL-33^{cit/cit} (-/-) mice.

Citrine⁺ IL33 expressing cells from each stromal phenotype are shown as proportions of the total stroma in (A) mesenteric lymph node, (B) gonadal fat, (C) mesenteric fat and (D) omental fat. Statistical significance was assessed by a Kruskal-Wallis test, followed by a Dunn's *post hoc* test if appropriate *p<0.05, **p<0.01, ***P<0.001. Horizontal lines represent the median. Group size n=4 IL-33^{cit/cit} mice on a Balb/c background pooled from two independent experiments. Four males were used and animals were aged between 13-14 weeks.

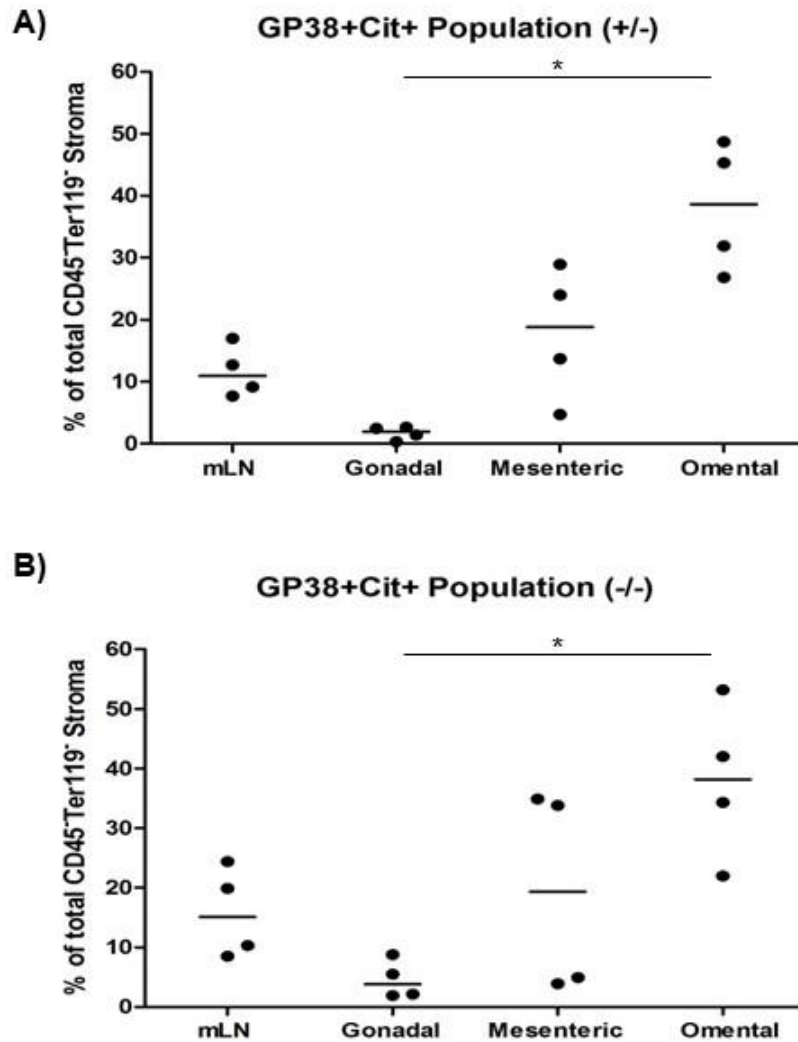


Figure 3.13: Comparison of Gp38⁺ Citrine⁺ populations in mLN and adipose deposits in IL-33^{cit/+} and IL-33^{cit/cit} mice.

(A) Gp38⁺ Citrine⁺ populations as a percentage of total stroma in IL-33^{cit/+} mice. (B) Gp38⁺ Citrine⁺ populations as a percentage of total stroma in IL-33^{cit/cit} mice. Statistical significance was assessed by a Kruskal-Wallis test, followed by a Dunn's *post hoc* test if appropriate *p<0.05, **p<0.01, ***P<0.001. Group size n=4 IL-33 mice on a Balb/c background, pooled from two independent experiments. Horizontal lines represent the median. Equal numbers of males and female IL-33^{cit/+} mice and four male IL-33^{cit/cit} animals were used. Animals were aged between 13-22 weeks old.

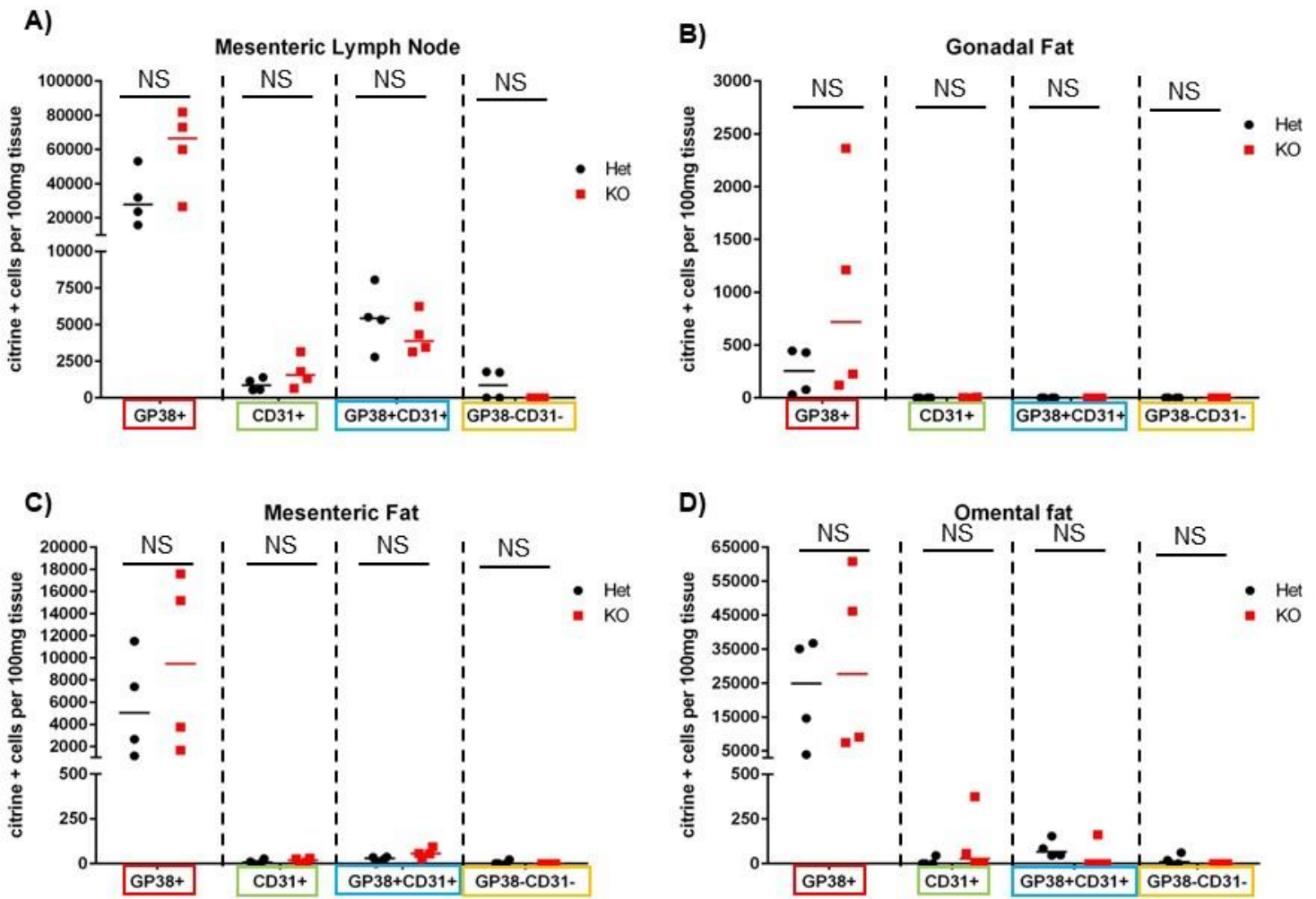


Figure 3.14: Comparison of citrine⁺ cells in IL-33^{cit/+} and IL-33^{cit/cit} mice. Citrine⁺ cell counts from the four phenotypes arising from Gp38 and CD31 staining are shown for (A) mesenteric lymph node, (B) gonadal fat, (C) mesenteric fat, and (D) omental fat. Statistical significance was assessed by an unpaired Mann-Whitney test *p<0.05, **p<0.01, ***P<0.001. Horizontal lines represent the median. Group size n=4 per genotype, IL-33^{cit/+} mice and IL-33^{cit/cit} mice on a Balb/c background, pooled from two independent experiments. Equal numbers of males and female IL-33^{cit/+} mice and four male IL-33^{cit/cit} animals were used. Animals were aged between 13-22 weeks old.

3.6. Further characterization of Gp38⁺citrine⁺ stromal populations

Gp38⁺CD31⁻ stromal cells are the main cell population that express IL-33 as shown by their frequency of citrine⁺ cells, compared to other stromal populations. It was therefore of interest to further characterize these Gp38⁺citrine⁺ cells. Two markers were selected for the initial pilot experiment: Sca-1 (*stem cell antigen-1*) and PDGFR α (*Platelet-derived growth factor receptor-alpha*). These markers were selected as they had previously been identified on embryonic adipocyte precursor populations (Bénézech *et al.* 2012). Sca-1 is a classical stem cell marker and it is also expressed on the cell surface in variety of stromal cell populations. In addition to expressing Sca-1, pre-adipocytes are also reportedly able to produce IL-33 (Wood *et al.*, 2009). It was therefore of interest to examine the Gp38⁺citrine⁺ IL-33 producing stromal population identified in this study for Sca-1 expression to confirm their identity as adipocyte precursors from adult tissues. Platelet-derived growth factor is the ligand for PDGFR α , and this ligand-receptor interaction plays a role in growth and proliferation, dysregulation of which are commonly implicated in malignancies (Kim *et al.*, 2012). Gp38⁺citrine⁺ (orange histograms) populations had high median proportions of Sca-1 and PDGFR α expression in all adipose tissues (>90%) excepting PDGFR α expression in the omentum (~50%), compared to fluorescence minus one control (blue peak) and isotype control (red peak) (Figure 3.15A-D and Figure 3.16A-B). This was the case in both the IL-33^{cit/+} and IL-33^{cit/cit} mice. Median weight normalized numbers of Gp38⁺citrine⁺Sca-1⁺ cells appear to follow the familiar tissue trend of gonadal<mesenteric<omental, although this is not as clear when examining the normalized numbers of Gp38⁺citrine⁺ PDGFR α ⁺ cells. In this case, the omentum has

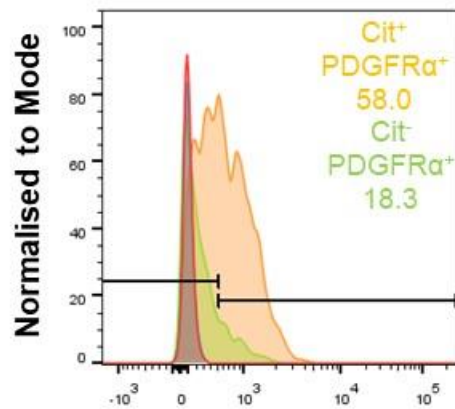
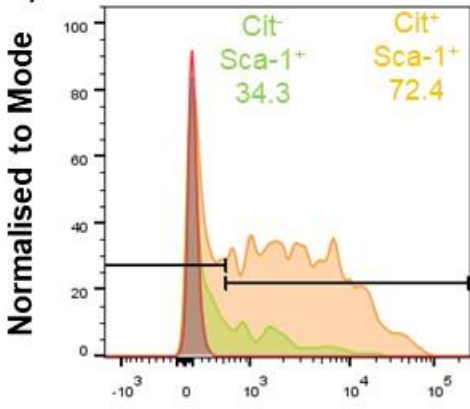
fewer Gp38⁺citrine⁺ PDGFR α ⁺ cells than then mesenteric fat. In addition, the omentum contains almost half as many Gp38⁺citrine⁺ PDGFR α ⁺ cells, compared to the Gp38⁺citrine⁺Sca-1⁺ counts in the same tissue. Conversely, gonadal and mesenteric fat have more than twice as many Gp38⁺citrine⁺PDGFR α ⁺ cells than Gp38⁺citrine⁺Sca-1⁺, although the proportions of Sca-1⁺ and PDGFR α ⁺ Gp38⁺citrine⁺ are similarly high (Figure 3.16 A-B). This may be due to differing cell viability across experiments, as panels for Sca-1 and PDGFR α were conducted at different times. Although these results are from a pilot study, they suggest that the Gp38⁺citrine⁺ cell populations in each tissue share characteristics consistent with the Gp38⁺CD31⁻ populations identified in a previous study – that is fibroblastic reticular cells that contain adipocyte precursors (Bénézech *et al.*, 2012).

It is also interesting to consider Sca-1 and PDGFR α expression in Gp38⁺Citrine⁻ populations in the adipose (green histograms). Both Sca-1 and PDGFR α were expressed by substantially smaller proportions of Gp38⁺Citrine⁻ stroma in all tissues, when compared to their Gp38⁺Citrine⁺ counterparts. This result suggests that Gp38⁺ cells that don't produce IL-33 are split into two populations: a small population expressing Sca-1 and PDGFR α , and a larger one that doesn't. There is also an interesting difference between the percentage of Gp38⁺citrine⁻ cells expressing Sca-1 in gonadal and mesenteric fat (a large portion) compared with the omentum (a very small proportion). This is one more differentiating feature of the omentum, suggesting that the stromal cells contained within it may have different functions to those within gonadal and mesenteric fat. The functional roles of both these IL-33⁻ populations are currently unknown but it would be interesting to compare their broader gene expression profiles

with that of Gp38⁺IL-33-producing stroma, which also express these additional markers, to shed some light into their functional differences.

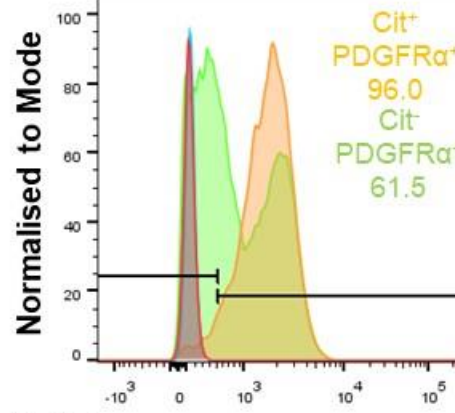
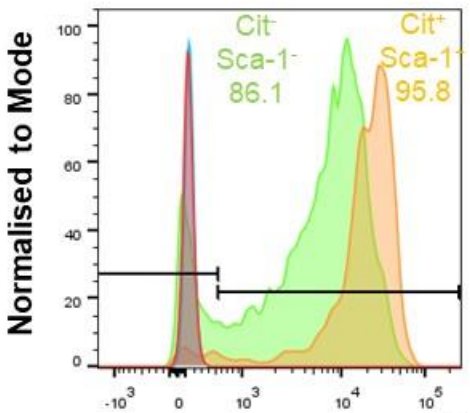
Mesenteric Lymph Node

A)



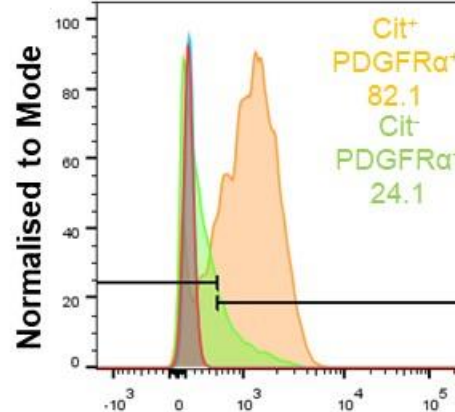
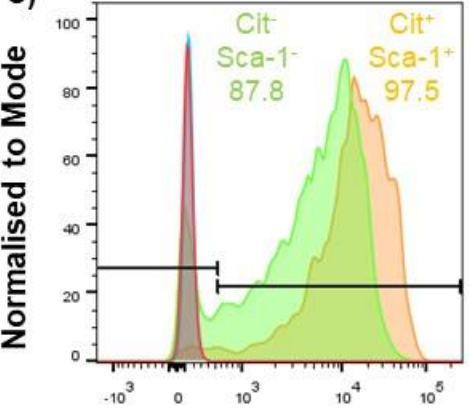
B)

Gonadal Fat



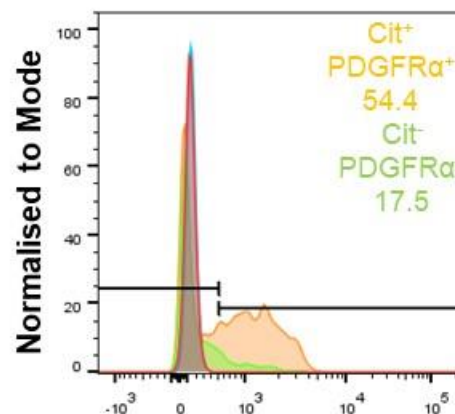
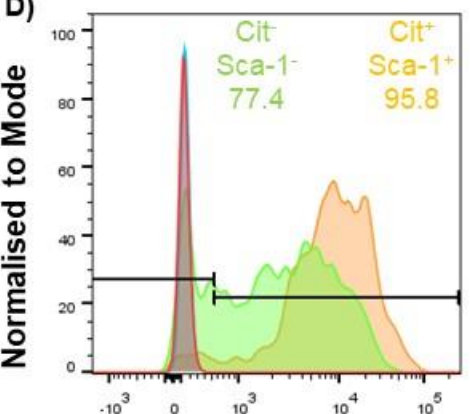
C)

Mesenteric Fat



D)

Omental Fat



Sca-1 →

PDGFRα →

Figure 3.15: Further characterization of Gp38⁺IL-33⁺ and Gp38⁺IL-33⁻ stromal populations in the mesenteric lymph node and adipose deposits of IL-33^{cit/+} and IL-33^{cit/cit} mice (pilot experiment). Representative histograms from an IL-33^{cit/+} mouse showing Sca-1 and PDGFR α expression for both Gp38⁺IL-33⁺ (orange) and Gp38⁺IL-33⁻ (green) stromal populations in (A) mesenteric lymph node, (B) gonadal fat (C) mesenteric fat and (D) omental fat. Blue peak represents the fluorescence minus one control and the red peak represents the isotype control. Controls were performed on a mLN sample and a pooled sample from all three types of adipose. The control peaks are virtually identical although the red peak extends slightly higher in the mLN samples, and the blue peak extends slightly higher in the fat samples and the colour change is visible. Indicative data for group size n=2 per genotype, pooled from two independent experiments. IL-33^{cit/+} mice were female and IL-33^{cit/cit} mice were male. Mice were aged between 13-15 weeks.

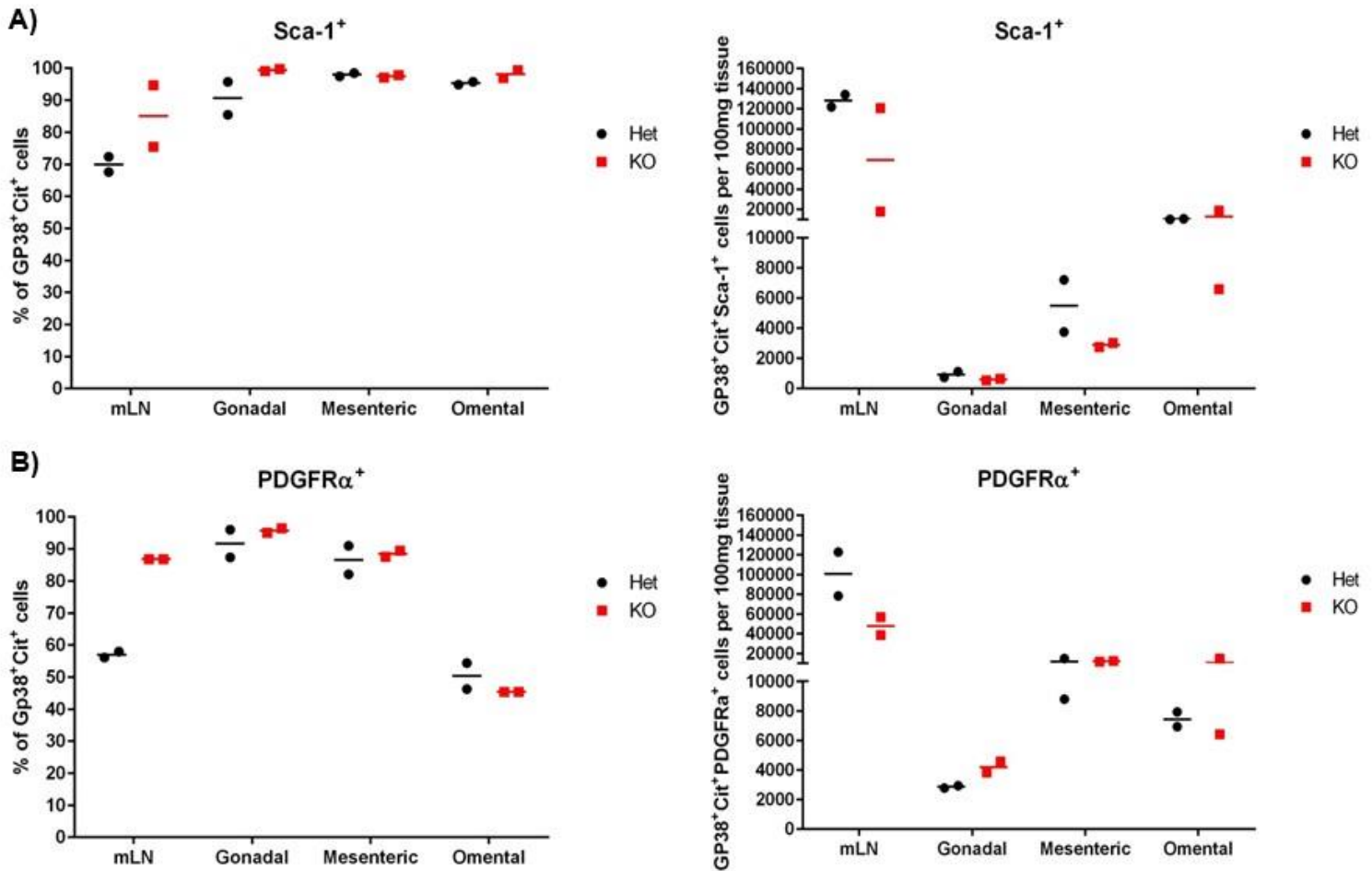


Figure 3.16: Further characterization of Gp38⁺IL33⁺ stromal populations in the mesenteric lymph node and adipose deposits of IL-33^{cit/+} and IL-33^{cit/cit} mice (pilot experiment). (A) Sca-1 expression is shown as a proportion of total Gp38⁺Cit⁺ stroma and as absolute numbers normalized to weight. (B) PDGFR α expression is shown as proportion of total Gp38⁺Cit⁺ stroma and as absolute numbers normalized to weight. Horizontal lines represent the median. n=2 per genotype pooled from two independent experiments. IL-33^{cit/+} mice were female and IL-33^{cit/cit} mice were male. Mice were aged between 13-15 weeks.

3.7. Effects of zymosan-induced peritoneal inflammation on Gp38⁺citrine⁺ stromal populations

Zymosan is a polysaccharide derived from the cell wall of the yeast species *Saccharomyces cerevisiae*. It is well established as an inducing agent of sterile peritoneal inflammation, through interaction with a heterodimer of TLR 2 (toll-like receptor) and TLR6 on macrophages (Underhill *et al.*, 1999; Ozinsky *et al.*, 2000) (Figure 3.17A). Previous work has shown that zymosan injected i.p into WT mice increases the size and number of FALCs (Bénézech *et al.*, 2015) at 72hr post-immunization. As the role of IL-33-producing stroma in adipose is unclear, it is of interest to examine whether their numbers increase during peritoneal inflammation.

Mice were injected with zymosan i.p and at 72hrs post immunization three subsets of stromal cells were examined: Gp38⁺, Gp38⁺citrine⁺, and Gp38⁺citrine⁺Sca-1⁺. IL-33^{cit/+} mice were used for the initial pilot experiment to determine whether zymosan increased the prevalence of the three key stromal subsets. The results of the pilot experiment suggest that zymosan treatment does not appear to increase the median proportions or median normalized counts of Gp38⁺ cells, Gp38⁺citrine⁺ cells, or Gp38⁺citrine⁺Sca-1⁺ cells in either the mLN or adipose tissues (Figure 3.17B-C) at this timepoint. In other words, IL-33-producing cells are not increasing in number in response to zymosan induced inflammation. However, as this is a pilot experiment using very small numbers of animals, more repeats should be conducted to confirm this conclusion.

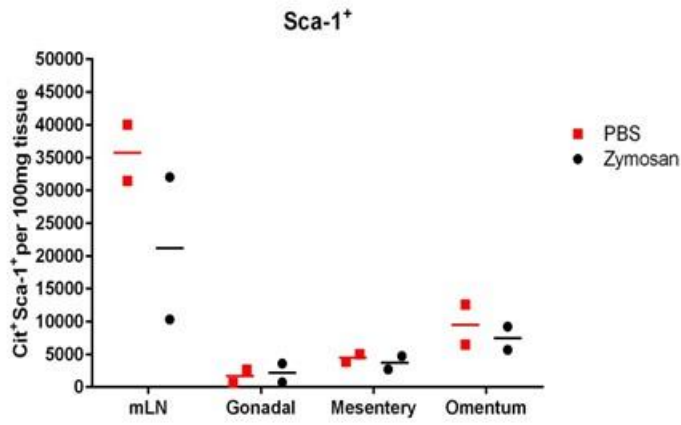
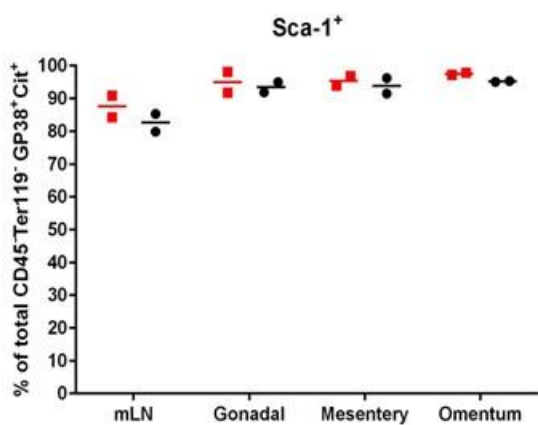
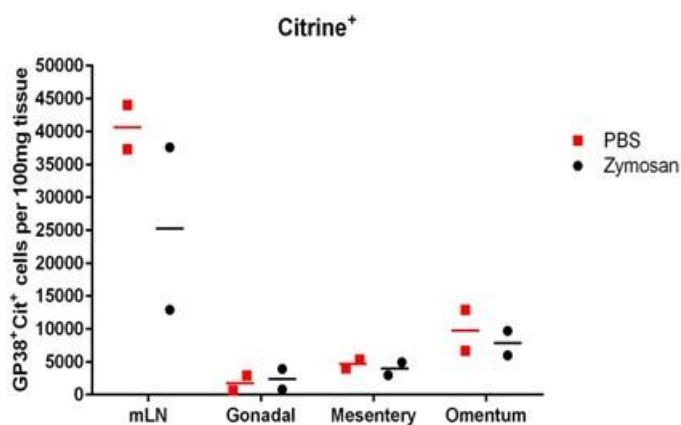
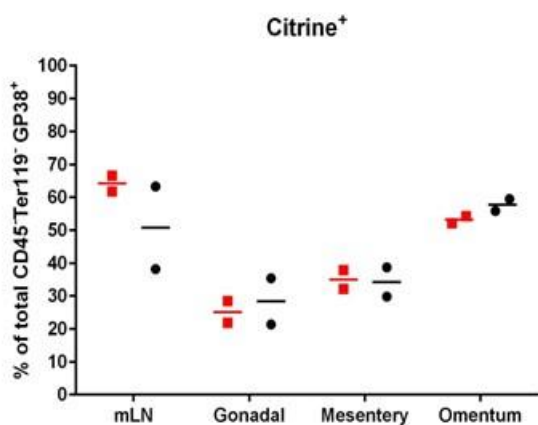
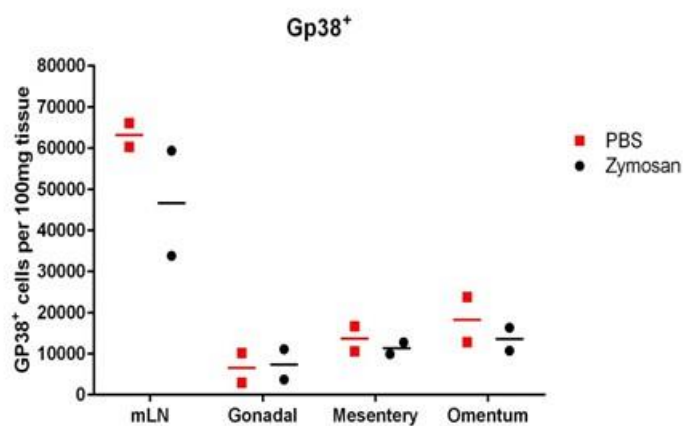
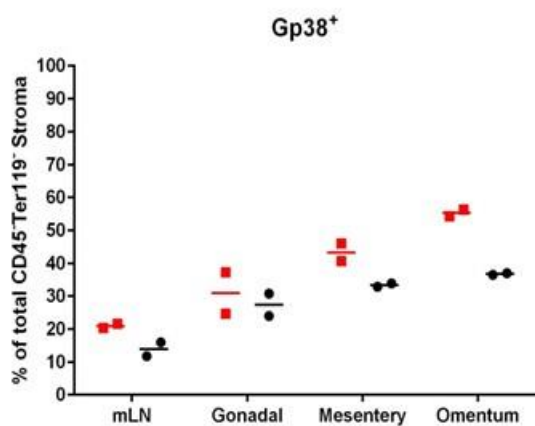
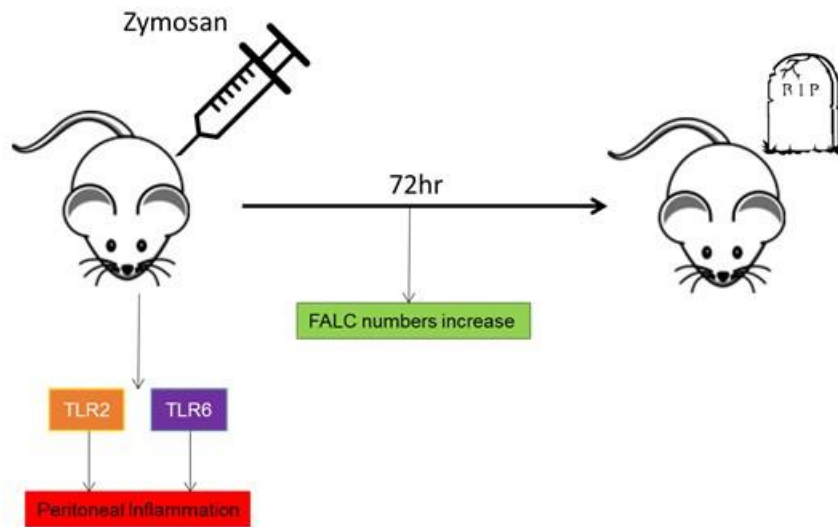


Figure 3.17: Effect of Zymosan-induced peritoneal inflammation on Gp38+IL-33+ stromal populations in IL-33^{cit/+} mice (Pilot experiment). (A) Experimental protocol illustrating zymosan injection of IL-33^{cit/+} and IL-33^{cit/cit} mice and harvesting of tissue after 72hr. Controls were injected with PBS. (B) Gp38⁺ stroma shown as a proportion of total stroma and as absolute numbers normalised to weight. (C) Citrine⁺ cells shown as a proportion of Gp38⁺ stroma and as absolute numbers normalised to weight. (D) Sca-1⁺ cells shown as a proportion of Citrine⁺Gp38⁺ stroma and as absolute numbers normalised to weight. Horizontal lines represent the median. Group size n=2 per treatment. IL-33^{cit/+} mice on a Balb/c background, from one independent experiment. Equal numbers of males and female IL-33^{cit/+} mice were used. Animals were aged matched (14 weeks). TLR – Toll-like Receptor

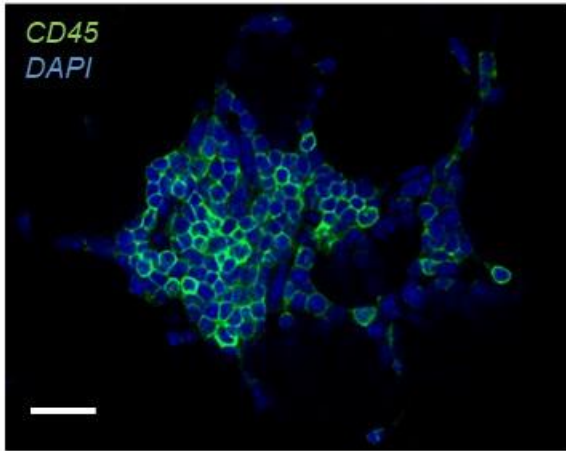
3.8. Components of FALCs identified by whole mount immunofluorescence and confocal microscopy

Much of this study has examined the immune and stromal cell composition of adipose deposits by flow cytometry, which allows construction of an overall picture of cell numbers and proportions. However, this method results in the loss of information regarding specific cellular locations, particularly in the FALC microenvironment. It is therefore of interest to develop a method to look in detail at the stromal and immune composition of the FALCs. One common method used to achieve this is immunofluorescence staining and in most tissues, frozen sections are cut, stained and then imaged. However, obtaining frozen sections from adipose tissues is technically challenging and therefore the whole mount method was used.

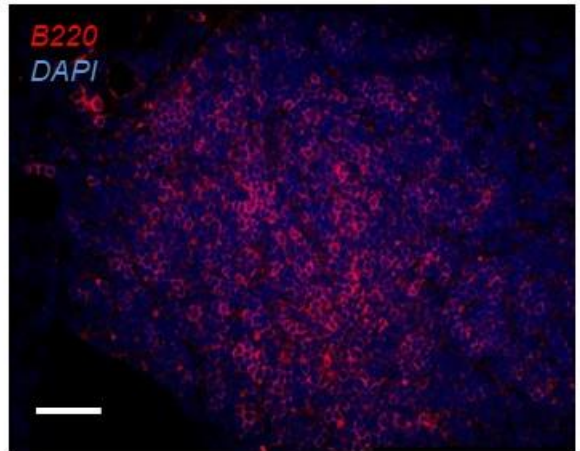
In previous work, the Caamano lab had successfully obtained whole mount immunofluorescence confocal images of some FALC components (Bénézech *et al.*, 2015). These stains were revisited with the fully optimized protocol, and staining with additional markers was also achieved. FALCs from the omental and mesenteric fat are most easily stained and visualized, primarily due to their prevalence in those tissues. Examples of both can be seen in Figure 3.18. A simple stain for the visualization of an omental FALC can be seen in Figure 3.18A. Anti-CD45 and DAPI staining clearly shows the morphology of the FALC and the concentration of lymphocytes in the center of the cluster. B cell follicles are known to form within FALCs (Bénézech *et al.*, 2015) and this is evident from the large number of B220⁺ cells present in an omental FALC (Figure 3.18B). There is also evidence for CD3⁺ and CD4⁺ T cells (Figure 3.18C) as shown in a mesenteric FALC. Images from staining for CD31⁺ blood endothelium and Lyve-1⁺ cells

(in this case, likely macrophages, rather than lymphatic endothelium) were obtained in a mesenteric FALC (Figure 3.18D/E). This suggests that blood vessels are present in FALCs but there is no evidence for lymphatic endothelium at this time. Imaging of IL-33 expressing cells was also achieved by whole mount immunofluorescence (Figure 3.19). An anti-IL-33 antibody was used on samples from WT BALB/C mice and the staining of anti-IL-33 can be seen overlaid with the DAPI nuclear stain, indicating a nuclear location for the anti-IL-33 antibody staining (white arrows Figure 3.19B). An IL-33^{cit/cit} mouse was used as a negative control, as cells from these mice do not produce IL-33. Here, the citrine⁺ nuclei are shown in green (white arrows), and anti-IL-33 antibody is shown in red. The staining pattern of anti-IL-33 in these samples is not consistent with nuclear staining and there is no co-staining with the citrine reporter protein (Figure 3.19C-D). This is to be expected as IL-33 is not present in these IL-33^{cit/cit} samples and the red staining observed is therefore non-specific staining. This give confidence that the pattern of nuclear staining observed with the anti-IL-33 antibody in Figure 3.19A-B is genuine.

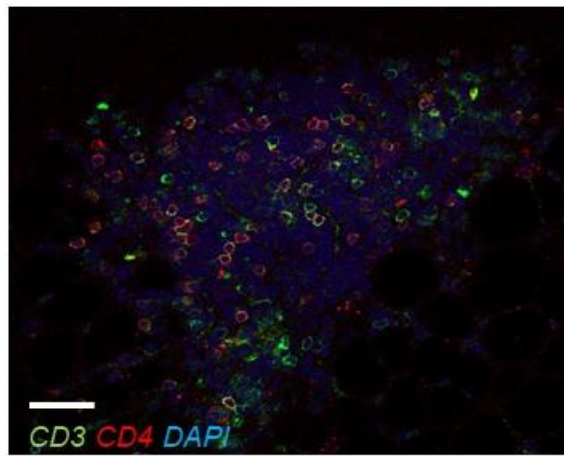
A)



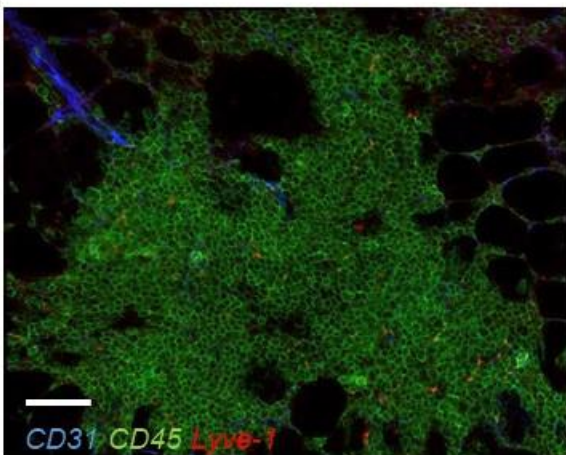
B)



C)



D)



E)

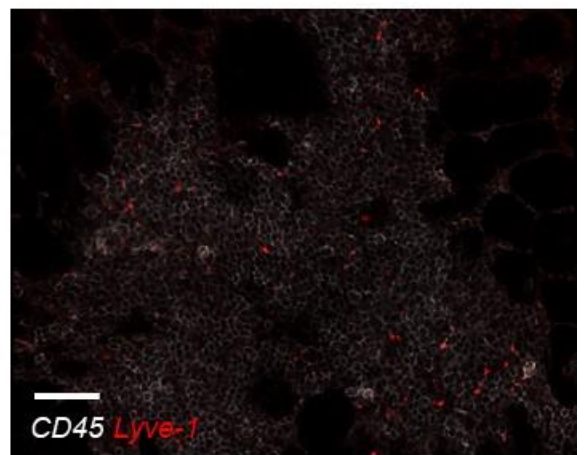
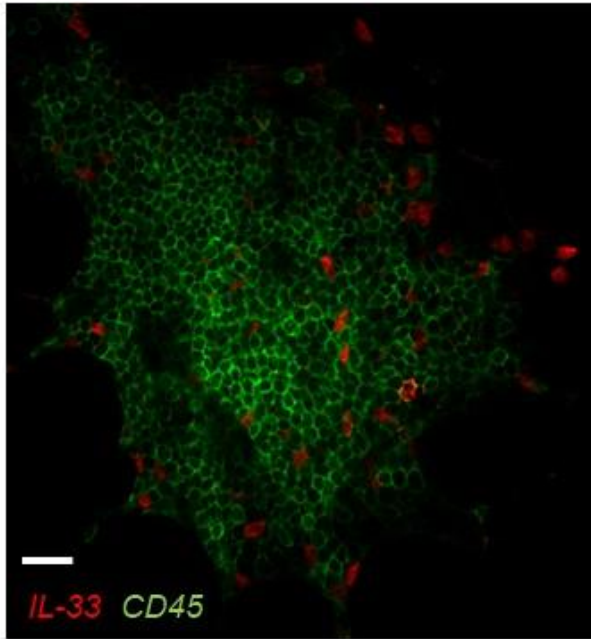
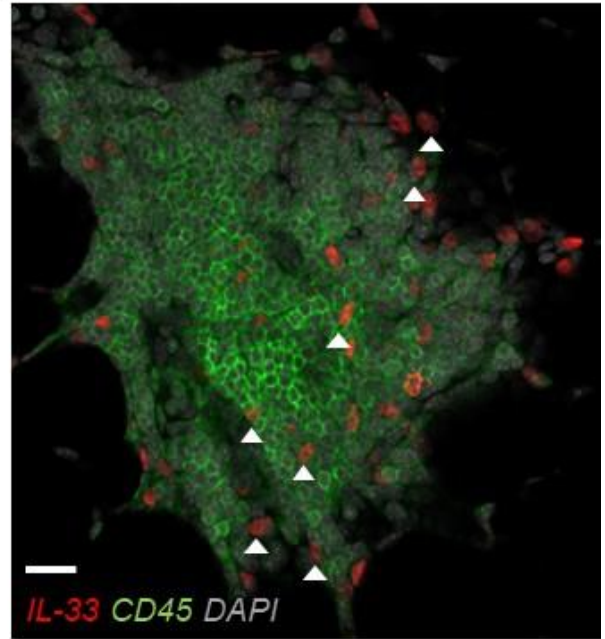


Figure 3.18: Components of FALC identified by whole mount immunofluorescence and confocal microscopy. (A) Basic visualisation of an omental FALC with FITC staining of CD45⁺ cells and a DAPI nuclear stain. (B) An omental FALC stained with B220⁺ (red) B cells and DAPI. (C) A mesenteric FALC with staining of CD3⁺ (green) and CD4⁺ (red) T cells. (D) A mesenteric FALC with CD31⁺ (blue) blood endothelium, CD45⁺ (green) cells, and Lyve-1⁺ cells (red). (E) The same mesenteric FALC as (D) but with CD45⁺ in white to allow better visualisation of Lyve-1⁺ cells (red) All images taken at 40x magnification Scale bar represents 20µm. All samples from C57/Bl6 WT mice.

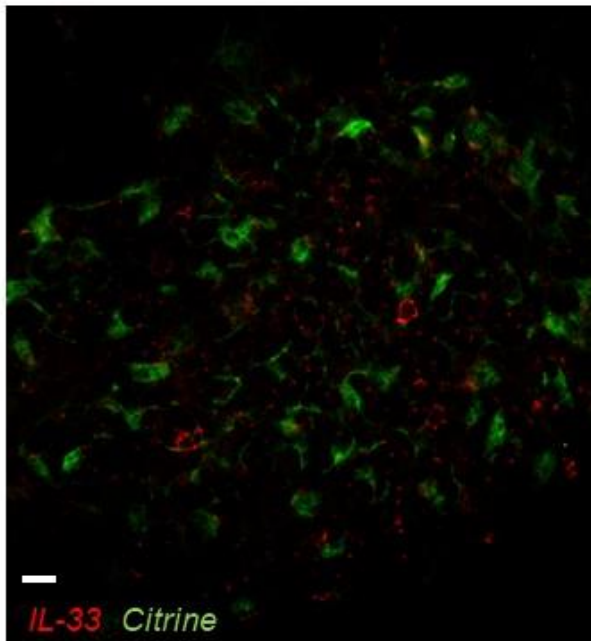
A)



B)



C)



D)

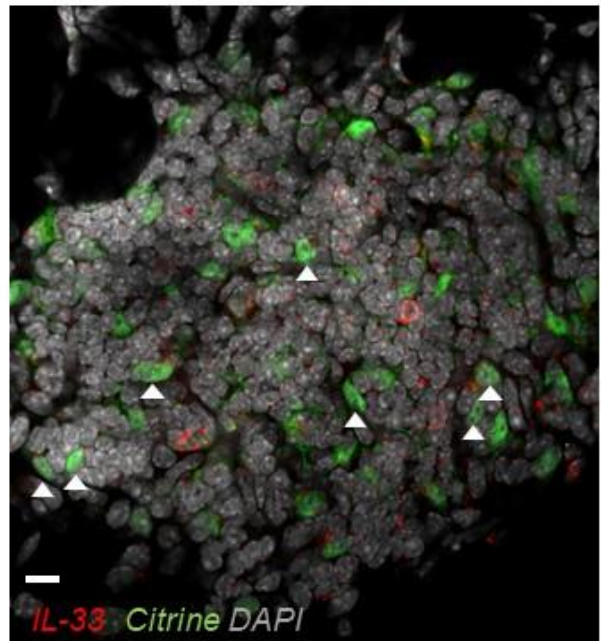


Figure 3.19: IL-33 expressing cells in FALC identified by whole mount immunofluorescence and confocal microscopy. (A) An omental FALC stained for CD45⁺ cells (green) and IL-33⁺ cells (red). The same FALC is shown in (B) with DAPI staining (grey) overlaid. (C) A second omental FALC from an IL-33^{cit/cit} mouse shows nuclear citrine (green) and staining with unconjugated anti-IL-33 and an Alexa Fluor 637 secondary antibody. The same FALC is shown in (D) with DAPI staining (grey) overlaid. Images were taken at 40x (A & B) and 60x (C & D) magnification. Scale bar represents 20µm. White arrows illustrate examples of IL-33 nuclear staining or the presence of nuclear citrine. Samples from IL-33^{cit/cit} or WT Balb/c mice. Figures C and D were contributed by Dr Sara Cruz Migoni.

4. Discussion

The data provided in this thesis has revealed that adipose deposits from distinct abdominal locations have some differential characteristics regarding their immune and stromal cell composition. Additional characterization of the stromal cell populations has been conducted and discovered that characteristics such as Sca-1, PDGFR α , and IL-33 expression do vary between tissue deposits. Taken together these data have further characterized the fat deposits under investigation and identified a potential new model tissue for further work in this area (the omentum). These results will have future applications to the wider field of obesity and metabolic homeostasis research. Numerous studies have highlighted the importance of adipocyte beiging processes to metabolic health and maintenance of the lean state. However, there is the unanswered key question of whether FALCs are involved in the beiging process in some way, given the presence of IL-33 and ILC2s in these structures. The characterization of fat depots and the identification of the omentum as a novel model tissue in this study will make further interrogation of beiging processes in FALCs easier, and in future could contribute to the identification of novel targets for pharmacological manipulation to counter obesity and metabolic dysregulation. The techniques developed during this study will assist in answering these broader questions through visualization of individual cells and key surface markers with confocal microscopy, or through application of flow cytometry techniques to other cell types from lean and obese mice, as well as human samples further down the line. Future experiments should include analysis of markers associated with beige adipocytes, such as UCP1, in each of the three depots investigated, and to what extent these are present during obesity. Thanks to the

confocal microscopy techniques refined in this study, the presence of these markers can be searched for in and around the FALC, which should shed some light on the role of these structures in the process of adipocyte beiging. Gene profiles from IL-33 producing cells and ILC2s could be compared across the tissues examined, in homeostasis and obesity, to see if there are clear differences in pro- and anti-inflammatory genes in these cells that may be contributing to their functions in beiging. Taken together these future experimental ideas should help dissect whether or not FALC and the cells within them play a role in the beiging process and how this is affected during obesity.

4.1. The presence of FALCs in adipose tissues

FALCs are easily identifiable in adipose tissue, although autofluorescence, particularly in gonadal fat, can present a problem when capturing images to document the FALC, as it is difficult to demonstrate whether or not FALC are present in the thicker areas of the deposit. In practice, it was simple to manually manipulate the tissue under the microscope to assess by eye whether FALCs were present in thicker areas of gonadal samples – they were not. However, due to the microscope and camera set up available it was technically difficult to capture images demonstrating this. Inclusion of an unstained or isotype control would be useful to show that autofluorescence is unavoidable in these samples, but as these images were intended for illustrative purposes, these controls were not included. An alternative measure could be to slice the samples into several thin strips before capturing the images, which would reduce the autofluorescence, as this would make it easier to demonstrate the lack of FALC in the thicker parts of the depot.

FALC prevalence varies widely between tissue type. FALCs as they are defined now were first identified by a group in 2010 (Moro *et al.*, 2010), but knowledge of FALCs in the omentum, commonly known in much of the literature as “milky spots”, goes back much further to 1863. Originally identified in rabbits (Recklinghausen, 1863), Louis-Antoine Ranvier designated them “milky spots” in 1874 (Ranvier, 1874). It has only been since 2009 however that the “milky spots”, or omental FALC have been considered an atypical secondary lymphoid organ (Rangel-Moreno *et al.*, 2009).

It is clear from the data that there are some stark differences in the density of FALCs in the omentum, compared to those in the mesenteric and gonadal fat. A previous study has also reported that, of the several deposits that have been studied, FALCs are most numerous in the omentum (Bénézech *et al.*, 2015). The FALC count data obtained for this thesis closely matches that of previous work, giving confidence that the large differences in FALC number seen across the deposits is a genuine phenomenon. The key to the differences seen in FALC numbers between the three adipose deposits analyzed may be to do with the levels of inflammation stimuli the organ typically encounters. Inflammation triggers an increase in the number and size of FALC, and if encountered often enough in certain tissues this could have led to evolutionary changes in their homeostatic state over time.

The omentum has been described for over a century as “the abdominal policeman” (Platell *et al.*, 2000) and reviews of its myriad uses during surgery suggests that the omentum is a complex and multifunctional organ (Platell *et al.*, 2000; Alagumuthu *et al.*, 2005). It is unsurprising then, given the various functions of the omentum in inflammation and the large numbers of macrophages and lymphocytes it contains, that

the omentum should contain huge numbers of FALCs in homeostasis. The omentum needs to be ready at all times to deal with infection or inflammation it may encounter as it comes into contact with different sites in the peritoneal cavity, and FALCs provide the omentum with a ready reservoir of immune cells that can be deployed. On the other hand, the mesenteric and gonadal fat are relatively fixed tissues compared to the omentum, so they may have exposure to relatively fewer inflammatory stimuli, and thus FALC numbers have remained lower in homeostasis.

In this study, the highest number of FALCs in a tissue (omentum) correlates with higher numbers of ILC2s and IL-33 producing cells, and the converse is also true (Gonadal, mesenteric fat). It would be interesting to see if the correlation between FALC numbers and other parameters explored in this study is maintained in inflammation conditions, as one of the limitations of this study is the lack of complete comparisons of homeostatic data with that gained from inflammation models. Other cell types could also be examined, such as macrophages, which are also known to be present in the omentum in high numbers.

4.2. Differential ILC profiles of adipose tissues

In this study, ILC1s, ILC2s, and ILC3s have been successfully identified in all three adipose deposits and the mLN. The mLN is used as a positive control for these experiments as the ILC profile for the mLN has been previously well-characterized (Mackley *et al.*, 2015). The adipose digestion protocol used for this study was not well-established and so successful staining of mLN ILCs in the absence of adipose ILCs would indicate that the adipose digestion protocol required further optimization. Once

the technique was fully optimized the mLN ILC data was included to provide a relative comparison to adipose ILC data.

The presence of ILC2s in adipose tissues has recently been established (Brestoff *et al.*, 2015; Lee *et al.*, 2015) and thus it was confirmatory that ILC2s comprised the highest proportions of ILCs in all three adipose deposits (Figure 3.5B). The ILC profile of gonadal and mesenteric fat is in fact very similar excepting significantly more ILC2s present in the mesenteric fat. This is of interest as one of the main critiques of rodent obesity studies is that too much focus is placed on gonadal fat, whereas mesenteric fat may be a more appropriate model for human disease. In this area at least, the two adipose deposits have very similar profiles. On the other hand, omental fat has a modestly different ILC profile to those of gonadal and mesenteric fat. When examining the numbers of total ILCs, omental fat has significantly more than gonadal fat, and a slight trend to containing more than mesenteric fat (Figure 3.4). Omental fat also contains significantly higher total numbers of ILC2s to gonadal fat and there is a slight trend suggesting there may be more than mesenteric fat (Figure 3.5). In addition, omental fat contains significantly more ILC3s than both gonadal and mesenteric fat and there is a strong trend suggesting ILC1s are more prevalent in the omentum as well (Figure 3.5). This suggests that omental fat displays some differential characteristics to gonadal and mesenteric fat in terms of their ILC profiles and that the omentum contains a relatively large reservoir of all type of ILCs in homeostasis, in contrast to the other adipose deposits. To date, there has been very little evidence for ILC3s in significant numbers in adipose tissue, and these data suggest that perhaps there are more ILC3s in the omental fat than previously thought. However, the data shown has been

normalized to 100mg of tissue for ease of comparison between tissues, and so with the average omentum weighing around 8-10mg it is unclear what the biological significance of 200-300 ILC3s per omentum might be, although they could be influencing the local response in some way, independent of the normalized cell number. The same could also be said for the omental ILC1 data. What does appear clear is that the presence of more FALCs seems to push the ILC composition of the adipose tissue to one that is less ILC2 centric.

One possible mechanism of a small number of ILCs influencing local responses could be via their cytokine production. As discussed in the introduction, ILCs are critical sources of a diverse array of cytokines, and these have substantial impacts on processes like macrophage polarization and induction of inflammation. One example of small numbers of ILC1s and ILC3s exerting substantial effects is in inflammatory bowel disease, where they contribute to the inflammatory pathology despite being relatively rare cell types, predominantly via secretion of IFN γ and other proinflammatory factors (Buonocore *et al.*, 2010; Geremia *et al.*, 2011; Bernink *et al.*, 2013). In the context of the omentum, perhaps the higher numbers of ILC1s and ILC3s observed create a basal level of inflammation in the environment at steady-state, compared with gonadal and mesenteric fat, which could go some way in explaining why there are many more FALC in the omentum in homeostasis. Other studies have demonstrated FALC increase in all tissues with inflammatory stimuli (Bénézech *et al.*, 2015), so it is not unreasonable to postulate that a greater number of FALC in homeostasis may be linked to a higher basal level of inflammation in the tissue. This could be investigated through assaying pro-inflammatory cytokine levels, such as IFN- γ , in WT ex-vivo samples for each depot by

ELISA. In addition, the relative proportions of M1 and M2 macrophages could be investigated between each tissue in WT mice, through cell sorting, and arrays investigating proinflammatory genes could be conducted, to see if the omentum has a more pro-inflammatory profile in homeostasis compared to gonadal and mesenteric fat. If this is the case, then obesity-induced changes may be more strongly felt in the omentum than the other deposits if a higher basal level of inflammation exists in homeostasis.

4.3. The location of ILC2s in mesenteric fat

As previously noted, the presence of ILC2s in adipose deposits has been well described, as has their role in the beiging process of white adipocytes (Brestoff *et al.*, 2015; Lee *et al.*, 2015). When ILC2s were first identified, they were reported to be present in the FALCs of mesenteric fat (Moro *et al.*, 2010), but preliminary immunofluorescence staining assays (data not shown) to identify ILC2s in FALC were unsuccessful, as were flow cytometry experiments on FALCs excised from the adipose deposit. One possible solution was to remove the FALC and assess the remaining tissue by flow cytometry. This had the surprising outcome of not affecting any of the populations that were examined such as total cellularity, total live lymphocytes, or ILC2s (Figure 3.7). An interpretation of these data is that the vast majority of ILC2s are not situated in FALCs as was previously described, but are instead distributed within the surrounding tissue, which provides a valuable insight into the location of ILC2s during homeostasis. However, there are some limitations with this experiment. The method of manually removing clusters with forceps could result in small clusters being missed, or the disturbance of cells in the cluster scattering them into the surrounding tissue, as

FALC are not surrounded by a fibrous capsule such as those enclosing lymph nodes. If there had been more time and resources for this study, perseverance at optimizing the method of digesting individual FALC could have provided further supporting data demonstrating few FALC resident ILC2s in homeostasis. Again, if time had allowed, repeating this series of experiments in a model of zymosan-induced peritoneal inflammation would have been interesting to conduct, as this model leads to an increase in the number of FALCs. If changes in the number of ILC2s were observed between naïve and FALC removed tissues in an inflammation model this could have provided an insight into whether ILC2s traffic from adipose tissue into FALCs during inflammation, or simply remain distributed in the adipose tissue.

4.4. IL-33^{cit/+} and IL-33^{cit/cit} mice as tools to investigate IL-33- producing stromal cells

This study used IL-33 reporter mice to explore the expression of this alarmin, thought to be important in driving ILC2 mediated effects in the tissue. The IL-33^{cit/+} and IL-33^{cit/cit} mice performed two major roles in this study. First, the mice allowed easy identification of IL-33-producing stroma cells in adipose tissues via flow cytometry, by using citrine as a reporter marker for IL-33. Second, the IL-33^{cit/cit} mice allowed investigation into some of the roles of IL-33 by assessing FALC numbers and stromal populations in animals where IL-33 is absent.

The stromal population containing the largest proportion of citrine⁺ cells were stromal cells of the Gp38⁺ phenotype. This was the case in both IL-33^{cit/+} and IL-33^{cit/cit} mice, demonstrating that an absence of IL-33 does not affect the proportions or absolute numbers of putative IL-33-producing cells, suggesting that IL-33 does not have a

significant role in inducing proliferation of this particular stromal population unlike its reported activity on ILC2s (Figures 3.10-3.14) (Molofsky *et al.*, 2013). In addition, FALC numbers from the adipose deposits of IL-33^{cit/+} and IL-33^{cit/cit} mice suggests that IL-33 does not play a conclusive role in the development of FALCs, although there is a trend in the gonadal and mesenteric fat data which hints that the absence of IL-33 may have a small effect on FALC numbers in these tissues (Figure 3.8).

Comparison of the Gp38⁺citrine⁺ populations across the three adipose deposits show a clear trend, that in the omentum the Gp38⁺citrine⁺ stromal phenotype comprises a significantly higher proportion of the total stroma, when compared to gonadal and mesenteric fat. This correlates with the trends seen in the ILC data for the omentum, and it follows that a tissue with the highest number of ILC2s would also contain a large proportion of IL-33-producing cells. The potential for a higher output of IL-33 may be a factor in the relatively high numbers of ILC2s seen in the omentum. However, a high proportion of IL-33-producing cells does not necessarily indicate a higher production of IL-33, as there may be negative feedback mechanisms in play that prevent all the cells capable of producing IL-33 from doing so. It would therefore be of interest to assess homeostatic IL-33 production in each tissue directly, perhaps by culturing *ex vivo* adipose samples and assaying the supernatant for IL-33 by ELISA, to see whether production of IL-33 follows the trends already identified in the ILC2 and IL-33-producing stroma data.

Although not investigated here, the regulation of IL-33 release within adipose tissues during obesity is an important point to discuss. A key study suggests that at some point during the development of obesity, IL-33 switches from having a protective role in

adipose tissues to being a proinflammatory signal, the expression of which becomes substantially upregulated (Zeyda *et al.*, 2013). This switch was associated with an increase in leptin levels, and was ameliorated in leptin deficient mice, suggesting a possible intervention pathway for novel therapies. The same study also suggests a role for fibroblast-derived IL-33 activation of endothelial cells in adipose tissues, which subsequently drives obesity-associated inflammation through a putative autocrine mechanism, within the depots (Zeyda *et al.*, 2013). It is unknown whether this increase in IL-33 expression is linked to fibroblast (pre-adipocyte) death in adipose tissue, but other studies have identified pre-adipocytes to be particularly susceptible to apoptosis in adipose tissues (Sorisky *et al.*, 2000). As such, this question would be an interesting avenue to explore, particularly in the context of FALC, as the present study demonstrates evidence of IL-33 producing stromal cells in these structures, but has not examined possible roles for fibroblast cell death in the release of IL-33, either in homeostasis or models of obesity.

Finally, FALC stromal cells have been previously characterized as expressing CXCL13 (Bénézech *et al.*, 2015). CXCL13 is known to be critical in the formation of FALCs via action as a B lymphocyte chemoattractant – B cells comprise the majority cell type in the clusters, which are known to play proinflammatory roles during obesity (Winer *et al.*, 2011; DeFuria *et al.*, 2013). In mice lacking CXCL13, FALCs do form but they contain a severely diminished number of B cells, underlying the importance of CXCL13 in this context (Bénézech *et al.*, 2015). However, the precise cellular source for CXCL13 in FALC is currently unknown. It would be of interest to examine the populations of

Gp38⁺citrine⁺ cells for expression of CXCL13, both by flow cytometry and by whole-mount immunofluorescence, to further characterize the stromal population of interest.

4.5. Further characterization of citrine⁺ stromal cells

In order to further characterize the phenotype of Gp38⁺citrine⁺ cells the presence of additional cell surface molecules was examined by flow cytometry. Sca-1 and PDGFR α were chosen for the pilot experiments as previous studies had detected the existence of these markers in embryonic adipose Gp38⁺ stromal populations (Bénézech *et al.*, 2012). The data showed that Gp38⁺citrine⁺ cells in all three adipose deposits had high proportions of Sca-1 expression. This was a confirmatory result as the putative identity of Gp38⁺CD31⁻ cells are thought to be adipocyte precursors and Sca-1 is a stem and stromal cell marker, whose presence has been detected on these populations previously, and has functional roles in proliferation. The Gp38⁺citrine⁺ populations in gonadal and mesenteric fat also have high proportions of cells that express PDGFR α , whose ligand-receptor interaction is involved in growth and renewal processes. When examining the population of Gp38⁺citrine⁻ cells, the proportion of cells expressing Sca-1 and PDGFR α was markedly lower than proportions seen in Gp38⁺citrine⁺ cells. This is interesting because the higher proportion of these markers in Gp38⁺citrine⁺ cells suggests that this population may have the ability to grow and proliferate above that of Gp38⁺ cells that do not produce IL-33. There are several in vitro experiments that could be conducted to support this theory, such as Ki67 proliferation assays.

However, in omental fat, only around half the Gp38⁺citrine⁺ population expresses PDGFR α . This could mean a number of different things. The lower level of PDGFR α

expression in the omentum could indicate a mixture of phenotypes exist within the broad classification of the Gp38⁺citrine⁺ population. Lower PDGFR α expression could also be the result of receptor internalization, via the Grb2 (Growth factor receptor-bound protein 2)-dynamin internalization mechanism (Rosenkranz *et al.*, 2000; Waterman *et al.*, 2002), or could also be the result of downregulation of the receptor. It could also be the result of contamination within the gating strategy for this tissue, whereby cells with very low expression of Gp38 and citrine do not express PDGFR α but are erroneously included with the main Gp38⁺ citrine⁺ population. This is unlikely however, as the PDGFR α data has been examined according to Gp38^{Hi}, Gp38^{Int}, and Gp38^{Lo} gates, and the proportion of Gp38^{Hi} citrine⁺ and Gp38^{Int} citrine⁺ cells expressing PDGFR α remains at approximately 50% (data not shown). This suggests that any contaminants in the gates exert a negligible effect.

Further work is required to establish the precise reason(s) for the lower proportion of PDGFR α expression seen in omental fat, not least the repetition of the original pilot experiment to give confidence that this result is genuine. It would also be of interest to sort purify the populations of Gp38⁺citrine⁺ stroma from each adipose deposit and conduct gene arrays, to investigate the relative levels of PDGFR α and other stromal markers of interest. This could help to rule in or out the receptor internalization hypothesis.

4.6. The effect of zymosan on adipose stromal populations

Zymosan is a well-known inducer of sterile peritonitis and results in expansion of FALC numbers and an influx of immune cells into the FALCs (Bénézech *et al.*, 2015). It was

therefore of interest to examine the effects of zymosan on the IL-33-producing stromal cell populations in the adipose deposits, as IL-33 acts as alarm signal during inflammation and exerts significant effects on ILC2s and other immune cells. The pilot experiment performed here suggests no clear trend exists regarding the effect of zymosan, at a 72hr timepoint, on three stromal cell phenotypes: the general Gp38⁺ population, Gp38⁺citrine⁺ cells, and Gp38⁺citrine⁺Sca-1⁺ cells. The evidence from the pilot experiment suggests that zymosan does not induce significant changes in the number of IL-33-producing cells in the stromal populations examined, but if time had allowed, these experiments would have been replicated to give more confidence to that conclusion. One limitation of this pilot study is the lack of good positive control to show that the zymosan has been active. There are qualitative visual tests that can be done, such as checking for increased FALC size under a light microscope and comparing to PBS controls, which were done. However, the best indication that the zymosan has worked properly would be to stain the FALCs with anti-CD45 FITC, count them, and the adipose deposits of zymosan treated mice should contain significantly more FALCs than those treated with PBS. Alas, this positive control method would have masked the citrine reporter protein required for stromal population identified by FACS, rendering it unsuitable for this experiment. Optimization was attempted by experimenting with anti-CD45 antibodies in different channels for FALC counts, as well as investigating use of an anti-IL-33 phycoerythrin antibody to use in place of the reporter, but neither approach gave satisfactory results in the timeframe required. If time had allowed, this pilot experiment would have been redesigned to incorporate a more appropriate positive control for zymosan activity. A further limitation of this experiment is the 72hr timepoint

examined, although this parameter was chosen, in part, to comply with institutional animal welfare regulations. Ideally, other timepoints after 72hr should also be investigated to allow for any possible lag in fibroblast proliferation, which has been previously reported in lymph nodes (Acton *et al.*, 2014). *Ex vivo* or *in vitro* assays could be performed to evaluate the best time course to try *in vivo*, such as Ki67 proliferation assays to determine when the stromal cells of interest begin to proliferate in response to zymosan.

Notwithstanding technical limitations, it would be of interest to gather data for ILC profiles and FALC counts in this zymosan model and compare them to the homeostatic data discussed in this study.

4.7. Development of a whole mount immunofluorescence staining method for confocal microscopy

One of the primary aims of this project was to develop and optimize a whole mount immunofluorescence technique for imaging FALCs by confocal microscopy. Extensive optimization has allowed the use of antibody combinations that include secondary antibody staining, alongside direct conjugates, with minimal non-specific fluorescence and background. This has dramatically improved image quality and has allowed clear imaging of individual components of the FALCs. It was in agreement with previous findings to detect B cells contained within the FALC, as other work has described the importance of FALC in B cell maturation (Bénézech *et al.*, 2015). B cells have been shown to play important roles during diet-induced obesity, in particular promotion of inflammation and insulin resistance via modulation of T cell cytokine production (Winer *et al.*, 2011; DeFuria *et al.*, 2013). As such, they represent a possible target for

pharmacological modulation in obesity and type 2 diabetes, although their specific roles in FALC during obesity are yet to be elucidated.

CD4⁺ T cells are also well known residents of the FALC (Moro *et al.*, 2010) and are detected again within the FALC in this study. Images also showed CD31⁺ blood vessels in the FALCs in corroboration with previous work (Moro *et al.*, 2010; Bénézech *et al.*, 2015). The co-staining with Lyve-1, which shows only what are thought to be Lyve-1⁺ macrophages rather than Lyve-1⁺ lymphatic vessels, is in agreement with other work where Lyve-1⁺ lymphatic vessels are not detected in the FALC (Bénézech *et al.*, 2015).

Co-staining for IL-33 alongside DAPI nuclear stain and anti-CD45 demonstrates that IL-33 is located in the nuclear compartment of non-lymphoid cells, in agreement with recent studies (Jackson-Jones *et al.*, 2016). Samples from an IL-33^{cit/cit} mouse stained for anti-IL-33 do not show anti-IL-33 staining that is consistent with nuclear staining, highlighted by the reporter protein citrine. Instead a small amount of background is visible, in contrast to the specific nuclear staining pattern seen in the WT mouse. These negative control images give confidence that the anti-IL-33 nuclear staining is indeed specific. It would be better if anti-IL33 staining could be performed using samples from an IL-33^{cit/+} mouse to observe co-staining between the anti-IL-33 antibody and the citrine reporter protein. However, the additional protocol steps required for intracellular staining with the anti-IL-33 antibody considerably weaken the citrine reporter signal, and no clear images featuring the co-staining were obtained. The images featuring co-staining in the negative control samples were obtained by a colleague, Dr Sara Cruz-Migoni, following further optimization and if time constraints had allowed the optimized protocol would have been applied to co-stained anti-IL-33 samples from IL-33^{cit/+} mice.

5. Concluding Remarks

One of the key aims of this study was to compare the FALC, ILC, and stromal profiles of gonadal, mesenteric, and omental fat in homeostasis to assess whether the tissues possess markedly different characteristics. The results of this study suggest that despite mesenteric fat being mooted as a more appropriate *ex-vivo* obesity model than gonadal fat, the physical differences between the two in the parameters examined are small. The only area in which there was a statistically significant difference between gonadal and mesenteric fat was in the number of ILC2s by tissue weight, where more were present in mesenteric fat (Figure 3.5). Arguably, perhaps this may be the most important difference of all the parameters examined, due to the fundamental role ILC2s play in metabolic homeostasis. However, this is not considered to be a sufficient body of evidence to advocate the replacement of gonadal fat with mesenteric fat in models of obesity. Further investigation is undoubtedly required, particularly in models of inflammation, where differences in ILC2 populations between tissues may well lead to broader effects on other parameters such as FALC numbers and IL-33 production. If this is shown to be the case, this would suggest there is a link between the regulation of ILC2s by IL-33 and the number of FALCs that form in a fat deposit. It is known that FALC numbers increase in response to inflammation (Bénézech *et al.*, 2015), and that IL-33 production increases in obesity and appears to play a more proinflammatory role, which drives an inflammation response (Zeyda *et al.*, 2013). A corresponding increase in ILC2s, given their roles in the beiging process, could suggest a mechanism that is attempting to restore the tissue to homeostasis. In future studies, it would be beneficial to explore to what extent IL-33 regulates ILC2s in homeostasis and whether this is

indeed perturbed in models of obesity, such as high fat diet. It would be particularly interesting to track these three parameters (FALC number, IL-33 production, and ILC2 number) in a murine model of diet-induced obesity, but extend the model past traditional endpoints to examine the effects a subsequent lean diet, and a return to the lean state, has on “ex-obese” mice. As this is very applicable to the human pattern of obesity and subsequent weight loss, it would shed light on whether obesity has any long-term effects on IL-33, ILC2s, and FALC in adipose, beyond the resolution of the disease.

With regard to the omental fat, this depot possesses slightly different FALC, ILC, and stromal profiles compared to the other fat deposits. Significantly more FALCs (Figure 3.1) were counted in the omentum vs gonadal fat, and trend towards having more than mesenteric fat. Both total and individual ILC population numbers either trend towards being, or are more significantly, present in greater numbers in the omentum, compared with gonadal and mesenteric fat (Figures 3.4-3.5). Similar results are seen in citrine-expressing stromal cell populations (Figure 3.13). The profiles are different enough that the omentum could almost be considered as an “outlier adipose tissue” in this regard. It appears to resemble the control lymphoid tissue (mLN) the closest of all the tissues examined. Coupling the results in this study with the existing knowledge of the myriad functions the omentum has, which are quite different to mesenteric and gonadal fat, suggests that the omentum is also unlikely to replace gonadal fat in obesity models. It is simply too different. However, the profile of the omentum does fit the criteria for a model tissue with which to further interrogate the role of FALCs in the beiging process. This investigation may not reveal a direct role for FALCs as a site for the beiging process. Instead, perhaps more likely, further exploration may reveal that FALCs act as cellular

reservoirs for the main players in the beiging process, or coordinate interactions between cells in order for appropriate cytokines and other factors to be produced. The omentum provides a good starting point model to explore these hypotheses as it fulfills the requirements for a tissue with high numbers of FALC, high numbers of ILC2s and high numbers of IL-33-producing stromal cells.

To facilitate these future studies into the role of FALCs in the beiging process, it was identified that an appropriate imaging protocol needed to be developed. The data presented in the latter part of this thesis, produced with the newly developed protocol, demonstrates that imaging is a viable approach to interrogate the localization of immune cells in adipose tissue at the required standard for future studies. Therefore, this thesis has achieved its original aims and in addition, by conducting additional pilot studies has exceeded the original brief, and laid the groundwork for follow on studies of immune and stromal cell characterization of abdominal adipose deposits in inflammation.

Appendix A: Supplementary Figures

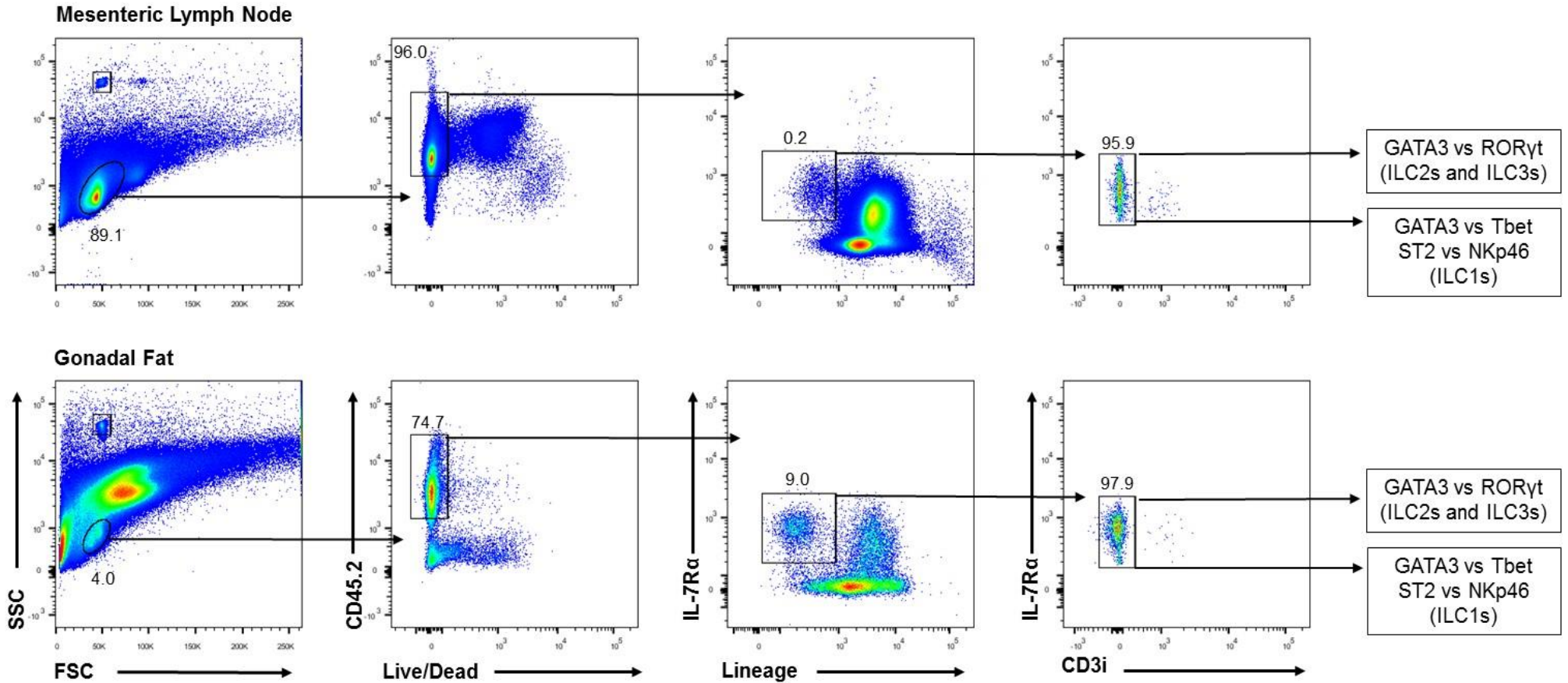


Figure S1: Full gating strategy for identifying ILCs in the mesenteric lymph node and gonadal fat. Representative flow cytometry plots showing the gating strategy for identification of a Live CD45.2⁺IL-7R α ⁺LIN⁻CD3i⁻ population of ILCs. Specific final plots to identify ILC1s as well as ILC2s and ILC3s can be seen in Figures 3.2-3.3.

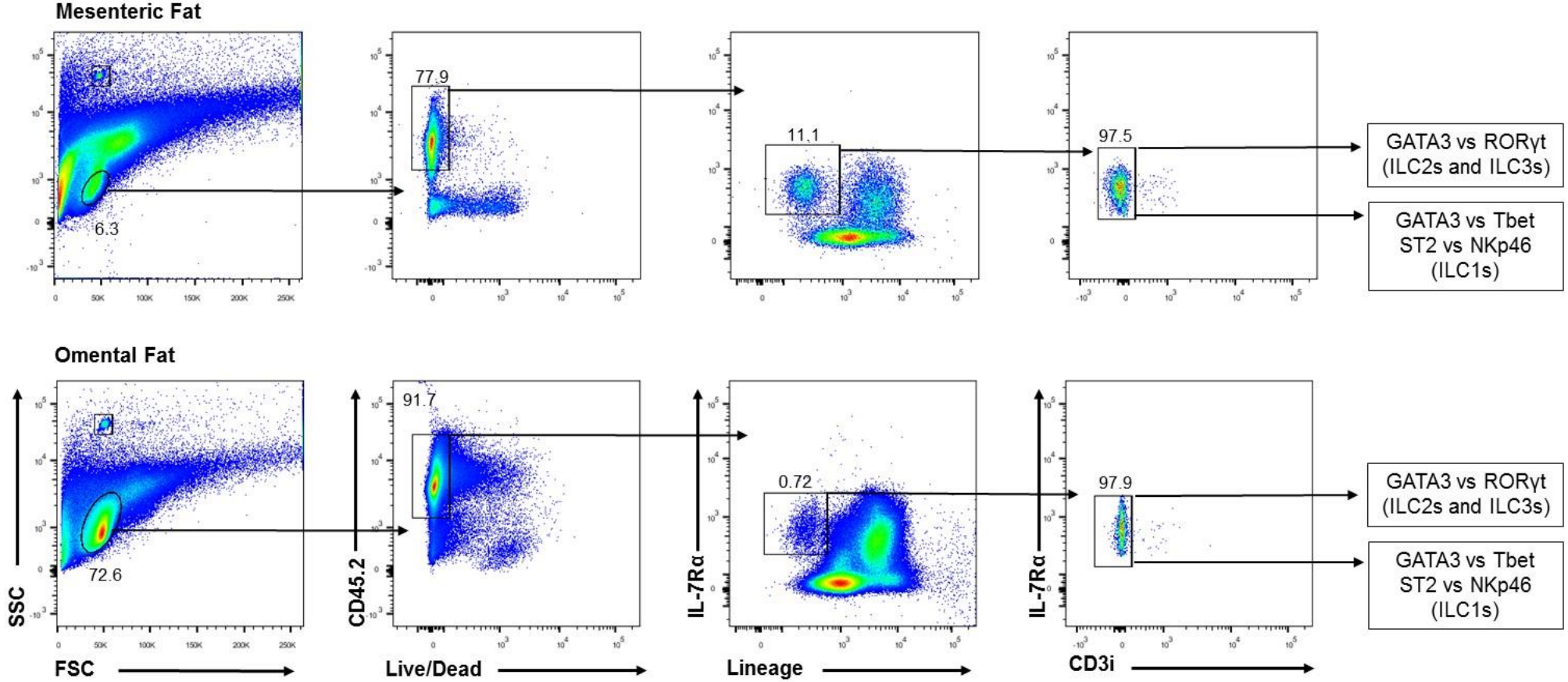


Figure S2: Full gating strategy for identifying ILCs in the mesenteric fat and omental fat. Representative flow cytometry plots showing the gating strategy for identification of a Live CD45.2⁺IL-7R α ⁺LIN⁻CD3i⁻ population of ILCs. Specific final plots to identify ILC1s as well as ILC2s and ILC3s can be seen in Figures 3.2-3.3.

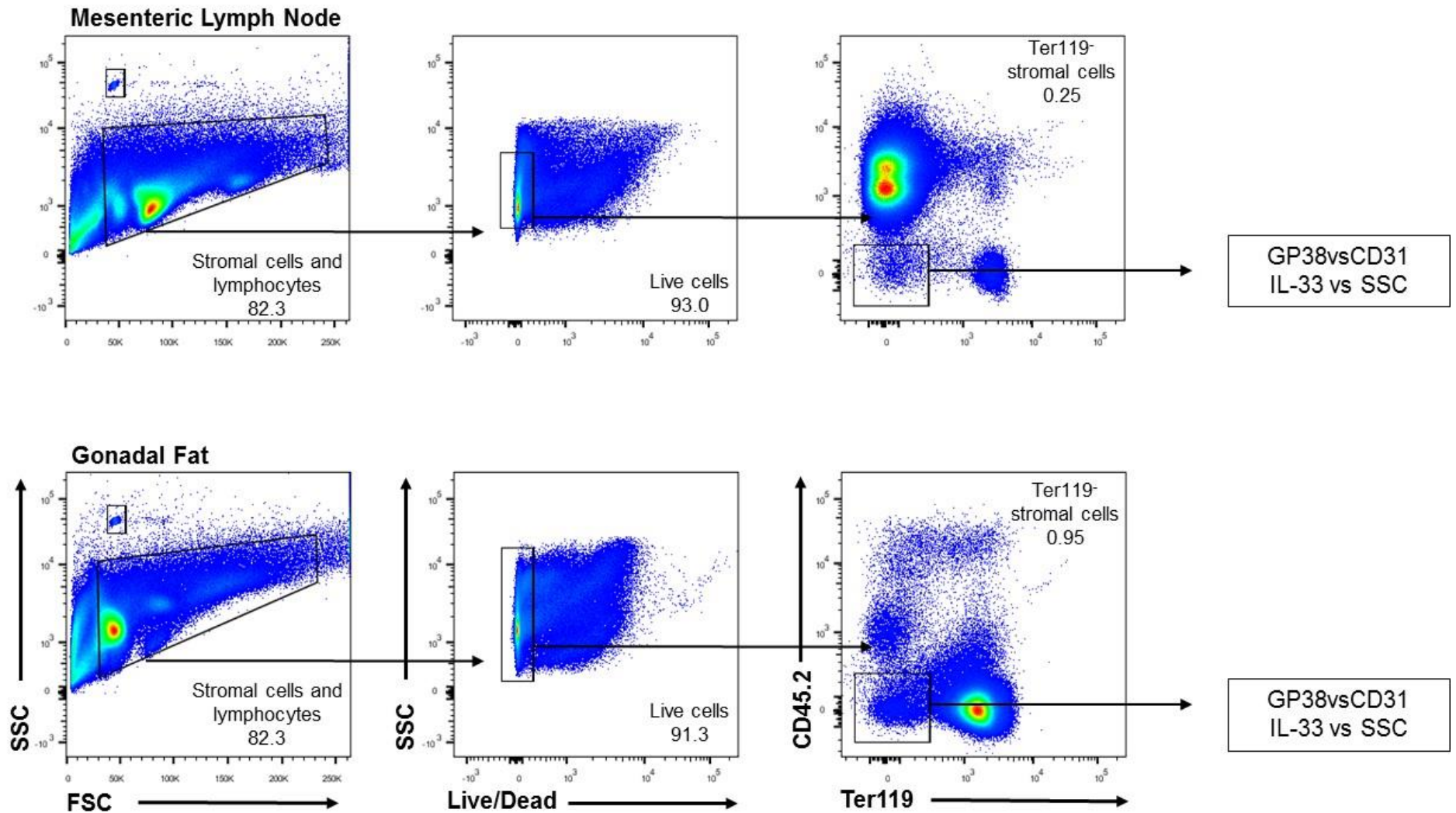


Figure S3: Full gating strategy for identifying IL-33 producing stromal cells in the mesenteric lymph node and gonadal fat of IL-33^{cit/+} mice. Representative flow cytometry plots showing the gating strategy for identification of LiveCD45⁺Ter119⁻ population of stromal cells. Specific final plots to identify IL-33 producing stroma in these tissues can be seen in figure 3.9. Plots are comparable to IL-33^{cit/cit} mice (data not shown).

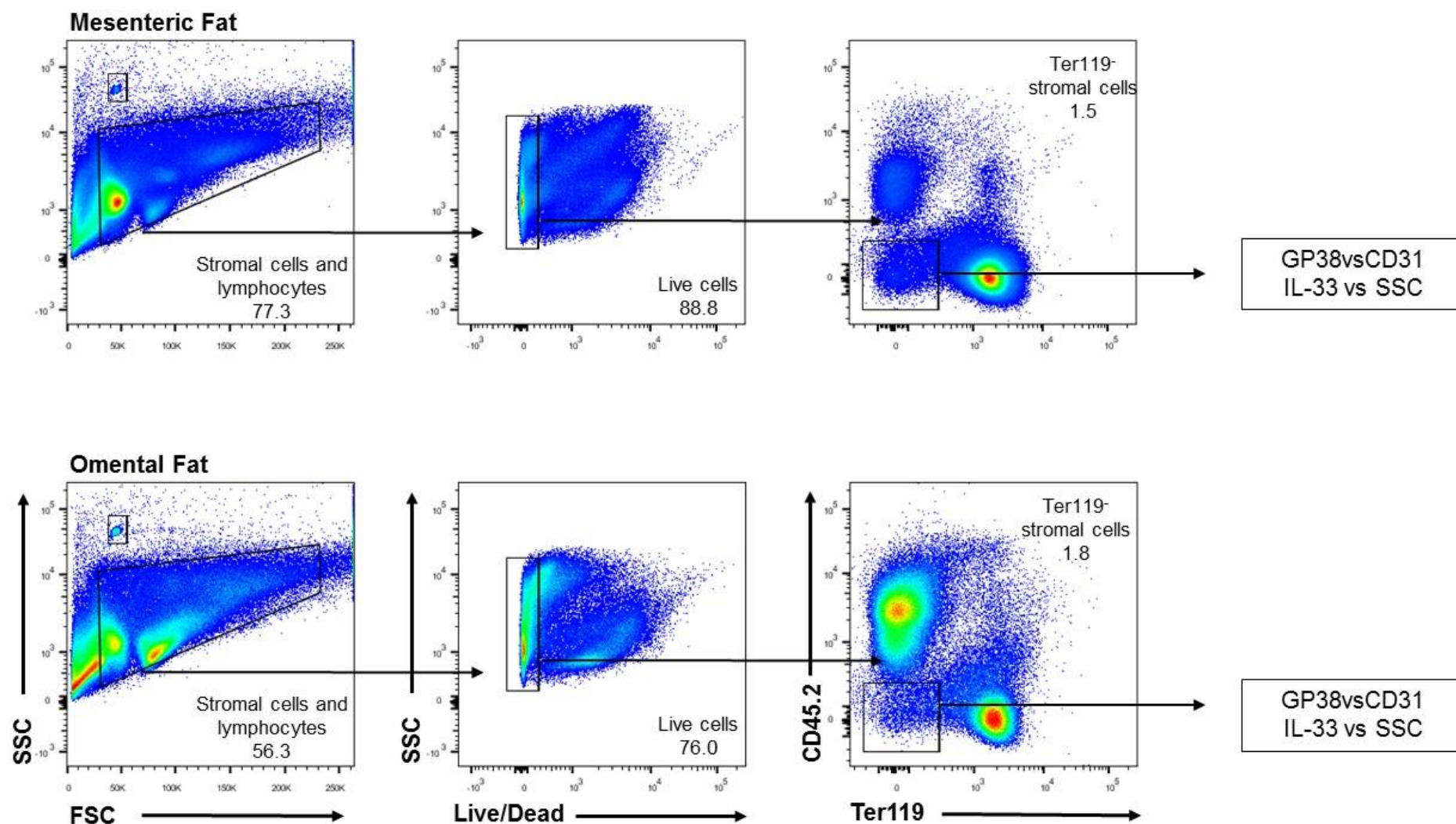


Figure S4: Full gating strategy for identifying IL-33 producing stromal cells in the mesenteric fat and omental fat of IL-33^{cit/+} mice. Representative flow cytometry plots showing the gating strategy for identification of LiveCD45⁺Ter119⁺ population of stromal cells. Specific final plots to identify IL-33 producing stroma in these tissues can be seen in figure 3.10. Plots are comparable to IL-33^{cit/cit} mice (data not shown).

Appendix B: List of References

- Acton, S.E., Farrugia, A.J., Astarita, J.L., Mourão-Sá, D., Jenkins, R.P., Nye, E., et al. (2014). Dendritic cells control fibroblastic reticular network tension and lymph node expansion. *Nature* 514: 498–502.
- Agarwal, V.K., and Bajaj, S. (1987). Salvage of end stage ischaemic extremity by omentopexy in Buerger's disease. *Indian J. Thorac. Cardiovasc. Surg.* 5: 12–17.
- Agrama, H.M., Blackwood, J.M., Brown, C.S., Machiedo, G.W., and Rush, B.F. (1976). Functional longevity of intraperitoneal drains: an experimental evaluation. *Am. J. Surg.* 132: 418–21.
- Alagumuthu, M., BhupatiB, D., SibaP, P., and Mangual, R. (2005). Review Article- The omentum: A unique organ of exceptional versatility. 68:.
- Artis, D., and Spits, H. (2015). The biology of innate lymphoid cells. *Nature* 517: 293–301.
- Barone, F., Nayar, S., and Buckley, C.D. (2013). The role of non-hematopoietic stromal cells in the persistence of inflammation. *Front. Immunol.* 3: 416.
- Bénézech, C., Luu, N.-T., Walker, J.A., Kruglov, A.A., Loo, Y., Nakamura, K., et al. (2015). Inflammation-induced formation of fat-associated lymphoid clusters. *Nat. Immunol.* 16: 819–28.
- Bénézech, C., Mader, E., Desanti, G., Khan, M., Nakamura, K., White, A., et al. (2012). Lymphotoxin- β receptor signaling through NF- κ B2-RelB pathway reprograms adipocyte precursors as lymph node stromal cells. *Immunity* 37: 721–34.
- Bernink, J.H., Peters, C.P., Munneke, M., Velde, A.A. te, Meijer, S.L., Weijer, K., et al. (2013). Human type 1 innate lymphoid cells accumulate in inflamed mucosal tissues. *Nat. Immunol.* 14: 221–9.
- Boos, M.D., Yokota, Y., Eberl, G., and Kee, B.L. (2007). Mature natural killer cell and lymphoid tissue-inducing cell development requires Id2-mediated suppression of E protein activity. *J. Exp. Med.* 204:.
- Brestoff, J.R., Kim, B.S., Saenz, S.A., Stine, R.R., Monticelli, L.A., Sonnenberg, G.F., et al. (2015). Group 2 innate lymphoid cells promote beiging of white adipose tissue and limit obesity. *Nature* 519: 242–6.

Broux, E. De, Parc, Y., Rondelli, F., Dehni, N., Tiret, E., and Parc, R. (2005). Sutured Perineal Omentoplasty After Abdominoperineal Resection for Adenocarcinoma of the Lower Rectum. *Dis. Colon Rectum* 48: 476–482.

Buonocore, S., Ahern, P.P., Uhlig, H.H., Ivanov, I.I., Littman, D.R., Maloy, K.J., et al. (2010). Innate lymphoid cells drive interleukin-23-dependent innate intestinal pathology. *Nature* 464: 1371–5.

Butland B, Jebb S, Kopelman P, et al. (2007). Tackling obesities: future choices – project report.

Carriere, V., Roussel, L., Ortega, N., Lacorre, D.-A., Americh, L., Aguilar, L., et al. (2007). IL-33, the IL-1-like cytokine ligand for ST2 receptor, is a chromatin-associated nuclear factor in vivo. *Proc. Natl. Acad. Sci.* 104: 282–287.

Chusyd, D.E., Wang, D., Huffman, D.M., and Nagy, T.R. (2016). Relationships between Rodent White Adipose Fat Pads and Human White Adipose Fat Depots. *Front. Nutr.* 3: 10.

Cicko, S., Meyer, A., Ehrat, N., Ayata, C.K., Zech, A., Hossfeld, M., et al. (2015). Extracellular ATP is a danger signal activating P2X7 Receptor in a LPS mediated inflammation (ARDS). *Eur. Respir. J.* 46:.

Cupedo, T., Vondenhoff, M.F.R., Heeregrave, E.J., Weerd, A.E. De, Jansen, W., Jackson, D.G., et al. (2004). Presumptive lymph node organizers are differentially represented in developing mesenteric and peripheral nodes. *J. Immunol.* 173: 2968–75.

DeFuria, J., Belkina, A.C., Jagannathan-Bogdan, M., Snyder-Cappione, J., Carr, J.D., Nersesova, Y.R., et al. (2013). B cells promote inflammation in obesity and type 2 diabetes through regulation of T-cell function and an inflammatory cytokine profile. *Proc. Natl. Acad. Sci.* 110: 5133–5138.

Deveaud, C., Beauvoit, B., Salin, B., Schaeffer, J., and Rigoulet, M. (2004). Regional differences in oxidative capacity of rat white adipose tissue are linked to the mitochondrial content of mature adipocytes. *Mol. Cell. Biochem.* 267: 157–166.

Faust, I.M., Johnson, P.R., Stern, J.S., and Hirsch, J. (1978). Diet-induced adipocyte number increase in adult rats: a new model of obesity. *Am. J. Physiol.* 235: E279-86.

Fletcher, A.L., Acton, S.E., and Knoblich, K. (2015). Lymph node fibroblastic reticular cells in health and disease. *Nat. Rev. Immunol.* 15: 350–361.

Fletcher, A.L., Malhotra, D., Acton, S.E., Lukacs-Kornek, V., Bellemare-Pelletier, A., Curry, M., et al. (2011). Reproducible isolation of lymph node stromal cells reveals site-dependent differences in fibroblastic reticular cells. *Front. Immunol.* 2: 35.

Geremia, A., Arancibia-Cárcamo, C. V., Fleming, M.P.P., Rust, N., Singh, B., Mortensen, N.J., et al. (2011). IL-23-responsive innate lymphoid cells are increased in inflammatory bowel disease. *J. Exp. Med.* 208: 1127–1133.

Giordano, A., Murano, I., Mondini, E., Perugini, J., Smorlesi, A., Severi, I., et al. (2013). Obese adipocytes show ultrastructural features of stressed cells and die of pyroptosis. *J. Lipid Res.* 54: 2423–36.

Grant, R., Youm, Y.-H., Ravussin, A., and Dixit, V.D. (2013). Quantification of adipose tissue leukocytosis in obesity. *Methods Mol. Biol.* 1040: 195–209.

Halim, T.Y.F., Krauss, R.H., Sun, A.C., and Takei, F. (2012a). Lung natural helper cells are a critical source of Th2 cell-type cytokines in protease allergen-induced airway inflammation. *Immunity* 36: 451–63.

Halim, T.Y.F., MacLaren, A., Romanish, M.T., Gold, M.J., McNagny, K.M., and Takei, F. (2012b). Retinoic-acid-receptor-related orphan nuclear receptor alpha is required for natural helper cell development and allergic inflammation. *Immunity* 37: 463–74.

Hams, E., Locksley, R.M., McKenzie, A.N.J., and Fallon, P.G. (2013). Cutting Edge: IL-25 Elicits Innate Lymphoid Type 2 and Type II NKT Cells That Regulate Obesity in Mice. *J. Immunol.* 191: 5349–5353.

Hardman, C.S., Panova, V., and McKenzie, A.N.J. (2013). IL-33 citrine reporter mice reveal the temporal and spatial expression of IL-33 during allergic lung inflammation. *Eur. J. Immunol.* 43: 488–98.

Hoyler, T., Klose, C.S.N., Souabni, A., Turqueti-Neves, A., Pfeifer, D., Rawlins, E.L., et al. (2012). The transcription factor GATA-3 controls cell fate and maintenance of type 2 innate lymphoid cells. *Immunity* 37: 634–48.

Jackson-Jones, L.H., Duncan, S.M., Magalhaes, M.S., Campbell, S.M., Maizels, R.M., McSorley, H.J., et al. (2016). Fat-associated lymphoid clusters control local IgM secretion during pleural infection and lung inflammation. *Nat. Commun.* 7: 12651.

Jarjour, M., Jorquera, A., Mondor, I., Wienert, S., Narang, P., Coles, M.C., et al. (2014). Fate mapping reveals origin and dynamics of lymph node follicular dendritic cells. *J.*

Exp. Med. 211:.

Joshi, A.D., Oak, S.R., Hartigan, A.J., Finn, W.G., Kunkel, S.L., Duffy, K.E., et al. (2010). Interleukin-33 contributes to both M1 and M2 chemokine marker expression in human macrophages. *BMC Immunol.* 11: 52.

Kiessling, R., Klein, E., Pross, H., and Wigzell, H. (1975). 'Natural' killer cells in the mouse. II. Cytotoxic cells with specificity for mouse Moloney leukemia cells. Characteristics of the killer cell. *Eur. J. Immunol.* 5: 117–21.

Kim, Y., Kim, E., Wu, Q., Guryanova, O., Hitomi, M., Lathia, J.D., et al. (2012). Platelet-derived growth factor receptors differentially inform intertumoral and intratumoral heterogeneity. *Genes Dev.* 26: 1247–62.

Klose, C.S.N., Kiss, E. a, Schwierzeck, V., Ebert, K., Hoyler, T., D'Hargues, Y., et al. (2013). A T-bet gradient controls the fate and function of CCR6-ROR γ t⁺ innate lymphoid cells. *Nature* 494: 261–265.

Konturek, S.J., Brzozowski, T., Majka, I., Pawlik, W., and Stachura, J. (1994). Omentum and basic fibroblast growth factor in healing of chronic gastric ulcerations in rats. *Dig. Dis. Sci.* 39: 1064–71.

Kozak, L.P., and Anunciado-Koza, R. (2008). UCP1: its involvement and utility in obesity. *Int. J. Obes.* 32: S32–S38.

Krist, L.F.G., Eestermans, I.L., Steenbergen, J.J.E., Hoefsmit, E.C.M., Cuesta, M.A., Meyer, S., et al. (1995). Cellular composition of milky spots in the human greater omentum: An immunochemical and ultrastructural study. *Anat. Rec.* 241: 163–174.

Lee, M.-W., Odegaard, J.I., Mukundan, L., Qiu, Y., Molofsky, A.B., Nussbaum, J.C., et al. (2015a). Activated Type 2 Innate Lymphoid Cells Regulate Beige Fat Biogenesis. *Cell* 160: 74–87.

Lee, M.-W., Odegaard, J.I., Mukundan, L., Qiu, Y., Molofsky, A.B., Nussbaum, J.C., et al. (2015b). Activated type 2 innate lymphoid cells regulate beige fat biogenesis. *Cell* 160: 74–87.

Loncar, D., Afzelius, B.A., and Cannon, B. (1988). Epididymal white adipose tissue after cold stress in rats. II. Mitochondrial changes. *J. Ultrastruct. Mol. Struct. Res.* 101: 199–209.

Loncar, D., Bedrica, L., Mayer, J., Cannon, B., Nedergaard, J., Afzelius, B.A., et al.

(1986). The effect of intermittent cold treatment on the adipose tissue of the cat. Apparent transformation from white to brown adipose tissue. *J. Ultrastruct. Mol. Struct. Res.* 97: 119–29.

Lu, Y.-C., Yeh, W.-C., and Ohashi, P.S. (2008). LPS/TLR4 signal transduction pathway. *Cytokine* 42: 145–151.

Lüthi, A.U., Cullen, S.P., McNeela, E.A., Duriez, P.J., Afonina, I.S., Sheridan, C., et al. (2009). Suppression of Interleukin-33 Bioactivity through Proteolysis by Apoptotic Caspases. *Immunity* 31: 84–98.

Mackley, E.C., Houston, S., Marriott, C.L., Halford, E.E., Lucas, B., Cerovic, V., et al. (2015). CCR7-dependent trafficking of ROR γ ⁺ ILCs creates a unique microenvironment within mucosal draining lymph nodes. *Nat. Commun.* 6: 5862.

Molofsky, A.B., Nussbaum, J.C., Liang, H.-E., Dyken, S.J. Van, Cheng, L.E., Mohapatra, A., et al. (2013). Innate lymphoid type 2 cells sustain visceral adipose tissue eosinophils and alternatively activated macrophages. *J. Exp. Med.* 210:

Moretta, A., Marcenaro, E., Sivori, S., Chiesa, M. Della, Vitale, M., and Moretta, L. (2005). Early liaisons between cells of the innate immune system in inflamed peripheral tissues. *Trends Immunol.* 26: 668–75.

Moro, K., Yamada, T., Tanabe, M., Takeuchi, T., Ikawa, T., Kawamoto, H., et al. (2010). Innate production of T(H)2 cytokines by adipose tissue-associated c-Kit(+)Sca-1(+) lymphoid cells. *Nature* 463: 540–4.

Morris, D.L., Cho, K.W., Delproposto, J.L., Oatmen, K.E., Geletka, L.M., Martinez-Santibanez, G., et al. (2013). Adipose tissue macrophages function as antigen-presenting cells and regulate adipose tissue CD4⁺ T cells in mice. *Diabetes* 62: 2762–72.

Neeland, I.J., Turer, A.T., Ayers, C.R., Powell-Wiley, T.M., Vega, G.L., Farzaneh-Far, R., et al. (2012). Dysfunctional adiposity and the risk of prediabetes and type 2 diabetes in obese adults. *JAMA* 308: 1150–9.

Neill, D.R., Wong, S.H., Bellosi, A., Flynn, R.J., Daly, M., Langford, T.K.A., et al. (2010). Nuocytes represent a new innate effector leukocyte that mediates type-2 immunity. *Nature* 464: 1367–70.

Nibbs, R.J., Kriehuber, E., Ponath, P.D., Parent, D., Qin, S., Campbell, J.D., et al.

(2001). The beta-chemokine receptor D6 is expressed by lymphatic endothelium and a subset of vascular tumors. *Am. J. Pathol.* *158*: 867–77.

O’Sullivan, T.E., Rapp, M., Fan, X., Weizman, O.-E., Bhardwaj, P., Adams, N.M., et al. (2016). Adipose-Resident Group 1 Innate Lymphoid Cells Promote Obesity-Associated Insulin Resistance. *Immunity* *45*: 428–41.

Odegaard, J.I., Lee, M.-W., Sogawa, Y., Bertholet, A.M., Locksley, R.M., Weinberg, D.E., et al. (2016). Perinatal Licensing of Thermogenesis by IL-33 and ST2. *Cell* *166*: 841–854.

Odegaard, J.I., Ricardo-Gonzalez, R.R., Goforth, M.H., Morel, C.R., Subramanian, V., Mukundan, L., et al. (2007). Macrophage-specific PPARgamma controls alternative activation and improves insulin resistance. *Nature* *447*: 1116–20.

Ohashi, K., Burkart, V., Flohe, S., and Kolb, H. (2000). Cutting Edge: Heat Shock Protein 60 Is a Putative Endogenous Ligand of the Toll-Like Receptor-4 Complex. *J. Immunol.* *164*: 558–561.

Ouchi, N., Parker, J.L., Lugus, J.J., and Walsh, K. (2011). Adipokines in inflammation and metabolic disease. *Nat. Rev. Immunol.* *11*: 85–97.

Ozinsky, A., Underhill, D.M., Fontenot, J.D., Hajjar, A.M., Smith, K.D., Wilson, C.B., et al. (2000). The repertoire for pattern recognition of pathogens by the innate immune system is defined by cooperation between toll-like receptors. *Proc. Natl. Acad. Sci. U. S. A.* *97*: 13766–71.

Palou, M., Priego, T., Sánchez, J., Rodríguez, A.M., Palou, A., and Picó, C. (2009). Gene expression patterns in visceral and subcutaneous adipose depots in rats are linked to their morphologic features. *Cell. Physiol. Biochem.* *24*: 547–56.

Pavert, S. a van de, Olivier, B.J., Goverse, G., Vondenhoff, M.F., Greuter, M., Beke, P., et al. (2009). Chemokine CXCL13 is essential for lymph node initiation and is induced by retinoic acid and neuronal stimulation. *Nat. Immunol.* *10*: 1193–1199.

Pichery, M., Mirey, E., Mercier, P., Lefrancais, E., Dujardin, A., Ortega, N., et al. (2012). Endogenous IL-33 Is Highly Expressed in Mouse Epithelial Barrier Tissues, Lymphoid Organs, Brain, Embryos, and Inflamed Tissues: In Situ Analysis Using a Novel IL-33-LacZ Gene Trap Reporter Strain. *J. Immunol.* *188*: 3488–3495.

Platell, C., Cooper, D., Papadimitriou, J.M., and Hall, J.C. (2000). The omentum. *World*

J. Gastroenterol. 6: 169–176.

Poltorak, A., He, X., Smirnova, I., Liu, M.Y., Huffel, C. Van, Du, X., et al. (1998). Defective LPS signaling in C3H/HeJ and C57BL/10ScCr mice: mutations in Tlr4 gene. *Science* 282: 2085–8.

Price, A.E., Liang, H.-E., Sullivan, B.M., Reinhardt, R.L., Eisley, C.J., Erle, D.J., et al. (2010). Systemically dispersed innate IL-13-expressing cells in type 2 immunity. *Proc. Natl. Acad. Sci. U. S. A.* 107: 11489–94.

Qiu, Y., Nguyen, K.D., Odegaard, J.I., Cui, X., Tian, X., Locksley, R.M., et al. (2014). Eosinophils and type 2 cytokine signaling in macrophages orchestrate development of functional beige fat. *Cell* 157: 1292–308.

Rangel-Moreno, J., Moyron-Quiroz, J.E., Carragher, D.M., Kusser, K., Hartson, L., Moquin, A., et al. (2009). Omental milky spots develop in the absence of lymphoid tissue-inducer cells and support B and T cell responses to peritoneal antigens. *Immunity* 30: 731–43.

Rankin, L.C., Girard-madoux, M.J.H., Seillet, C., and Mielke, L.A. (2016). Europe PMC Funders Group Complementarity and redundancy of IL-22-producing innate lymphoid cells. *17*: 179–186.

Ranvier, L. (1874). Du développement et de l'accroissement des vaisseaux sanguins. *Arch Physiol Norm Pathol.* 6: 429–46.

Recklinghausen, F. (1863). Ueber Eiter- und Bindegewebskörperchen. *Arch. Für Pathol. Anat. Und Physiol. Und Für Klin. Med.* 28: 157–197.

Ricardo-Gonzalez, R.R., Red Eagle, A., Odegaard, J.I., Jouihan, H., Morel, C.R., Heredia, J.E., et al. (2010). IL-4/STAT6 immune axis regulates peripheral nutrient metabolism and insulin sensitivity. *Proc. Natl. Acad. Sci. U. S. A.* 107: 22617–22.

Robinson, D.S., Hamid, Q., Ying, S., Tsicopoulos, A., Barkans, J., Bentley, A.M., et al. (1992). Predominant TH2-like bronchoalveolar T-lymphocyte population in atopic asthma. *N. Engl. J. Med.* 326: 298–304.

Rosenkranz, S., Ikuno, Y., Leong, F.L., Klinghoffer, R.A., Miyake, S., Band, H., et al. (2000). Src family kinases negatively regulate platelet-derived growth factor alpha receptor-dependent signaling and disease progression. *J. Biol. Chem.* 275: 9620–7.

Sato-Takayama, N., Vosshenrich, C.A.J., Lesjean-Pottier, S., Sawa, S., Lochner, M.,

Rattis, F., et al. (2008). Microbial flora drives interleukin 22 production in intestinal NKp46+ cells that provide innate mucosal immune defense. *Immunity* 29: 958–70.

Schmitz, J., Owyang, A., Oldham, E., Song, Y., Murphy, E., McClanahan, T.K., et al. (2005). IL-33, an Interleukin-1-like Cytokine that Signals via the IL-1 Receptor-Related Protein ST2 and Induces T Helper Type 2-Associated Cytokines. *Immunity* 23: 479–490.

Shiao, S.L., McNiff, J.M., and Pober, J.S. (2005). Memory T cells and their costimulators in human allograft injury. *J. Immunol.* 175: 4886–96.

Shibley, P.G., and Cunningham, R.S. (1916). STUDIES ON ABSORPTION FROM SEROUS CAVITIES. *Am. J. Physiol. -- Leg. Content* 40:.

Sonnenberg, G.F., Monticelli, L.A., Elloso, M.M., Fouser, L.A., and Artis, D. (2011). CD4(+) lymphoid tissue-inducer cells promote innate immunity in the gut. *Immunity* 34: 122–34.

Sorisky, A., Magun, R., and Gagnon, A. (2000). Adipose cell apoptosis: death in the energy depot. *Int. J. Obes.* 24: 3–7.

Spits, H., Artis, D., Colonna, M., Diefenbach, A., Santo, J.P. Di, Eberl, G., et al. (2013). Innate lymphoid cells--a proposal for uniform nomenclature. *Nat. Rev. Immunol.* 13: 145–9.

Strissel, K.J., Stancheva, Z., Miyoshi, H., Perfield, J.W., DeFuria, J., Jick, Z., et al. (2007). Adipocyte Death, Adipose Tissue Remodeling, and Obesity Complications. *Diabetes* 56: 2910–2918.

Uhm, M., Saltiel, A.R., Brestoff, J.R., Kim, B.S., Saenz, S.A., Stine, R.R., et al. (2015). White, Brown, and Beige; Type 2 Immunity Gets Hot. *Immunity* 42: 15–17.

Underhill, D.M., Ozinsky, A., Hajjar, A.M., Stevens, A., Wilson, C.B., Bassetti, M., et al. (1999). The Toll-like receptor 2 is recruited to macrophage phagosomes and discriminates between pathogens. *Nature*, Publ. Online 16 December 1999; | doi10.1038/35005543 39.

Vidal-Puig, A.J., Considine, R. V, Jimenez-Liñan, M., Werman, A., Pories, W.J., Caro, J.F., et al. (1997). Peroxisome proliferator-activated receptor gene expression in human tissues. Effects of obesity, weight loss, and regulation by insulin and glucocorticoids. *J. Clin. Invest.* 99: 2416–22.

Vineberg, A.M., Kato, Y., Pirozynski, W.J., Vineberg, A., Niloff, P., Vineberg, A., et al. (1966). Experimental revascularization of the entire heart. Evaluation of epicardiectomy, omental graft, and/or implantation of the internal mammary artery in preventing myocardial necrosis and death of the animal. *Am. Heart J.* 72: 79–93.

Walker, J.A., Barlow, J.L., and McKenzie, A.N.J. (2013). Innate lymphoid cells--how did we miss them? *Nat. Rev. Immunol.* 13: 75–87.

Waterman, H., Katz, M., Rubin, C., Shtiegman, K., Lavi, S., Elson, A., et al. (2002). A mutant EGF-receptor defective in ubiquitylation and endocytosis unveils a role for Grb2 in negative signaling. *EMBO J.* 21: 303–13.

WHO, IASO, and IOTF (2000). The Asia-Pacific perspective: redefining obesity and its treatment.

Winer, D.A., Winer, S., Shen, L., Wadia, P.P., Yantha, J., Paltser, G., et al. (2011). B cells promote insulin resistance through modulation of T cells and production of pathogenic IgG antibodies. *Nat. Med.* 17: 610–617.

Wood, I.S., Wang, B., and Trayhurn, P. (2009). IL-33, a recently identified interleukin-1 gene family member, is expressed in human adipocytes.

Wu, D., Molofsky, A.B., Liang, H.-E., Ricardo-Gonzalez, R.R., Jouihan, H.A., Bando, J.K., et al. (2011). Eosinophils Sustain Adipose Alternatively Activated Macrophages Associated with Glucose Homeostasis. *Science* (80-.). 332:.

Yang, H., Wang, H., Chavan, S.S., and Andersson, U. (2015). High Mobility Group Box Protein 1 (HMGB1): The Prototypical Endogenous Danger Molecule. *Mol. Med.* 21 *Suppl 1*: S6–S12.

Yang, Y.-K., Chen, M., Clements, R.H., Abrams, G.A., Aprahamian, C.J., and Harmon, C.M. (2008). Human Mesenteric Adipose Tissue Plays Unique Role Versus Subcutaneous and Omental Fat in Obesity Related Diabetes. *Cell. Physiol. Biochem.* 22: 531–538.

Yoneshiro, T., Aita, S., Matsushita, M., Okamatsu-Ogura, Y., Kameya, T., Kawai, Y., et al. (2011). Age-Related Decrease in Cold-Activated Brown Adipose Tissue and Accumulation of Body Fat in Healthy Humans. *Obesity* 19: 1755–1760.

Zenewicz, L.A., Yancopoulos, G.D., Valenzuela, D.M., Murphy, A.J., Stevens, S., and Flavell, R.A. (2008). Innate and adaptive interleukin-22 protects mice from inflammatory

bowel disease. *Immunity* 29: 947–57.

Zeyda, M., Wernly, B., Demyanets, S., Kaun, C., Hämmerle, M., Hantusch, B., et al. (2013). Severe obesity increases adipose tissue expression of interleukin-33 and its receptor ST2, both predominantly detectable in endothelial cells of human adipose tissue. *Int. J. Obes.* 37: 658–665.